1-1-2019

The Genetics Of Vein Of Galen Malformation And Assessment Of Candidate Genes In Xenopus Tropicalis

Jonathan Read Gaillard

The Genetics of Vein of Galen Malformation and Assessment of Candidate Genes in *Xenopus tropicalis*

A Thesis Submitted to the Yale
University School of Medicine
in Partial Fulfillment of the Requirements for the
Degree of Doctor of Medicine

By

Jonathan Read Gaillard

2019

I. Abstract

GENETICS OF VEIN OF GALEN MALFORMATION AND ASSESSMENT OF CANDIDATE GENES IN *XENOPUS TROPICALIS*

Jonathan R. Gaillard, Daniel D. Duran, Mustafa Khokha, Engin Deniz, and Kristopher T. Kahle. Section of Pediatric Neurosurgery, Department of Neurosurgery, Yale University, School of Medicine, New Haven, CT.

The Vein of Galen Malformation (VOGM) is a specific subtype of arteriovenous malformation (AVM) that becomes evident in weeks 6-11 of embryonic development. VOGM comprise less than 1% of all vascular malformations, yet represent 30% of all pediatric intracranial vascular malformations. Depending on their specific characteristics, i.e. its feeding vessels, it can present clinically as devastating congestive heart failure in neonates, hydrocephalus in children, or seizures and headaches in young adults. Advances in treatment provide improved survival, primarily through endovascular surgery. The genetic and molecular etiology of VOGM remains relatively unknown, with the only associated genes being in the context of other syndromes, including seven mutations in p120-RasGAP (*RASA1*) in Cutaneous Malformations-Arteriovenous Malformations (CM-AVM), as well as one mutation each in *activin A receptor type II-like 1* (*ACVRL1*) mutation and *Endoglin* (*ENG*) in Hereditary Hemorraghic Teleangiectasia.

Our limited knowledge of the molecular genetics of VOGM has hindered the development of novel therapies. We hypothesized that the apparent sporadic occurrence of VOGM may frequently be attributable to damaging de novo mutation events or incomplete penetrance

of rare transmitted variants. Unbiased whole-exome sequencing (WES) can overcome these barriers for gene discovery. We recruited 55 patients, including 52 parent-offspring trios. WES revealed statistically significant rare, damaging *de novo* mutations in chromatin modifier genes involved in brain and vascular development ($p=8.9 \times 10^{-4}$). VOGM probands also had inherited, missense deleterious and loss of function, in ephrin signaling genes, specifically a whole exome significant mutation burden in *EPHB4* ($p=7.47 \times 10^{-10}$). Finally, we observed a whole exome significant inherited mutation in Claudin 14 ($p= 6.44 \times 10^{-7}$). Inherited mutations demonstrated incomplete penetrance and variable expressivity with mutation carriers often exhibiting cutaneous vascular abnormalities suggesting a two-hit mechanism. The identified mutations account for 30% of studied VOGM cases.

To functionally validate candidate mutations and establish causality, we developed a screening platform using *Xenopus tropicalis* by using CRISP/Cas9 gene editing and observing the effects of candidate gene knockdown on vasculogenesis and brain vasculature.

CRISPR/Cas9 knockdown of *EPHB4* and *CLDN14* yielded significantly abnormal vasculogenesis ($p=0.0028$ and $p=0.0001$ respectively) observed by in situ hybridization. We implemented and modified established clearing techniques to allow visualization of the full thickness of the *Xenopus* brain vasculature. The evolutionary precursor to the vein of Galen, the posterior vascular plexus (PVP), and the mesencephalic veins (MSV), were imaged. *EPHB4* and *CLDN14* CRISPR/Cas9 knockdown revealed significant decreases in MSV length ($p<0.0001$ and $p=0.0006$ respectively) but there was no significant decrease

in PVP area. Attempted rescue with wild-type vs. mutant human *CLDN14* mRNA did not lead to significant improvement of the phenotype.

Together these findings are the first step in better understanding the mechanism and pathogenesis of VOGM and potential novel therapeutic targets. While *Xenopus* is not a perfect model system, it does show promise as a tool to assess candidate VOGM that merit further study in mammalian systems harboring a true vein of Galen.

II. Acknowledgements

I would like to thank my thesis advisor Dr. Kristopher T. Kahle who to took me into his lab even though I was just a 2nd year student who was still debating whether to pursue neurosurgery. Though I have instead chosen pediatric neurology, much of what I have learned during this project has given me great insight and ideas for my own future endeavors. Dr. Kahle's enthusiasm for research and energy knows no bounds. He has set the bar very high for what I hope to accomplish in my own future career as a physician scientist, a goal I aim to achieve.

I would like to thank Dr. Mustafa Khokha and Dr. Jun Lu as part of my MHS thesis committee. Thank you for all your help and input both on this thesis, my growth as a future scientist, and the work I have performed in your labs.

This work would not have been possible without HHMI Medical Fellows program which gave me the funding and support to be able to pursue a comprehensive research project. Without HHMI I may not have realized my interest and excitement in more basic and translational research. Because of this work, I have become more determined to become a physician scientist.

I would like to especially thank my post-doc and now neurosurgery resident, Daniel Duran from the Kahle lab, who took me under his wing and made sure I knew how to make packages, how to differentiate Vein of Galen Malformations, how to confirm possible hits. He will make an amazing neurosurgeon.

I would also like to thank Kahle Lab, Khokha Lab, Deniz Lab, and Lifton lab members who taught me a lot and helped make lab more like my second family. Together, we published the genetics work presented in this thesis at: Daniel Duran et al. Mutations in Chromatin Modifier and Ephrin Signaling Genes in Vein of Galen Malformation, Neuron, Dec 2018, ISSN 0896-6273, https://doi.org/10.1016/j.neuron.2018.11.041.

Finally, I would like to thank my family. My loving parents who were my first points of inspiration to become a physician scientist. They are amazing role models and helped throughout this whole process from HHMI applications to thesis. And to my loving wife Aveline who has supported me through my entire work here at Yale, even when I have gone in on the weekends and stayed late in lab. I love you will all my heart.

Table of Contents

IV. Introduction to Vein of Galen Malformations

IV. Introduction to Vein of Galen Malformations

Please note, some of the text below includes figures and text, taken and adapted from the article:

Duran, D., Karschnia, P., ***Gaillard, J.R****., Karimy, J.K., Youngblood, M.W., DiLuna, M.L., Matouk, C.C., Aagaard-Kienitz, B., Smith, E.R., Orbach, D.B., Rodesch, G., Berenstein, A., Gunel, M., & Kahle, K.T.* ***Human Genetics and molecular mechanisms of vein of Galen malformation.*** *J Neurosurg Pediatr. 2018 Apr;21(4):367-374.*

It is reproduced here with permission from Journal of Neurosurgery.

The Vein of Galen Malformation (VOGM) is a specific type of Arteriovenous Malformation (AVM) that offers a unique opportunity to understand the pathogenesis of AVMs providing insight into disease causing mutations in arterio-venous differentiation. Although it is estimated that VOGM makes up only 1% of all intracranial vascular malformations, VOGM represent 30% of all pediatric intracranial vascular malformations (Deloison et al., 2012; Long et al., 1974). VOGM starts in weeks 6-11 of embryonic development (Raybaud et al., 1989). VOGM are phenotypically varied in their presentation depending on their feeding vessels. In severe cases, the VOGM can be detected in utero by ultrasound and can present clinically as devastating congestive heart failure in neonates, or in less severe cases present with hydrocephalus in children, or seizures and headaches in young adults (Amacher and Shillito, 1973). VOGM rarely present with stroke and do not rupture, thereby leading to improved outcomes through diagnosis and treatment. The study of the genetics of VOGM will prove invaluable to the study of other AVMs by unveiling

pathways and mechanisms that are responsible for dysregulated arterio-venous differentiation.

Advances in treatments provide improved survival, primarily through endovascular surgery, and less frequently, radiosurgery (Lasjaunias et al., 1995; Lasjaunias et al., 2006). Previously, with clipping and microsurgery mortality was 80-100%, however, endovascular surgery greatly reduced mortality to 15% (Khullar et al., 2010). However, the genetic and molecular etiology of VOGM remains relatively unknown, limiting the creation of novel therapies that may further reduce mortality and morbidity by intervening at even earlier. At present, the fundamental lack of information regarding the genetic and molecular etiology of VOGM leaves physicians unprepared for the increased population of VOGM patients, some of whom will likely be born to parents who themselves were treated for VOGM.

Here we review the pathophysiology, diagnosis, and management of infants and children with VOGM and the limited genetic landscape. We examine studies on arteriovenous malformations, specifically the arteriovenous specification and in model organisms. A comprehensive understanding of the key genetic drivers and the associated molecular mechanisms of VOGM may identify targets for the development of novel pharmacotherapeutic strategies, if not genetic counseling for VOGM patients who will one day have families of their own.

The pathophysiology of VOGM/ Importance of Brain AVMs and VOGM

Brain AVMs occur in approximately 1.3/100,000 person-years (Gabriel et al., 2010). VOGM themselves represent <1% of all vascular malformations yet account for approximately 30% of all pediatric cerebrovascular malformations (Deloison et al., 2012; Long et al., 1974). Jaeger and colleagues reported the first VOGM patient **(Jaeger et al., 1937)**, a 4-year-old child who presented at 8 months of age with hydrocephalus due to the vein of Galen occluding the sylvian aqueduct (Jaeger et al., 1937).

The development of VOGM was still largely debated until the late 1980s. **Raybaud and colleagues** (Raybaud et al., 1989) found that between gestational weeks 6 and 11 the affected embryo develops arteriovenous fistulas that feed into the embryonic structure named the median prosencephalic vein of Markowski. The arteriovenous fistula creates a persistent turbulent flow which prevents the natural regression of the median vein and thereby maintains the patency of the median prosencephalic vein which enlarges in size and occupies the same location as the vein of Galen (Raybaud et al., 1989). This creates a misnomer as the VOGM does not actually affect the vein of Galen proper.

VOGMs fall into two distinct angioarchitectural patterns: choridal (**Fig. 1A**) and mural (**Fig. 1B**). Choridal malformations are characterized by numerous feeder vessels and "pseudoniduses" that communicate with the medial prosencephalic vein. In contrast, mural VOGMs present a small number of larger-caliber fistulas into this structure (Lasjaunias et al., 2006). One or more arteries can directly feed into the median prosencephalic vein and certain arteries are found in different classes of VOGM. The arteries include the posterior

choroidal artery, anterior cerebral artery (neonates>child), middle cerebral artery (neonates>>child), anterior choroidal arteries (neonates only), anterior thalamoperforate arteries, or branches of the middle meningeal arteries (Raybaud et al., 1989). Care must be taken to differentiate true VOGMs, which arise from the median prosencephalic vein, from AVMs that drain into a dilated but already formed vein of Galen, specifically named Vein of Galen Dilitations (VGAD) (Lasjaunias et al., 1987).

In the natural history of the disease, patients are phenotypically variable in their presentation. Significant cerebral damage or multiorgan damage are contraindications to pursuing intervention (de Koning et al., 1997; Rodesch et al., 1994; Swanstrom et al., 1994; Yuval et al., 1997). Patients who present in the neonatal period present high-output cardiac failure, which is fatal without intervention within days or weeks of birth (Amacher and Shillito, 1973; Hoffman et al., 1982; Johnston et al., 1987). Patients who fail medical management in the neonatal period undergo emergent endovascular embolization. Unlike in traditional AVMs, VOGM rarely present with hemorrhage (Suh et al., 2001). In a series of 34 patients, two with mural lesions and one with a choroidal lesion developed hemorrhage; with one presenting with subarachnoid hemorrhage at 19 hours of age, one with acute intraventricular hemorrhage at 5 months of age, and the third due to intra-operative complication causing intraventricular hemorrhage (Meyers et al., 2000). Another patient had a subdural hemorrhage and intracerebral hemorrhage as an unforeseen consequence to a shunting procedure (Suh et al., 2001). Other case series have also noted few hemorrhages (Halbach et al., 1998).

Patients who are medically managed or asymptomatic at birth, or those who do not receive definitive treatment can undergo continued, and unless acted upon, permanent, changes to the vascular and ventricular systems of the brain. Many patients experience hydrocephalus and a large retrospective series found hydrocephalus as the second most common presenting symptom, 46.8% of all patients with a greater preponderance in infants (73%) as compared to children, adults (30%), or neonates (15%) (Zerah et al., 1992). Similar percentages have been reported in other cases (17/22) (Amacher and Shillito, 1973). The development of hydrocephalus is likely due to the elevated pressure in the venous sinuses, preventing the normal reabsorption of CSF (Mickle et al., 1994; Zerah et al., 1992). However, some patients develop persistent venous insufficiency which has resulted in hydrocephalus, progressive atrophy, and parenchymal calcification in what has been termed "brain melting" by some (Brunelle, 1997; Lasjaunias, 1997). It has been postulated that attempts to manage the hydrocephalus accelerates parenchymal deterioration by reversing flow in the medullary veins from a cerebro-fugal direction to a cerebro-petal one, thus decreasing parenchymal perfusion and leading to parenchymal deterioration (Brunelle, 1997; Lasjaunias, 1997; Zerah et al., 1992). Other VOGM patients develop seizures (Hoffman et al., 1982), and VOGM presents in teenagers and adults as persistent headaches. There is one report of a VOGM rupturing in a 62-year-old woman (Tsai et al., 2015).

Since the report of the first patient with a VOGM in 1937, there have been several classification systems for VOGM patients based on their age and presenting features

(Amacher and Shillito, 1973; Gold et al., 1964) and a score for clinical management and whether or not intervention would have any merits (Lasjaunias et al., 2006).

Gold and colleagues created the first classification system with three groups: neonates with cardiac insufficiency, infants and young children with hydrocephalus and convulsions, and older children to adults with headaches and subarachnoid hemorrhage (Gold et al., 1964). Amacher and Shilito added a fourth category to the system and created more specific criteria (Amacher and Shillito, 1973). Group 1 presented at during the neonatal period with severe cardiac failure and cranial bruit, Group 2 was a mix of patients that presented in neonatal or infancy period with mild heart failure, craniomegaly within 1-6 month of birth, and cranial bruit (Amacher and Shillito, 1973). Group 3 presented in infancy (1-12 months of age) with craniomegaly and cranial bruit while Group 4 presented late (>3 years) with headache, exercise syncope, and calcified rim in pineal regions (Amacher and Shillito, 1973).

Lasjaunias published the experience at L' Hôpital Bicêtre with examining 317 and treating 223 VOGM patients from 1981 to 2002 (Lasjaunias, 2003), and later refined it into the Bicêtre score, a clinical scoring system to determine management particularly neonates (Lasjaunias et al., 2006). The max score of 21 is based on five categories: cardiac (5 points), cerebral (5 points), respiratory (5 points), hepatic (3 points), and renal (3 points) function, examining effectiveness of medications, seizures, required respiratory support, and urine output (Lasjaunias et al., 2006). The score helps guide neonatal and infant management such as the decision to forgo treatment in patients with severe brain or multiorgan damage

(score <8), and the need for emergent embolization in patients who fail medical management (Lasjaunias, 2003; Lasjaunias et al., 2006).

Diagnosis of VOGM

While many tests have been used to evaluate suspected VOGM in the past, including auscultation for cranial bruit, skull film, cardiac catheter, air contrast, and 99m TC scan angiogram was the most conclusive (**Fig. 1A,B**) (Amacher and Shillito, 1973). More recently, Magnetic resonance angiogram and CT angiogram (**Fig. 1C,D**) have been used to both diagnose and plan for embolization.

Early diagnosis is important for the management of the newborn with VOGM in case urgent endovascular therapy is needed. Pre-natal ultrasound can assist with early detection of VOGM to gather the appropriate resources for the management of the newborn. The 20-year experience of one center demonstrated that 40-50% of VOGM are diagnosed in utero (Lasjaunias, 2003). Other studies have shown similar numbers with 4/13 patients another series that were diagnosed prenatally (Jones et al., 2002). In utero MRI can also assist with classification of VOGM subtype and management decisions (**Fig. 1E,F**) (Breysem et al., 2003; Huisman et al., 2002). MRI and MRA of a mother pregnant with a VOGM fetus at 31weeks 4 days revealed severely dilated dural venous sinuses, intracranial veins, cerebral ventriculomegaly, periventricular white matter injury with hemorrhage, global cardiomegaly, fetal hydrops, and polyhydramnios (Wagner et al., 2015).

Occasionally, prenatally diagnosed patients require early delivery, whether it be due to fetal demise or for more effective cardiac evaluation and management (Doren et al., 1995; Yuval et al., 1997). In utero evidence of cardiac dysfunction is a poor prognosis (Yuval et al., 1997). Patients that are stable enough in the neonatal period, can undergo less invasive imaging techniques to plan for surgery at a later date.

Treatment and outcomes of VOGM

Treatment of VOGM was limited until the use of radiosurgery and endovascular therapy. Surgical clipping led to 100% mortality with minimal improvement to 80% with the advent of microsurgery (Khullar et al., 2010). During this period, most patients died post-operatively. It was not until radiosurgery, and more specifically embolization, that significantly improved survival. This was further improved by changing from a transveous (Casasco et al., 1991), to an arterial approach (Lasjaunias et al., 1991). One case series of 14 patients spanned the transition from clipping to endovascular techniques (Ciricillo et al., 1990). Ciricillo et al. treated five infants between 1978-1983 with craniotomy and clipping of feeding vessels, all of whom died perioperatively, while six of eight neonates who underwent endovascular intervention survived (Ciricillo et al., 1990).

Over time came improvements with experience, patient selection, medical management, timing of interventions, and institutional preparedness. At first, endovascular therapy was efficient for infants and children, however it still had a high rate of morbidity and mortality in the neonatal period with mortality ranging from 23-75% and morbidity 21-88% in

several series (Brunelle, 1997; Casasco et al., 1991; Lasjaunias et al., 1995; Lasjaunias et al., 1989; Lylyk et al., 1993).

Although embolization can be performed in the neonatal period when intensive cardiac management fails, it has better outcomes when delayed until at least 5 months of age (Lasjaunias, 2003). Embolization is also performed in cases where the patient deteriorates whether due to seizures, failure to thrive, worsening cardiac failure, or developmental delay (Bhattacharya and Thammaroj, 2003). The delay in first embolization allows the infant to grow to better tolerate surgery, vessels to increase in size, and for the cerebral vasculature to mature, thereby reducing the risk of adverse side effects of treatment. Additionally, complete occlusion of the shunt has led to poor outcomes as the immature cerebral vasculature does not tolerate the dramatic increase in blood volume and pressure after the shunt is closed (Jones et al., 2002). Using a series of 2-3 surgeries, the VOGM is closed, with the target of a 1/3 reduction of the shunt in the first procedure (Lasjaunias, 2003; Lasjaunias et al., 2006).

These improvements led to significant reductions in mortality with survival of 90% in the 216 cases that underwent embolization, with 74% of children neurologically normal, 15.6% with a mild-moderate deficit or delay, and 10.4% with significant delay or deficit (Lasjaunias, 2003). Other institutions have reported similar decreases in mortality with ~80% survival (Li et al., 2011; Mitchell et al., 2001). Morbidity has also improved alongside mortality. Most patients survive with little or no neurological impairment after

treatment with rates 66.7% (Li et al., 2011), 67% (Rodesch et al., 1994) and others (Mitchell et al., 2001) reporting similar rates.

Today neonates and infants remain disproportionately affected, with one third having no or little impairment, one third having moderate neurological impairment, and one third having severe, devastating neurological impairment or death (Khullar et al., 2010). Centralized care has become crucial as well to appropriate treatment. The implementation of a multidisciplinary team involving obstetrics, cardiology, neonatology, neurosurgery, and others, as well as appropriate diagnostic and therapeutic strategies, from prenatal detection to timing of the intervention, has also improved patient outcomes (Berenstein et al., 2012). The implementation of such a strategy at a single, high-volume center, has reduced neonatal mortality rate from 50% to 11% in less than 2 decades (Berenstein et al., 2012; Friedman et al., 1991).

The genetics of VOGM

Despite significant improvements in the clinical treatment of VOGM, the genetic and molecular etiology of VOGM is relatively unknown. The only genes associated with VOGM are in the context of other syndromes. There are seven *RASA1* (p120-RasGAP) mutations in the context of Capillary Malformation – Arteriovenous malformation (CM-AVM, OMIM#608354) (Heuchan et al., 2013; Revencu et al., 2008), and one activin A receptor type II-like 1 (*ACVRL1*) mutation (Chida et al., 2013) and one Endoglin (*ENG*) mutation(Tsutsumi et al., 2011) in the context of Hereditary Hemorrhagic Teleangiectasia

(HHT, OMIM #187300). A list of all mutations associated with VOGM prior to this work can be found in Table 1.

RASA1 encodes Ras GTPase-activating protein 1, which inhibits the activity of the RAS cyclic AMP pathway (Scheffzek et al., 1996; Trahey et al., 1988; Tsygankova et al., 2000) RASA1 is ubiquitously expressed with particularly high levels in the brain and other ectoderm-derived tissues (Mollat et al., 1994). Activation of RASA1 improves the GTPase activity of RAS, changing active RAS-GTP to inactive RAS-GDP. RAS1 plays a crucial role in the balance of RAS-GTP : RAS-GDP and an impaired RASA1 would lead to a persistent active, GTP bound RAS configuration and a constitutive RAS activation (Sung et al., 2016; Vigil et al., 2010).

Rasa1 knockout mice exhibit developmental arrest by E9.25 and death by E10.5 (Henkemeyer et al., 1995). Examination of the *Rasa1* knockout mice revealed aberrant yolk sac angioarchitecture, reduced caliber of the dorsal aorta, and sprouting of aberrant ventral dorsal aortic branches suggesting delayed primitive endothelial cell reorganization and eventual embryonic lethality (Henkemeyer et al., 1995). However, heterozygous *Rasa1* mice did not demonstrate any vascular phenotypes.

Mutations in RASA1 have been associated with CM-AVM (Boon et al., 2005; Revencu et al., 2008) which presents with phenotypic heterogeneity. Revencu and colleagues reported findings on 314 individuals across 132 kindreds with *RASA1* mutations and CM-AVM syndrome (Revencu et al., 2013). This work revealed that 97% of affected individuals

demonstrated cutaneous manifestations while only 23% presented with a non-cutaneous AVM, of which 42.6% occurred within the CNS and only 3 were true VOGMs (Revencu et al., 2013). Another group led by Heuchan (Heuchan et al., 2013), having noted the connection between VOGM and RASA1 mutations, sequenced *RASA1* in 11 individuals with VOGM. Four of the 11 carried mutations in *RASA1*. Eight different mutations in *RASA1* have been reported in associating with VOGM (**Table 1**).

Patients with HHT similarly have phenotypic variability, with some having teleangiectasias on the skin and mucosa, and AVMs in the lungs, liver, and CNS. One study revealed that only 3.7% of patients with HHT demonstrate a CNS vascular lesion with only Dural AV fistulas, cavernous malformations, and parenchymal AVMs described in the cohort of 321 patients (Maher et al., 2001). The two genes most commonly associated with HHT are *ENG* and *ACVRL1* (*ALK1*) which have been associated with HHT types 1 (OMIM no. 187300) and 2 (OMIM no. 600376), respectively (Abdalla et al., 2000; Bayrak-Toydemir et al., 2006; McAllister et al., 1994). There are several cases of VOGMs in patients with diagnosed HHT or with a positive family history (Revencu et al., 2013; Tsutsumi et al., 2011). One report by Tsutsumi and colleagues (Tsutsumi et al., 2011) demonstrated that a mother with clinical HHT gave birth to a child with a choroidal VOGM with a mutation identified in the *ENG* gene (p.Gln558fs). Another report revealed a patient with subarachnoid hemorrhage secondary to VOGM underlain by a mutation in ACVRL1 (p.Arg218Trp) which was also carried by the sister and mother (Chida et al., 2013). However, it is unclear if this was a true VOGM or a VGAD due to the lack of imaging.

Functional expression

With the use of whole exome sequencing, and the increasing prevalence of whole genome sequencing, more and more data are generated in the search of causes for genetic disease. Despite technological advances, sequencing itself does not result in a clear genetic diagnosis or causal gene (Neveling et al., 2013). Even when large cohorts allow for whole exome-wide significant findings, studies must be made to investigate mechanism of action to reveal possible avenues of intervention. The need for validation will only increase as whole exome sequencing becomes more common place with new initiatives such as the NIH's Newborn Sequencing in Genomic Medicine and Public Health.

To this end, we have elected to use *Xenopus tropicalis*, an established model for genetics research, to screen candidate genes. Unlike *Danio rerio* (zebrafish) or *Xenopus laevis*, *X. tropicalis* is diploid, which makes it well suited for loss of function studies via gene depletion. *Xenopus* is closer to *Homo sapiens* compared to zebrafish (Ureta-Vidal et al., 2003). *Xenopus* is the closest vertebrate model to humans that has the advantages of speed and lower cost compared to zebrafish and mouse. *X. tropicalis* grow quickly and reach sexual maturity faster than *X. laevis* (Hirsch et al., 2002) and live and reproduce for more than a decade when cared for properly (Tinsley and Kobel, 1996). Both *Xenopus tropicalis* and *Xenopus laevis* lay thousands of embryos that can easily be manipulated with microinjection with mRNA for gain of function studies, or with morpholino or CRISPR/Cas9 for loss of function studies.

Recent work has shown that F0 CRISPR/Cas9 is highly efficient and can cause biallelic gene modification in as little as two hours after injection and well before the onset of zygotic gene expression, with subsequent phenotype detection within 3 days at $35 cost (Bhattacharya et al., 2015). CRISPR/Cas9 has been shown to be more specific and to have fewer off-target effects than morpholinos (Gentsch et al., 2018).

Xenopus makes an ideal system for the study of the developing vasculature. Embryos develop externally and are transparent allowing direct visualization of the heart and tail vessels. Previous studies have generated a fate map of future vasculature of a 32-cell embryo (Mills et al., 1999), which allows directed targeting of specific vasculature. Additionally, much work has gone into the development of the heart, dorsal aorta, intersegmental vessels, including the signaling between endothelial cells, hematopoietic cells, and surround tissues have been extensively studied. The available tools for *Xenopus* have increased over time including in-situ markers, direct visualization, and transgenic animals.

The APJ receptor, also known as *msr,* is a *in situ* hybridization marker both for vasculogenesis (development of the heart, posterior cardinal veins, dorsal aorta, viteline vein network), as well as for angiogenesis of the intersegmental vessels and tail veins (Cox et al., 2006; Devic et al., 1996). *Msr* has been the marker of choice in assessing the effect of drugs on vascular development (Cha et al., 2012; Kalin et al., 2009). *Xenopus* embryos are transparent, which allows direct visualization of blood vessels, especially in the tail which is thin; however, direct visualization remains difficult in other regions and organs

particularly in the brain. The creation of *Xflk-1*:GFP transgenic *X. laevis* (Doherty et al., 2007) with *flk1* being a marker on endothelial cells, and its replication in *X. tropicalis*, has allowed direct visualization not only of patent vessels but the stages of angiogenesis from endothelial cell migration and sprouting to lumenization. This has greatly improved the ability to perform live imaging and study vasculogenesis and angiogenesis *in vivo*.

In summary, VOGM will likely become an even more common manifestation of vascular disease due to the growing population of successfully treated patients. Patients and their families will continue to ask the questions "Why did I (or my family member) have a Vein of Galen Malformation?" and "How will this impact my own children in the future?" These questions must be met, not only for VOGM patients and their families, but for the potential insights into other AVMs and novel therapeutic targets. Whole exome sequencing lends itself to an unbiased approach of gene discovery. Any potential genetic findings will require functional testing to elucidate the mechanism of this disease.

Figure 1. Representative images of VOGMs.
Lateral representative projections of digital subtraction angiography vertebral artery contrast injections depicting choroidal VOGM **(A)** and mural VOGM **(B)**. 3-T time-of-flight MR angiography 3D renderings depicting choroidal VOGM **(C)** and mural VOGM **(D)**. Fetal T2-weighted MR images depicting a dilated vein of Markowski in a patient with VOGM, axial projection **(E)** and sagittal projection **(F)**.

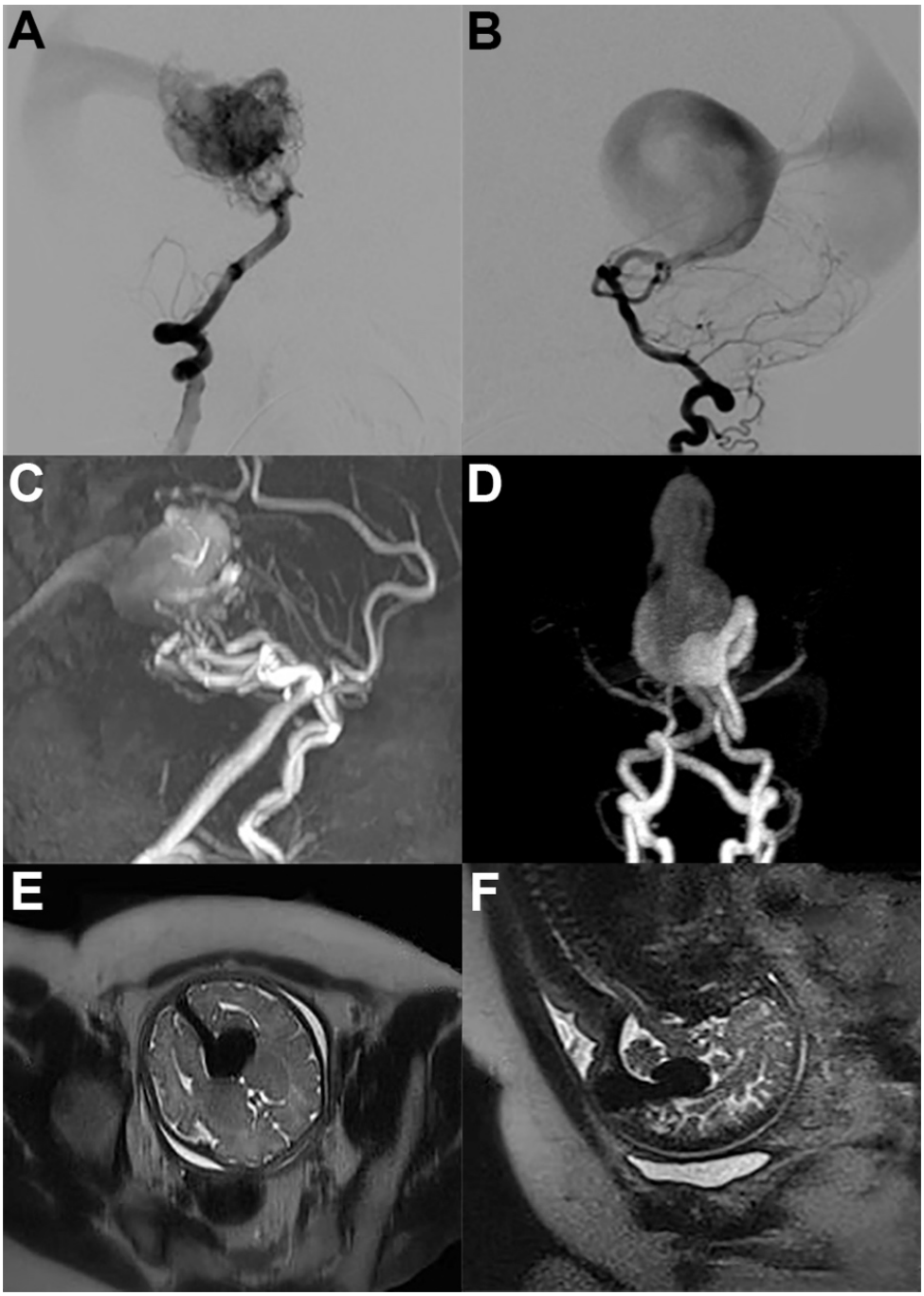

Table 1. VOGM-associated genetic variants

No.	Gene	Coding variant	Exon	Type of mutation	Protein variant	Year of publication	Source
1	*RASA1*	c.2977del	24	frameshift deletion	p.Arg993Valfs	2013	Revencu et al
2	*RASA1*	c.2125C>T†	16	stop gain	p.Arg709*	2013	Revencu et al, Heuchan et al
3	*RASA1*	c.3024del	24	frameshift deletion	p.Glu1008Aspfs	2013	Revencu et al
4	*RASA1*	c.2288A>T	17	missense	p.Glu763Val	2008	Revencu et al
5	*RASA1*	c.2532_2536del	19	frameshift deletion	p.Leu845Thrfs	2008	Revencu et al
6	*RASA1*	c.2119C>T	16	missense	p.Arg707Cys	2013	Heuchan et al
7	*RASA1*	c.2912T>C	23	missense	p.Leu971Ser	2013	Heuchan et al
8	*RASA1*	c.1678G>T	12	stop gain	p.Glu560*	2013	Chida et al
9	*ACVRL1*‡	c.652C>T	6	missense	p.Arg218Trp	2013	Chida et al
10	*ENG*	c.1672_1684del	12	frameshift deletion	p.Gln558fs	2011	Tsutsumi et al

† Reported separately by two publications

‡ Although the case in this report is presented as a true VOGM, imaging in this report does not demonstrate clear fistulas to the vein of Markowski

V. Statement of Purpose

The Vein of Galen Malformation (VOGM) is a specific type of arteriovenous malformation (AVM) that starts in embryonic development weeks 6-11 (Raybaud et al., 1989). Patients have variable clinical presentations from devastating congestive heart failure at birth to headaches in young adults (Amacher and Shillito, 1973). The advent of endovascular treatment greatly decreased mortality from 100-80% down to 15% (Khullar et al., 2010). However, the multiple staged endovascular surgeries and follow up are costly and the lack of understanding of the genetic and molecular etiology of VOGM hinder the development of novel therapies that may prevent VOGM or at the very least the more devastating neonatal presentations. Only 10 mutations distributed amongst three genes have been associated with VOGM. There are seven *RASA1* (p120-RasGAP) mutations in the context of Capillary Malformation – Arteriovenous malformation (CM-AVM, OMIM#608354) (Heuchan et al., 2013; Revencu et al., 2008), and one activin A receptor type II-like 1 (*ACVRL1*) mutation (Chida et al., 2013) and one Endoglin (*ENG*) mutation (Tsutsumi et al., 2011) in the context of Hereditary Hemorrhagic Teleangiectasia (HHT, OMIM #187300). Uncovering the genetics of VOGM would provide a better understanding of VOGM, AVMs, and neurovascular development. The overall aim of this project is to investigate the developmental regulation of vasculogenesis and angiogenesis with regards to arteriovenous malformations. In order to accomplish this goal, we propose the following aims:

Specific Aim 1: Establishing a large and precisely phenotyped VOGM patient cohort

In this aim we will establish a VOGM patient cohort with an innovative and collaborative social media recruitment platform. Probands that satisfy our inclusion criteria,

demonstrate: 1) a true VOGM, with an ectatic fistula feeding into the median prosencephalic vein and not a VGAD; 2) the availability of both biological parents to contribute DNA; are actively recruited from Yale School of Medicine and our collaborating institutions (Boston Children's Hospital, USA). We will also employ a social media recruitment strategy utilizing Facebook, approved by the Yale University IRB/HIC (Kristopher Kahle, PI; HIC/HSC Protocol#: 1602017144), which allows us to efficiently identify and rapidly obtain DNA from VOGM patients around the world using mailed consent forms and buccal swab kits. This process has been employed both by our group and others to significant effect in studying genetic disease (Furey et al., 2018; Timberlake et al., 2016). We place emphasis on collecting DNA from all nuclear family members due our hypothesis of phenotypic variability. For each index case, we obtain full medical records, prior clinical genetic testing, and importantly, any full brain CT-angiogram, MR-angiogram, traditional angiogram, and neuroradiology reports.

Specific Aim 2: Identification of novel VOGM-causing genes using whole exome capture and massively parallel DNA sequencing. In this aim we will utilize WES and bioinformatics to identify novel VOGM-causing mutations. All trios are sequenced at the Yale Center for Genomic Analysis (YCGA). Resulting sequence is analyzed with computational pipelines that enable the rapid identification of rare/novel/*de novo* variants which are predicted to alter the function of the encoded protein, are specific for the disease, and are not detected in published and internal reference SNV sequence databases of unaffected patients (Furey et al., 2018). Assuming that there are single loci which account for VOGM, we predict that we will detect several novel VOGM genes which we predict

will cluster in pathways related to arterio-venous specification ((Fish and Wythe, 2015)), the axon guidance and neuro-vascular development pathways (Klagsbrun and Eichmann, 2005), or in pathways related to *RASA1*, *ENG*, and *ACVRL1*. We anticipate it will be possible to identify multiple independent mutations in the same genes or genetic pathways in different individuals with similar phenotypes.

Specific Aim 3. Functional assessment of discovered VOGM genes using CRISPR gene editing in *Xenopus tropicalis*. In this aim, we plan to develop a novel method of functionally validating candidate mutations that utilizes CRISPR gene editing in *Xenopus tropicalis* coupled with in situ hybridization, quantitative Optical Coherence Tomography (qOCT), and confocal imaging of the brain to assess the functional impact of discovered VOGM-causing mutations *in vivo*. To do this, we will employ F0 CRISPR gene editing in *Xenopus tropicalis*, a rapid, diploid amphibian system (Bhattacharya et al., 2015), to examine vasculogenesis, angiogenesis, and brain vasculature. F0 CRISPR/Cas9 is highly efficient and can cause biallelic gene modification in as little as two hours after injection and well before the onset of zygotic gene expression, with subsequent phenotype detection within 3 days at $35 cost (Bhattacharya et al., 2015). To phenotype embryos, we will employ in situ hybridization of vessel marker msr at the time of vasculogenesis and early angiogenesis (Devic et al., 1996), and examine the brain vasculature *in vivo* using transgenic *Xflk1:GFP* ((Doherty et al., 2007) to examine the vasculature throughout the animal as well as in the brain at the evolutionary precursor of the median prosencephalic vein. This work will help establish *Xenopus* as a means of studying brain vasculature, will

provide insight into the mechanism of VOGM and guide future investigations and mechanisms for therapeutic strategies.

VI. Mutations in chromatin modifier and Ephrin signaling genes in Vein of Galen Malformation

VI. Mutations in chromatin modifier and Ephrin signaling genes in Vein of Galen Malformation

Please note, the work presented here has been published as:

Duran, D., Zeng, X., Jin, S.C., Choi, J., Nelson-Williams, C., Yatsula, B., ***Gaillard, J.,*** *Furey, C.G., Lu, Q., Timberlake, A.T., Mansuri, M.S., Sorscher, M.A., Loring, E., Klein, J., Lu, Q., Montejo, J.D., Vera, A., Hu, J.K., Allocco, A., Karimy, J.K., Panchagnula, S., Youngblood, M.W., Zhang, J., DiLuna, M.L., Matouk, C.C., Mane, S., Tikhonova, I., Castaldi, C., López-Giráldez, F., Knight, J., Haider, S., Alper, S.L., Komiyama, M., Ducruet, A.F., Zabramski, J.M., Dardik, A., Walcott, B.P., Stapleton, C.J., Aagaard-Kienitz, B., Rodesch, G., Jackson, E., Smith, E.R., Orbach, D.B., Berenstein, A., Bilguvar, K., Vikkula, M., Gunel, M., Lifton, R.P., Kahle, K.T.* ***Mutations in Chromatin Modifier and Ephrin Signaling Genes in Vein of Galen Malformation. Neuron..*** *2019. 101(3):429-443.e4*

It is reproduced here with permission and many thanks to Elsevier.

INTRODUCTION

Embryogenesis requires vascular development to meet hemodynamic and nutritive demands. Arterio-venous (A-V) specification in model organisms is genetically-determined and results in the differential expression of genes in arteries and veins prior to establishment of circulation (Fish and Wythe, 2015). For example, during development Ephrin-B2 and its receptor Eph-B4 are exclusively expressed in arteries or veins, respectively (Adams et al., 1999; Gerety et al., 1999; Wang et al., 1998). Murine deletion of *Efnb2* or *EphB4* impairs A-V specification and causes arterio-venous malformations (AVMs), high-flow vascular lesions characterized by direct connections of arteries to veins without intervening capillaries. A-V specification requires orchestrated activity of multiple

signaling cascades (e.g., Eph-Ephrin, Hedgehog, VEGF, TGF-beta, and Notch) and transcriptional networks (e.g., HEY and HES, SOX factors, and COUP-TFII) (Fish and Wythe, 2015). Nonetheless, the genetic determinants of A-V specification in humans remain incompletely understood.

During normal brain development, primitive choroidal and subependymal arteries that perfuse deep brain structures are connected via an intervening capillary network to the embryonic precursor of the Vein of Galen (i.e., the median prosencephalic vein of Markowski [MPV]). The MPV returns deep cerebral venous blood to dural sinuses that drain into the internal jugular veins (Raybaud et al., 1989). Vein of Galen malformations (VOGMs), the most common and severe neontal brain AVMs (Deloison et al., 2012; Long et al., 1974), directly connect primitive choroidal or subependymal cerebral arteries to the MPV, exposing it to dangerously high blood flow and pressures that can result in high-output cardiac failure, hydrocephalus, and/or brain hemorrhage (Recinos et al., 2012). VOGMs are also often associated neurodevelopmental delay and congenital heart defects (CHDs) (McElhinney et al., 1998). While endovascular partial obliteration of anomalous A-V connections has improved VOGM outcomes (Altschul et al., 2014; Mitchell et al., 2001), many VOGMs remain refractory to intervention, which are also are inaccessible to many patients.

Limited knowledge of the molecular pathophysiology of VOGMs has hindered development of early diagnostic and targeted therapeutic strategies. Considered isolated, sporadic congenital lesions, rare VOGMs have been associated with Mendelian disorders,

including 8 cases of autosomal dominant (AD) capillary malformation-arteriovenous malformation (CM-AVM) syndrome type 1 (CM-AVM1) caused by *RASA1* mutation (OMIM# 608354) (Duran et al., 2018a; Revencu et al., 2013); 2 cases of AD CM-AVM syndrome type 2 (CM-AVM2) caused by *EPHB4* mutation (Amyere et al., 2017), and single cases of AD Hereditary Hemorrhagic Telangiectasia (HHT) type 1 (HHT1) due to *ENG* mutation (OMIM# 187300) (Tsutsumi et al., 2011) and AD HHT type 2 (HHT2) caused by *ACVRL1* mutation (OMIM# 600376; 1 case) (Chida et al., 2013).

Traditional genetic approaches have been limited in their ability to identify additional causative genes for VOGM because cases are rare and most often sporadic (Xu et al., 2010). This limitation motivates application of whole-exome sequencing (WES) to large numbers of affected subjects and their families, searching for genes mutated in probands more often than expected by chance. This unbiased approach has aided the study of other genetically heterogeneous neurodevelopmental disorders (de Ligt et al., 2012; Epi et al., 2013; Iossifov et al., 2014; Iossifov et al., 2012; Krumm et al., 2015; Neale et al., 2012; O'Roak et al., 2011; O'Roak et al., 2012; Rauch et al., 2012; Sanders et al., 2012; Timberlake et al., 2016; Timberlake et al., 2017; Vissers et al., 2010; Willsey et al., 2017), including those associated with brain malformations (Barak et al., 2011; Bilguvar et al., 2010; Mishra-Gorur et al., 2014; Nikolaev et al., 2018), CHDs (Homsy et al., 2015; Jin et al., 2017; Zaidi et al., 2013), and congenital hydrocephalus (Furey et al., 2018). We hypothesized that VOGMs might arise from damaging *de novo* mutation events or incomplete penetrance of rare transmitted variants.

RESULTS

VOGM cohort characteristics and whole exome sequencing

We recruited 55 probands with radiographically confirmed VOGMs (see **STAR Methods**) treated by endovascular therapy, including 52 parent-offspring trios with a single affected offspring and 3 singleton cases. 62% of probands were diagnosed prenatally or within one month after birth; only one was diagnosed after age 2. Common features at diagnosis included high output cardiac failure (62%), macrocephaly (64%), hydrocephalus (60%), and prominent face/scalp vasculature (49%). Among the CHDs found in 9% were partial anomalous pulmonary venous return, patent ductus arteriosus, and pulmonary valve stenosis. **Supplementary Table 1** summarizes cohort demographics, clinical features, and radiographic classification, including angio-architectural subgroups (Lasjaunias et al., 2006). 37 of the 55 patients in our cohort presented with "choroidal" type lesions, defined as VOGMs with numerous feeder vessels and "pseudoniduses" that communicate with the MPV (Lasjaunias et al., 2006). The remaining 18 probands presented with "mural" VOGMs, characterized by fewer vessels of larger caliber that fistulize into the MPV (Lasjaunias et al., 2006). See **Supplementary Figure 1 for** representative VOGM images.

DNA was isolated and WES performed as described (Timberlake et al., 2016). WES from 1,789 control trios comprising parents and unaffected siblings of autism probands were analyzed (Fischbach and Lord, 2010; Krumm et al., 2015) by our in-house informatics pipeline. In both cases and controls, ≥ 94.6% of targeted bases had ≥ 8 independent reads and ≥ 89.8% had ≥ 15 independent reads. (See **Supplementary Table 2** for exome

metrics). Variant calling was by Genome Analysis Toolkit (GATK) HaplotypeCaller (McKenna et al., 2010; Van der Auwera et al., 2013), and allele frequency annotation by the Exome Aggregation Consortium (ExAC) and the Genome Aggregation Database (gnomAD) (Lek et al., 2016) (see **STAR Methods**). *De novo* mutation identification was by TrioDeNovo (Wei et al., 2015). MetaSVM was used to infer the impact of missense mutations (Dong et al., 2015). Missense variants were considered damaging if predicted deleterious by MetaSVM (D-mis). Inferred loss-of-function (LoF) mutations, including stop-gains, stop-losses, frameshift insertions/deletions, and canonical splice site mutations were also considered damaging. Mutations in genes of interest were validated by PCR amplification and Sanger sequencing (**Supplementary Figure 2**).

Enrichment in damaging *de novo* mutations in VOGM probands

The *de novo* mutation rate in probands was 1.56×10^{-8} per base pair, with 1.21 *de novo* coding region mutations per proband (**Supplementary Table 3**), consistent with expectation and prior results (Homsy et al., 2015; Timberlake et al., 2017; Ware et al., 2015). Total *de novo* mutation burden in controls was also as previously reported (Timberlake et al., 2017). The distribution of types of *de novo* coding mutations in probands was compared to that expected from the probability of mutation of each base in the coding region and flanking splice sites (Samocha et al., 2014). While synonymous mutations and inferred tolerated missense (T-mis) mutations in probands were not significantly enriched, *de novo* D-mis mutations in probands were marginally enriched ($P = 0.01$; enrichment = 2.05-fold; **Supplementary Table 3**). In contrast, control subjects displayed no enrichment in any class of coding region mutation **(Supplementary Table**

3). The observed excess of damaging *de novo* mutations in probands over that expected predicts these mutations contribute to ~13% of VOGM cases.

One gene, *KEL*, exhibited more than one protein-altering *de novo* mutation (**Figure 1**). Among the 52 trios analyzed, we observed a near-significant enrichment of protein-altering *de novo* mutations in *KEL* (one-tailed *Poisson* test $P = 4.2 \times 10^{-6}$; Benjamini-Hochberg false discovery rate [BH-FDR] = *0.08*). One of these mutations caused premature termination (p.Gln321*) and the other was a missense mutation p.Gly202Ser (CADD = 22.6), both impacting the KELL polypeptide's peptidase domain (**Figure 1**).

We analyzed the burden of *de novo* mutations in genes highly intolerant to heterozygous LoF mutation (LoF-intolerant genes; pLI ≥ 0.9) (Lek et al., 2016), consistent with loss of one gene copy markedly impairing reproductive fitness. *de novo* D-mis mutations were marginally enriched (6 mutations; *P = 0.02*; enrichment = 2.82-fold; **Table 1)**, of which four (3 D-mis and the only LoF mutation) occurred in genes encoding chromatin modifiers (*KMT2D*, *SMARCA2*, *SIRT1*, and *KAT6A*) (**Figure 2**). The 547 genes in the chromatin modifier gene ontology term GO:0016569 include 272 LoF-intolerant chromatin modifier genes; mutations in this set are enriched ($P = 8.9 \times 10^{-4}$; enrichment = 9.63-fold; **Table 1**), but *de novo* mutations in the LoF-intolerant chromatin modifier gene set were not enriched in controls (**Table 1)**. A case-control analysis using the two-tailed binomial exact test (Sanders et al., 2012; Willsey et al., 2017) further supported this result (**Supplementary Table 4**). In an orthogonal analysis of all genes using the permutation-based test (1 million iterations), the probability of finding 4 or more damaging *de novo* mutations in LoF-

intolerant chromatin modifiers among a total of only 19 damaging *de novo* mutations in all genes was also low (empirical $P = 3.5 \times 10^{-3}$; expected number = 0.66; see **STAR Methods**). Damaging *de novo* mutations in chromatin modifiers were thus identified in ~7% of all VOGM probands (**Supplementary Table 5**). Missense mutations occur in key functional domains of the encoded proteins at positions conserved through worm (*KAT6A* and *KMT2D*) and yeast (*SMARCA2*) (**Figure 2, panel C; Supplementary Table 5**). Clinical characteristics of probands harboring these mutations are shown in **Figure 2** and **Supplementary Table 5**.

Enrichment of rare damaging transmitted mutations in *EPHB4*

We next assessed the total burden in all probands of rare (minor allele frequency [MAF] ≤ 2×10^{-5}) *de novo* and transmitted D-mis and LoF mutations in LoF-intolerant genes (see **STAR Methods)**. The probability of the observed number of rare variants in each gene occurring by chance was calculated by comparing observed to the expected burden, adjusting for gene lengths (Besse et al., 2017). Analysis of damaging variants in LoF-intolerant genes revealed genome-wide significant enrichment (Bonferroni multiple testing threshold = 2.63×10^{-6}) of mutations only in *EPHB4* (pLI = 0.99), with one LoF and three independent D-mis mutations (one-tailed binomial $P = 7.47 \times 10^{-10}$; BH-FDR = 2.40×10^{-6}; enrichment = 341.13-fold; **Figure 3, panel A; Table 2**).

Independent case-control gene burden analyses for damaging variants in all probands versus a cohort of 3,578 autism parental and ExAC controls showed a significant mutation burden in *EPHB4* vs. autism parental controls (one-tailed Fisher's $P = 1.68 \times 10^{-6}$, odds

ratio = 89.97, 95% CI [19.29, Inf]) and vs. ExAC controls (one-tailed Fisher's $P = 1.98 \times 10^{-6}$, odds ratio = 49.76, 95% CI [16.39, Inf]); **Supplementary Table 6**). The Bonferroni-corrected threshold for the 3,230 LoF-intolerant genes, 1.55×10^{-5}, was also surpassed by the *CAD* gene (one-tailed binomial $P = 4.17 \times 10^{-6}$; BH-FDR = 0.01; enrichment = 101.08-fold).

All *EPHB4* mutations were transmitted; three of these have allele frequencies of zero in ExAC and gnomAD, while one has a MAF of 1.13×10^{-5} in gnomAD. All D-mis mutations in *EPHB4* alter highly conserved amino acid residues (**Figure 4, panel C; Table 2**). Mutations p.Lys650Asn and p.Phe867Leu lie in the tyrosine kinase domain of the vein-specific (Gerety et al., 1999) Eph-B4 receptor. p.Ala509Gly lies in one of two EphB4 extracellular fibronectin III domains believed to bind extracellular matrix (**Figure 4, panel C**).

7 additional family members without diagnosed VOGM in these kindreds carried the same mutations. However, three *EPHB4* mutation carriers exhibited uncommon cutaneous vascular lesions. Thus in kindred VGAM-115, the mutation-carrying father had an abdominal port wine stain, and the proband's mutation carrier sibling had atypical left cheek and posterior thigh capillary malformations (**Supplementary figure 3, panels A & B**). Similarly, the mutation-carrying mother in kindred KVGAM-33 had an atypical capillary malformation on her left arm, while the proband's mutation carrier sibling had an atrial septal defect (**Figure 4, panel B**). Vascular and cardiac abnormalities were absent among non-mutation carriers in these families. All VOGMs associated with *EPHB4*

mutations were of the choroidal subtype (**Figure 4, panels A & B**). Together, these findings provide evidence of incomplete penetrance and variable expressivity of *EPHB4* mutations. Interestingly, 2 of 54 CM-AVM2 patients with *EPHB4* mutations also had VOGM (Amyere et al., 2017).

Wild type and VOGM-mutant Eph-B4 (p.Ala509Gly; p.Lys650Asn; p.Phe867Leu) were expressed in mammalian cells (see **STAR Methods**), and levels of Eph-B4 tyrosine (Tyr)-phosphorylation, an index of tyrosine kinase activity (Ferguson et al., 2015; Lisabeth et al., 2013), were compared. Eph-B4 kinase domain mutants p.Lys650Asn and p.Phe867Leu showed reduced or absent phosphorylation, respectively (**Figure 4, panel D**). In contrast, the extracellular fibronectin III domain mutant p.Ala509Gly showed unchanged phosphorylation.

Eph-B4 Tyr phosphorylation creates docking sites for signaling molecules via a phosphotyrosine-SH2 domain interaction, facilitating Eph-B4 downstream signaling (Pawson and Scott, 1997; Wang et al., 2002). *RASA1*-encoded Ras GTPase-activating protein 1 (Ras-GAP) binds to these docking sites and regulates downstream signaling pathways (Kawasaki et al., 2014; Roth Flach et al., 2016). We immunoprecipitated wild type or VOGM-mutant Eph-B4 from mammalian cells co-expressing Ras-GAP. Ras-GAP co-immunoprecipation with *EPHB4* mutant p.Lys650Asn was reduced, and Ras-GAP failed to bind Eph-B4 mutant p.Phe867Leu (**Figure 4, panel E**). In contrast, wild type Eph-B4 and Eph-B4 p.Ala509Gly bound Ras-GAP with similar affinity. These results are consistent with the cytoplasmic mutations impairing receptor kinase activity. The

extracellular mutation alters the fibronectin domains, likely to affect signaling by altering binding to extracellular matrix ligands (a hypothesis not yet tested).

Recurrent rare damaging transmitted mutations in *CLDN14*

Expansion of the analysis to include the burden of rare (MAF $\leq 2 \times 10^{-5}$) D-mis and LoF mutations in *all* genes identified one additional gene, *CLDN14,* with genome-wide significant damaging mutation burden (one-tailed binomial $P = 6.44 \times 10^{-7}$; BH-FDR = 0.01; enrichment = 190-fold; **Figure 3, panel B; Table 2**). Comparing *CLDN14* mutation burden by case-control analysis against both autism parental controls (odds ratio = Inf, 95% CI [38.42, Inf]; one-tailed Fisher's $P = 3.38 \times 10^{-6}$; **Supplementary Table 6a**) and ExAC controls, odds ratio = 67.82, 95% CI [17.66, Inf]; one-tailed Fisher's $P = 1.65 \times 10^{-5}$; **Supplementary Table 6b**) supported the significance of this finding. The three rare damaging *CLDN14* mutations were all heterozygous transmitted missense mutations (5.5% of probands; **Figure 5**). Two are identical (p.Val143Met) and present in unrelated VOGM probands, with MAF of *0* in Non-Finnish Europeans in ExAC. Beagle v3.3.2 kinship analysis (Browning and Browning, 2011; Stuart et al., 2015) and trio analysis using 139 phased genotypes flanking the mutation revealed that p.Val143Met variant lies on a segment shared identically by-descent from a common ancestor by the two probands, with a minimum shared segment of 0.34 Mb. Nonetheless, these probands shared no other rare variants, indicating that they do not share a recent common ancestor. The other rare damaging variant, p.Ala113Pro, is absent in ExAC, with MAF 8.28×10^{-6} in gnomAD.

CLDN14 encodes Claudin-14, a tight junction protein expressed in epithelia and endothelial cells of brain and kidney (Kniesel and Wolburg, 2000; Wattenhofer et al., 2005). Claudin extracellular loops make homo- or heterotypic interactions with adjacent cells to form the tight junction barrier (Van Itallie and Anderson, 2013). p.Val143Met alters a highly conserved residue in the second extracellular loop of Claudin-14, and is predicted to be deleterious by MetaSVM, CADD, Polyphen2, and SIFT. p.Ala113Pro lies in the second intracellular loop of Claudin-14(**Figure 5, panel C; Supplementary Figure 4**).

Interestingly, in one of the families (KVGAM20) harboring the recurrent Claudin-14 mutation p.Val143Met, cutaneous vascular lesions segregated with the mutation among family members. The mother who transmitted the mutation had a port wine stain on her left thigh, while her children (proband and carrier sibling) had similar atypical capillary malformations in the nuchal area. This VOGM proband also had a midline atypical capillary malformation on her lower back (**Supplementary Figure 3, panels G-J**).

Enrichment of mutations in genes in the Ephrin signaling pathway

To search for pathways enriched for rare damaging mutations in VOGM, LoF-intolerant genes harboring damaging *de novo* and/or rare (MAF $\leq 2 \times 10^{-5}$) damaging transmitted mutations, along with *KEL* and *CLDN14*, were input into Ingenuity Pathway Analysis (IPA; May 2018 version; total 128 input genes) (Kramer et al., 2014). Axonal guidance signaling, essential for vascular patterning and regulated by Ephrin-Eph receptor signaling (Adams and Eichmann, 2010), was the most significantly enriched canonical pathway ($P = 6.61 \times 10^{-8}$; BH-FDR = 1.33×10^{-5}), including Ephrin receptor signaling pathway genes

(also significant). Nine additional IPA pathways were significant after B-H correction (**Supplementary Table 7**). Because IPA does not adjust for gene length, we tested each of these pathways in the case-control analysis (see **STAR Methods**) using ethnicity-matched autism parents and ExAC controls. Axonal guidance and Ephrin receptor signaling pathways showed significant enrichment in cases (**Supplementary Tables 8**).

We further analyzed mutation burden in genes in these two pathways by binomial test, comparing observed to expected values as corrected for gene size (see **STAR Methods**). Significant enrichment in both axonal guidance and Ephrin receptor signaling pathways was observed in cases, whereas analyses of synonymous variants in cases as well as rare damaging variants in autism parents and ExAC controls showed no significant enrichment (**Supplementary Tables 9**). Lastly, we found that most of the signal in the axonal guidance pathway was attributable to the Ephrin receptor signaling pathway because, after removal from analysis of the latter genes, the axonal guidance pathway was no longer significantly enriched (**Supplementary Table 10**). Detailed variant information of damaging mutations in genes that contributed to the significant result is described in **Supplementary Table 11**.

Of note, *EFNB2* (pLI = 0.94), encoding the Eph-B4 ligand Ephrin-B2, harbored the rare D-mis mutation p.Arg277His in a neonate with a choroidal VOGM (**Supplementary Figure 5**). *EFNB2* is represented in the IPA axonal guidance and Ephrin receptor signaling gene sets, but this specific *EFNB2* variant was not included as input in our pathway analysis because its MAF slightly exceeded our threshold of 2×10^{-5} (MAF of 1.88×10^{-5} and 2.89×10^{-5} in ExAC and gnomAD, respectively). The proband's *EFNB2* mutation-carrying

mother, while not having VOGM, exhibited multiple atypical nuchal capillary malformations. Of note, *Ephrin-b2* knockout mice phenocopy *eph-b4* knockout mice, exhibiting CNS and systemic AVMs, defects in cerebral angiogenesis, and embryonic lethality (Wang et al., 2010b).

Rare damaging mutations in genes implicated in Mendelian AVM syndromes

VOGM is a rare feature in patients with CM-AVM types 1 and 2 due to mutation in RASA1 (Duran et al., 2018a; Revencu et al., 2013) and *EPHB4* (Amyere et al., 2017), respectively. VOGM has also previously been associated with single cases of Hereditary Hemorrhagic Telangiectasia (HHT) type 1 due to *ENG* mutation (Tsutsumi et al., 2011) and HHT type 2 due to *ACVRL1* mutation (OMIM# 600376) (Chida et al., 2013).

Our VOGM cohort included no *ENG* mutations. We found one damaging mutation in *RASA1* (p.Arg709*, **Supplementary Table 11**), encoding the Eph-B4 binding partner and effector Ras GTPase-activating protein 1 (Ras-GAP) (Kawasaki et al., 2014), in a patient with a mural VOGM. This patient and mutation has been previously reported (Revencu et al., 2013)and was independently ascertained in the present study.

A single patient with a choroidal VOGM had a damaging p.Arg484Gln mutation in *ACVRL1* (**Supplementary Table 12**), encoding ALK1, a receptor kinase in the TGF-β signaling pathway highly expressed in developing human vasculature (Zhang et al., 2017). This mutation altering a conserved residue in the ALK1 kinase domain was reported in HHT2 with isolated pulmonary hypertension (ClinVar accession RCV000198604.1;

rs863223408) (Harrison et al., 2005). However, neither the *ACVRL1*-mutant VOGM proband nor family members carrying the mutation exhibited HHT-associated findings (e.g., epistaxis or telangiectasia) or other vascular abnormalities. *ACVRL1* (ALK1) is a known regulator of Ephrin-B2-Eph-B4 signaling (Kim et al., 2012; Roman and Hinck, 2017; Zhang, 2009), and *acvrl1* deficient mice exhibit markedly enlarged cerebral vessels with arteriovenous shunting and altered Eph-B4 expression (Walker et al., 2011).

Unrelated probands with mural VOGMs carried two rare damaging mutations (p.Gly39Ser and p.Asn373Ser) in the *ACVRL1* paralog, *ACVR1* (pLI = 0.96); **Supplementary Table 12; Supplementary Figure 6, panels A & B**), a gene not previously implicated in VOGM. The *ACVR1* p.Asn373Ser VOGM proband also had an atrial septal defect and partial anomalous pulmonary venous return (**Supplementary Figure 6, panel B**), and two mutation carriers in the family had cutaneous capillary malformations (**Supplementary Figure 6, panel B**). Neither the proband nor other family members had common HHT features (Abdalla et al., 2003). *ACVR1* encodes the receptor serine-threonine receptor kinase ALK2 coordinating with TGF-beta type 2 receptors and co-receptors such as Endoglin (*ENG*) (Barbara et al., 1999; Chen et al., 1998; Wolfe and Myers, 2010). p.Gly39Ser alters a conserved residue in the extracellular ligand binding domain (**Supplementary Figure 6, panel C**). p.Asn373Ser alters a conserved residue predicted to be structurally critical to the cytoplasmic serine-threonine kinase (**Supplementary Figure 6, panels D & E**).

DISCUSSION

The rarity and the sporadic nature of VOGM have hindered its genetic understanding. This study, the largest trio-based genomic analysis of VOGM to date, has provided the following novel insights. First, probands exhibit an excess of damaging *de novo* mutations (~13% of cases); among these, mutations in chromatin modifier genes with essential roles in brain and heart development are enriched, and inferred to impact ~8% of cases. Second, there is a prevalence of rare inherited damaging mutations in the Ephrin signaling genes, including a genome-wide significant burden in *EPHB4*, (another ~16% of probands). Third, inherited mutations show incomplete penetrance and variable expressivity, with mutation carriers often exhibiting cutaneous vascular lesions, suggesting a two-hit mechanism. Thus, while rare mutations of large effect contribute to a significant fraction of VOGM cases, mutations in many additional genes likely contribute to disease pathogenesis. Our results support this hypothesis, suggesting potential pathogenic roles for *de novo KEL* mutations and rare, inherited *CLDN14* mutations. However, the small number of observations and lack of replication studies require validation and extension by larger follow-up studies. Of note, analysis of rare homozygous and compound heterozygous genotypes (MAF $\leq$ 0.001) revealed no genes with more than one such genotype. See **Supplementary Table 13** for proband information and identified likely pathogenic mutations.

Genes encoding covalent histone modifiers and chromatin remodelers have been implicated in autism (De Rubeis et al., 2014), CHD (Jin et al., 2017), congenital hydrocephalus (Furey et al., 2018), and other congenital disorders (Feinberg, 2018). In our

cohort, 4/55 probands had *de novo* mutations in chromatin modifiers. Enrichment of these mutations in our cohort and the conservation of the mutated residues in critical domains of protein function are consistent with each of these mutations contributing to VOGM pathogenesis. All four genes (*KMT2D*, *SMARCA2, SIRT1, KAT6A)* are highly expressed in the developing human and murine brain (Machida et al., 2001; Ogawa et al., 2011; Pollen et al., 2015; Tham et al., 2015) and essential for neuronal and/or vascular development (Griffin et al., 2008; Potente et al., 2007; Van Laarhoven et al., 2015). *SMARCA2*, *KAT6A*, *KMT2D* are mutated in Mendelian diseases that feature intellectual disability and/or epilepsy (Dentici et al., 2015; Morin, 2003). Mendelian phenotypes associated with *KAT6A* and *KMT2D* mutations include vascular defects and CHD (Arboleda et al., 2015; Van Laarhoven et al., 2015). Multiple mutated chromatin modifiers are shared among patients with CHD and autism (Homsy et al., 2015; Jin et al., 2017; Zaidi et al., 2013) ~87% of CHD patients with LoF *de novo* mutations in chromatin modifier genes exhibit neurodevelopmental phenotypes (Jin et al., 2017). These observations suggest that neurodevelopmental phenotypes in VOGM patients currently attributed to secondary CNS damage may instead reflect primary impairment from genetic mutation.

The role of Eph-B4 in A-V specification is well established in model systems (Mosch et al., 2010; Zhang and Hughes, 2006). Heterozygous missense variants in *EPHB4* have also been reported in two families with non-immune *hydrops fetalis* and/or atrial septal defect (HFASD; OMIM # 617300) (Martin-Almedina et al., 2016) and 54 families with CM-AVM2, featuring isolated cutaneous capillary malformations (63%) and associated AVMs (35%) (Amyere et al., 2017). We found damaging mutations in *EPHB4* in 7% of VOGM

probands in this cohort. Two of 52 prior CM-AVM2 patients with *EPHB4* mutations were reported to have VOGMs (Amyere et al., 2017). During preparation of this manuscript, (Vivanti et al., 2018) reported 3 transmitted damaging mutations in *EPBH4* among whole exome sequences from 19 VOGM case-parent trios, and two additional mutations from targeted sequencing of 32 other singleton VOGM probands. *Eph-b4* antisense morpholino knockdown in zebrafish embryos disrupts angioarchitecture of the dorsal longitudinal vein, homolog of the human Vein of Galen precursor (Aurboonyawat et al., 2007). We conclude that heterozygous *EPHB4* germline mutations contribute to a spectrum of vascular pathology, and *EPHB4* is a *bona fide* VOGM risk gene.

Our analysis also demonstrated enrichment of rare heterozygous damaging mutations in Ephrin signaling genes (**Supplementary Table 11**). These genes are expressed in the embryonic human brain and vasculature (Guo et al., 2012), regulate neurovascular development, and can be mapped into a single experimentally-supported STRING interactome (**Supplementary Figure 7**, see **STAR Methods**). Cutaneous vascular lesions are a common hallmark of developmental vascular disorders such as *RASA1*- and *EPHB4*-mutated CM-AVM (Amyere et al., 2017; Revencu et al., 2013); *ENG1*- and *ACVRL1*-mutated HHT (Chida et al., 2013); and *RASA1*-mutated Parkes Weber syndrome (Brouillard and Vikkula, 2007). We found similar cutaneous vascular lesions in VOGM kindreds harboring mutations in *EFNB2*, *EPHB4*, *EPHA4*, *ACVR1*, and *CLDN14*. These findings further implicate these genes in a Eph-B4-RASA1 signaling network (**Supplementary Figure 8**).

Transmitted VOGM-associated mutations show incomplete penetrance. Moreover, many of the identified VOGM-associated genes harbouring damaging *de novo* and inherited mutations have been implicated in other Mendelian diseases, sometimes producing different phenotypes. These observations highlight the pleiotropy with variable expressivity resulting from these mutations. These features have been described in other diseases. For example, haploinsufficiency for the identical chromatin modifier genes results in CHD (Zaidi et al., 2013) or autism (Iossifov et al., 2014), or both. Variable expressivity of VOGM and associated features could arise from environmental modifiers (Stuart et al., 2015). in concert with the rare mutations identified and/or specific genetic modifiers (Timberlake et al., 2016). Co-mutation of genes in KVGAM20, VGAM100, and KVGAM45 could be important in this regard (see **Supplementary Table 13**). Sequencing additional exomes from VOGM kindreds will help clarify this issue.

The mechanisms by which syndromes characterized by abnormal A-V specification present with multifocal distributions of lesions remains poorly understood. Since 68% of VOGM families with full clinical data had capillary malformations or other uncommon cutaneous vascular lesions, and that identified mutations in probands were found in all family members with these cutaneous lesions, provide evidence linking VOGM and the cutaneous lesions to the same mutations (**Supplementary Table 13**). This is consistent with a two-hit mechanism, in which phenotypic expression relies upon an inherited mutation and a second, post-zygotic mutation in the other wild-type allele (Brouillard et al., 2002; Pagenstecher et al., 2009). This mechanism has been shown for other hereditary multifocal vascular malformations such as *RASA1*-mutated CM-AVM1 (Revencu et al.,

2013), glomuvenous malformations (OMIM# 138000), cutaneomucosal venous malformation (OMIM# 600195), and cerebral cavernous malformations (OMIM# 116860) (Pagenstecher et al., 2009). In this context, phenotypic expression depends on the cell types in which somatic mutations occur, and could explain the low penetrance of VOGM arising from transmitted mutations. Further work, including exome sequencing of lesional VOGM tissue, will test this hypothesis.

Although the identified *de novo KEL* mutations and inherited *CLDN14* mutations will require further validation by WES of additional VOGM patients and functional studies, several observations suggest the importance of the current findings. *KEL*, encoding the Kell blood group transmembrane glycoprotein, was the only gene in our study that harbored more than one protein-altering *de novo* mutation (see **Figure 1**). Both the premature termination and p.Gly202Ser mutations in Kell alter its peptidase domain, shown to generate vasoactive endothelin peptides via cleavage of the endothelin-3 pro-protein (Lee et al., 1999). Endothelins provide vascular-derived axonal guidance cues (Makita et al., 2008) involved in Ephrin-dependent vascular patterning (Adams and Eichmann, 2010).

CLDN14 was the only other gene besides *EPHB4* with genome-wide significant enrichment of transmitted damaging mutations. Recessive LoF genotypes in *CLDN14* cause sensorineural deafness type 29 (OMIM # 614035); in contrast, VOGM-associated *CLDN14* mutations are heterozygous and D-mis, and include a recurrent missense mutation, suggesting gain-of-function or neomorphic effects, and phenotypic

heterogeneity. Claudin-14 is a tight junction protein in brain epithelia and endothelial cells (Kniesel and Wolburg, 2000; Wattenhofer et al., 2005). The regulation of tight junction formation by Claudins can impact endothelial cell permeability, integrity, and proliferation (Gonzalez-Mariscal et al., 2007; Morita et al., 1999). The recurrent VOGM-associated Claudin-14 mutation in lies in the large 2nd extracellular loop that likely plays a role in tight junction formation. Endothelial cells heterozygous, but not homozygous, for *CLDN14* exhibit disruption of ZO-1-positive cell-cell junctions, abnormal distribution of basement membrane laminin, increased VEGF-stimulated angiogenesis, and significantly enhanced cell proliferation – suggesting a gene dosage effect (Baker et al., 2013). Functional interactions have been reported between Claudins and Ephrin-B2-EphB4 bi-directional signaling (Tanaka et al., 2005a). In support of a possible Ephrin-Claudin-14 interaction is the fact that one of the families harboring the recurrent Claudin-14 mutation p.Val143Met had CM-AVM-like cutaneous vascular lesions that segregated with the mutation in family members (see **Figure 5, panel B**). The role of Claudin-14 in potential EphB4-dependent A-V specification will be a topic of future investigation.

These findings suggest mutation carrier offspring may be at increased risk of VOGMs, as well as capillary malformations and potentially other AVMs. However, not all mutation carriers develop capillary malformations, making absence of capillary malformations an unreliable clinical marker for transmission risk in affected families. These observations suggest the importance of family history and mutation-based screening for risk assessment. The narrow developmental window of gestational weeks 6-11 during which PVM fistulas form (Raybaud et al., 1989) poses a challenge to improved early therapeutic strategies for

VOGM. Thus, attempted diagnosis with intention to treat must occur before the safe gestational age threshold for amniocentesis (Shulman et al., 1994). These difficulties highlight the need for continued genetic research on VOGM, with focus on mechanistic implications of recently discovered VOGM-associated mutations.

Eph-B4 kinase domain mutations remove inhibition of downstream RAS/MAPK/ERK1/2 and PI3K/AKT/mTORC1 signaling cascades (Kim et al., 2002; Salaita and Groves, 2010; Xiao et al., 2012). We showed select VOGM-associated Eph-B4 mutations result in decreased binding of Eph-B4 to RASA1(see **Figure 4, panel E**). PI3K/AKT/mTORC1 up-regulation has been noted in capillary malformations of *RASA1*-mutant CM-AVM1 patients (Kawasaki et al., 2014). Therapy targeting Eph-B4-Ras-GAP-mTOR signaling may represent a viable therapeutic approach for VOGM and, perhaps, CM-AVM spectrum lesions.

MAIN TABLES AND LEGENDS

Table 1. Enrichment of damaging *de novo* mutations in chromatin modifiers intolerant to LoF mutation in VOGM

Table 1. Enrichment of damaging *de novo* mutations in chromatin modifiers intolerant to LoF mutation in VOGM												
	Cases, N = 52						Controls, N=1,789					
	Observed		Expected		Enrichment	*p*	Observed		Expected		Enrichment	*p*
	N	Rate	N	Rate			N	Rate	N	Rate		
LoF-intolerant genes (n = 3,230)												
Total	14	0.27	15.6	0.30	0.90	0.69	504	0.28	527	0.29	0.96	0.85
Syn	2	0.04	4.3	0.08	0.46	0.93	127	0.07	145.6	0.08	0.87	0.95
Mis	11	0.21	9.8	0.19	1.12	0.39	339	0.19	331.7	0.19	1.02	0.33
D-Mis	6	0.12	2.1	0.04	2.82	0.02	64	0.04	72.7	0.04	0.88	0.86
LoF	1	0.02	1.5	0.03	0.69	0.77	38	0.02	49.7	0.03	0.76	0.96
Damaging	7	0.13	3.6	0.07	1.96	0.07	102	0.06	122.4	0.07	0.83	0.97
All chromatin genes (n = 547)												
Total	4	0.08	2.3	0.04	1.73	0.20	65	0.04	78.3	0.04	0.83	0.94
Syn	0	0.00	NA	NA	NA	NA	12	0.01	21.3	0.01	0.56	0.99
Mis	3	0.06	1.5	0.03	2.06	0.18	47	0.03	49.4	0.03	0.95	0.65
D-Mis	3	0.06	0.3	0.01	8.80	5.12×10^{-03}	12	0.01	11.6	0.01	1.03	0.50
LoF	1	0.02	0.2	3.85×10^{-03}	4.53	0.20	6	3.35×10^{-03}	7.6	4.25×10^{-03}	0.80	0.76
Damaging	4	0.08	0.6	0.01	7.12	2.66×10^{-03}	18	0.01	19.2	0.01	0.94	0.64
Intolerant chromatin genes (n = 272)												
Total	4	0.08	1.6	0.03	2.56	0.07	47	0.03	52.7	0.03	0.89	0.80
Syn	0	0.00	NA	NA	NA	NA	9	0.01	14.2	0.01	0.63	0.95
Mis	3	0.06	1	0.02	3.04	0.08	35	0.02	33.3	0.02	1.05	0.41
D-Mis	3	0.06	0.3	0.01	11.40	2.48×10^{-03}	7	3.91×10^{-03}	9	0.01	0.78	0.79
LoF	1	0.02	0.2	3.85×10^{-03}	6.55	0.14	3	1.68×10^{-03}	5.2	2.91×10^{-03}	0.58	0.89
Damaging	4	0.08	0.4	0.01	9.63	8.91×10^{-04}	10	0.01	14.2	0.01	0.71	0.90

LoF: loss-of-function; N: the number of de novo mutations; Rate: the number of de novo mutations divided by the number of individuals in the cohort; Enrichment: ratio of observed to expected numbers of mutations; Intolerant genes: Genes with a pLI ≥ 0.9; D-Mis: Damaging missense mutations as predicted by MetaSVM; Damaging: D-Mis + LoF. Chromatin genes used for analysis were extracted from the Biomart database using GO:0016569 as the input.

Table 2. Transmitted mutations in *EPHB4* and *CLDN14* in VOGM

Table 2. Transmitted mutations in *EPHB4* and *CLDN14* in VOGM									
Family	**Type of VOGM**	**Ethnicity**	**Gene**	**Mutation**	**Domain affected**	**ExAC MAF***	**gnomAD MAF***	**pLI**	**MetaSVM**	**CADD**
VGAM115	Choroidal	European	*EPHB4*	p.(Glu432fs1)	N/A	< 9.06E-06	< 4.76E-06	0.99	N/A	N/A
KVGAM25	Choroidal	European	*EPHB4*	p.(Ala509Gly)	Fibronectin III	3.30E-05	1.13E-05	0.99	D	25
KVGAM33	Choroidal	Mexican	*EPHB4*	p.(Lys650Asn)	Tyrosine kinase	< 8.24E-06	< 4.06E-06	0.99	D	29.9
KVGAM18	Choroidal	European	*EPHB4*	p.(Phe867Leu)	Tyrosine kinase	< 9.03E-06	< 5.17E-06	0.99	D	31
VGAM100	Choroidal	Mexican	*CLDN14*	p.(Ala113Pro)	Second intracellular segment	< 8.37E-06	8.28E-06	0	D	24.2
KVGAM20	Choroidal	European	*CLDN14*	p.(Val143Met)	Second extracellular segment	9.43E-06	1.24E-05	0	D	31
KVGAM51	Mural	European	*CLDN14*	p.(Val143Met)	Second extracellular segment	9.43E-06	1.24E-05	0	D	31

* For variants not observed in public databases, their minor allele frequency is calculated as less than 1 out of total number of alleles sampled at the closest locus with allele number available

FIGURES AND LEGENDS

Figure 1. Protein-altering *de novo KEL* mutations in Vein of Galen malformation (VOGM)

(A) Representative digital subtraction angiography images demonstrating mural and choroidal VOGMs in KVGAM45-1 and KVGAM10-1, respectively.

(B) Pedigrees depicting kindred structures. Note that probands carrying *de novo* mutations in *KEL* are the only members of families KVGAM45 and KVGAM10 with VOGMs; none of the family members in these two families have any disease phenotypes or cutaneous manifestations. Red 'D' denotes protein-altering mutation, '+' denotes wild type sequence.

(C) Mutations identified by exome sequencing were confirmed by direct PCR amplification with custom primers followed by Sanger sequencing.

(D) Linear representation of the KEL polypeptide, with functional domains as dark rectangles. Amino acid modifications are mapped (in red) on the protein structure. Conservation of the wild-type amino acid substituted by the missense mutations is depicted below. TM = Transmembrane domain.

Figure 1. Protein-altering *de novo KEL* mutations in Vein of Galen malformation (VOGM)

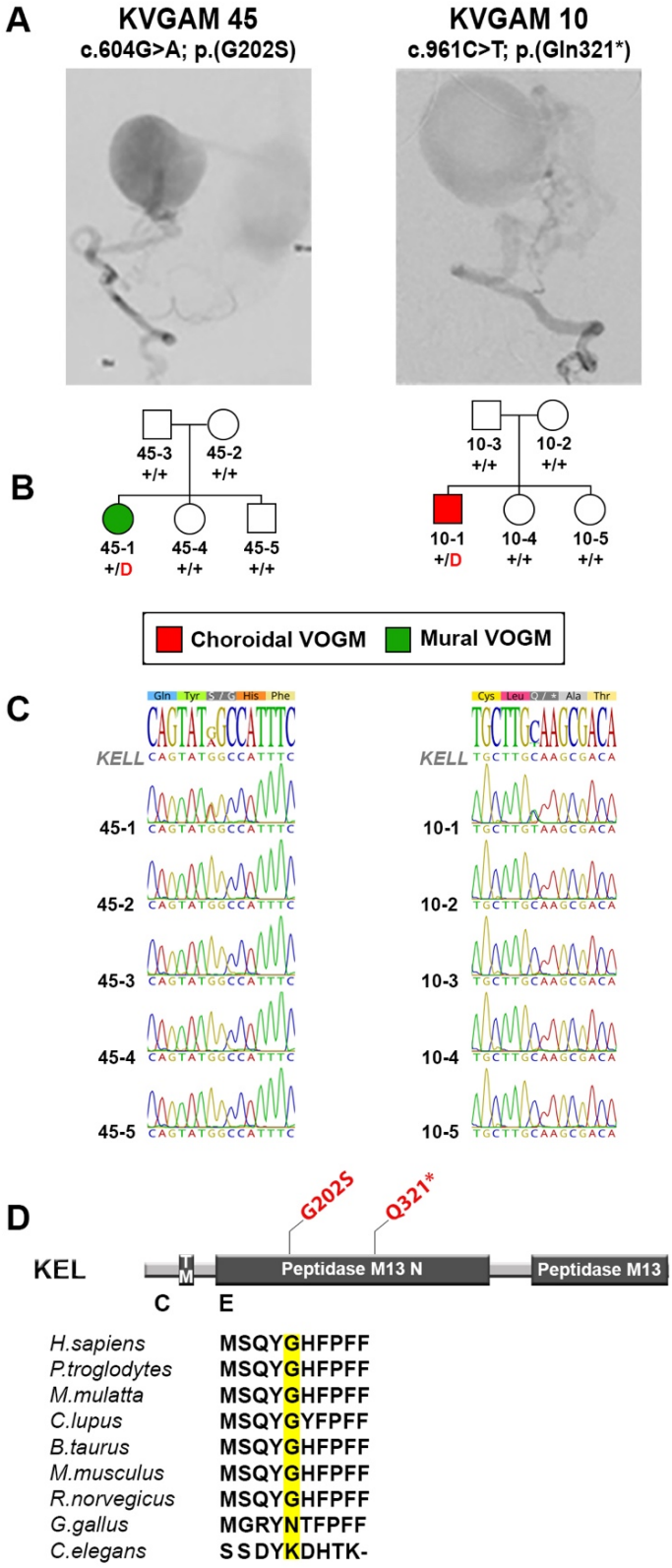

Figure 2. Damaging *de novo* mutations in chromatin modifiers in VOGM

(A) Magnetic resonance angiographies and a digital subtraction angiography reconstruction demonstrating VOGM in probands from four pedigrees.

(B) Pedigree structures of VOGM kindreds. For each kindred, the gene and mutation, the angiographic image, and pedigree structure are shown. Subjects with atypical capillary malformations are denoted by blue symbols. Red 'D' denotes damaging mutation, '+' denotes wild type sequence.

(C) Linear representation of functional domains of SIRT1, KMT2D, SMARCA2, and KAT6A, with location of VOGM mutations. Functional domains are represented by dark rectangles. Amino acid changes (red) are located on the protein structure. For missense mutations, phylogenetic conservation of the wild-type amino acid is shown, with the mutated amino acid in yellow. SIR2 = Sirtuin catalytic domain, SIR2 Domain; PHD = Zinc Finger PHD type; MOZ_SAS = Histone acetyltransferase domain, MYST-type; zf-H = PHD-like zinc binding domain; FYRN = F/Y-rich domain - F/Y-rich N-terminus motif; FYRC = F/Y-rich domain - F/Y-rich C-terminus motif; SET = Su(var)3-9, Enhancer-of-zeste and Trithorax; QLQ = Glutamine-Leucine-Glutamine domain; HAS = Helicase-SANT associated domain; BRK = BRK domain; SNF2_N = SNF2-related, N-terminal domain; Hel_C = Helicase C-terminal domain; SnAC = Snf2-ATP coupling, chromatin remodeling complex; BD = Bromodomain.

(D) Schematic of histone mark modifications by SIRT1, KMT2D, SMARCA2, and KAT6A.

Figure 2. Damaging *de novo* mutations in chromatin modifiers in VOGM

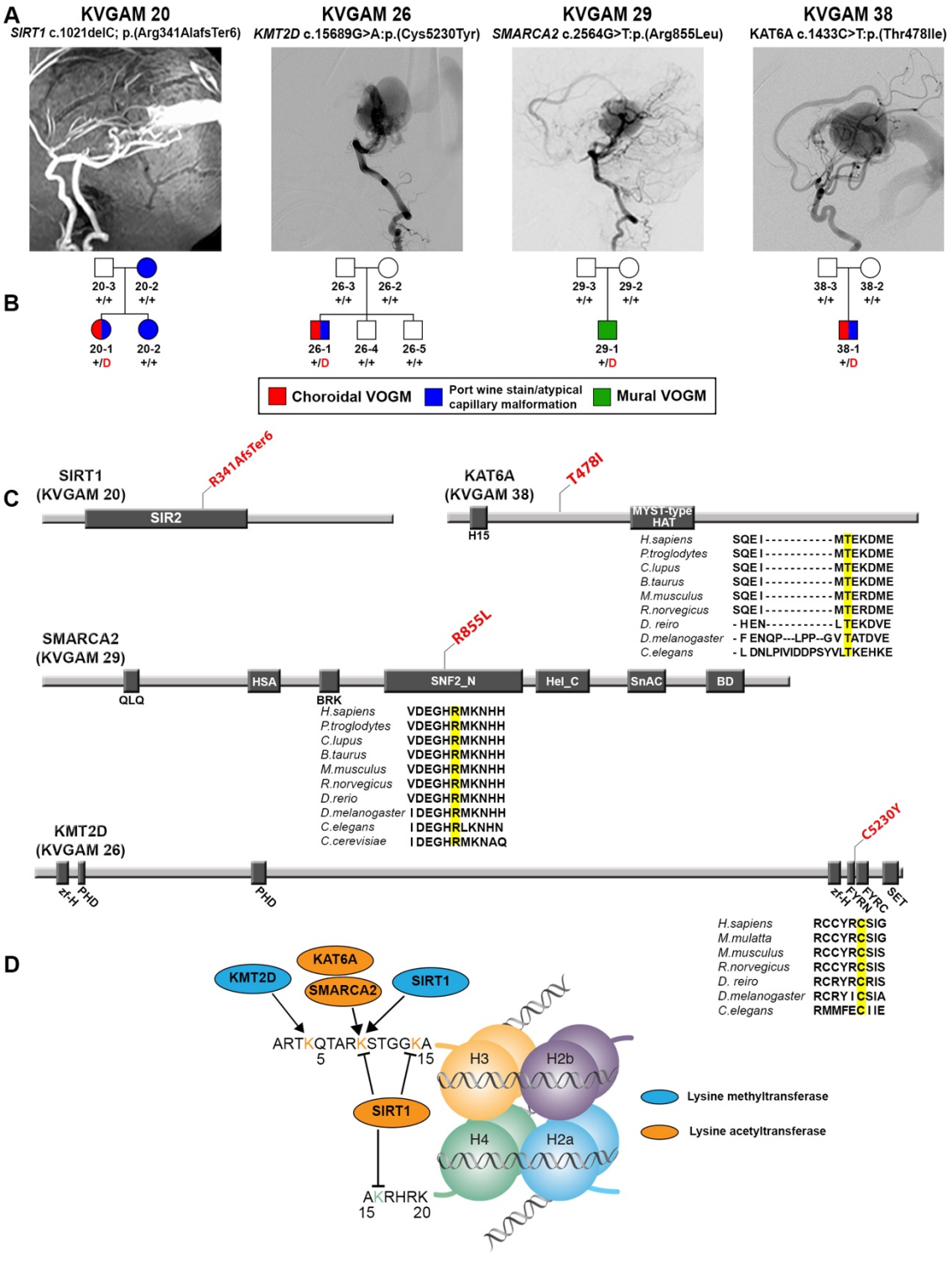

Figure 3. Exome-wide significant enrichment of rare damaging transmitted mutations in *EPHB4* and *CLDN14*

(A) Quantile-quantile plots of observed vs. expected binomial test p-values for rare damaging (D-mis+LoF) variants with MAF $\leq 2 \times 10^{-5}$ in the Genome Aggregation database (gnomAD) in LoF-intolerant genes (pLI $\geq$ 0.9).

(B) Quantile-quantile plots of observed vs. expected binomial test p-values for rare damaging (D-mis+LoF) variants with MAF $\leq 2 \times 10^{-5}$ in gnomAD for all genes. MAF = Minor allele frequency; D-mis = Missense mutations predicted to be deleterious per MetaSVM; LoF = Canonical loss-of-function mutations (stop-gains, stop-losses, frameshift insertions or deletions, and canonical splice site mutations).

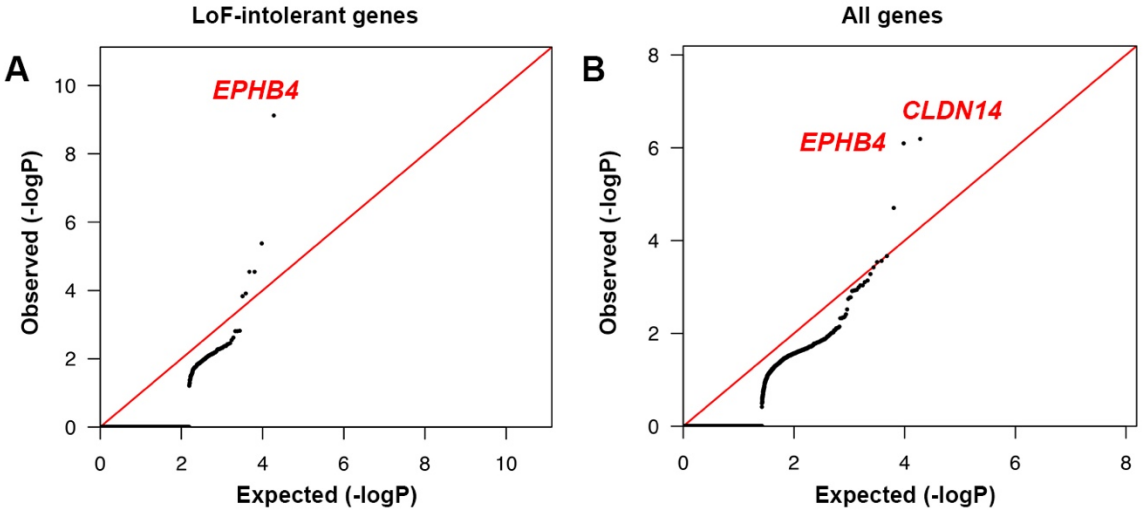

Figure 4. Damaging *EPHB4* mutations in choroidal VOGM

(A) Vascular imaging of probands from coronal reconstruction of computed tomography and magnetic resonance angiography demonstrating VOGMs.

(B) Pedigree structures of the kindreds, showing gene, mutation, and angiographic image. A carrier with atrial septal defect in family KVGAM 33 is in yellow. Red 'D' denotes damaging mutation, '+' denotes wild type sequence.

(C) Eph-B4 functional domains (dark rectangles) with location of VOGM mutations (red), and phylogenetic conservation of wild-type amino acid (yellow) at each mutated position. LB = ligand binding domain; CRD = Cysteine-rich domain; FNIII = Fibronectin III domain; TM = Transmembrane domain; TK = Tyrosine kinase domain; SAM = Sterile alpha motif.

(D) Representative immunoblots showing effects of Ala509Gly, Lys650Asn, and Phe867Leu mutations on resting state Eph-B4 tyrosine phosphorylation in HEK 293T cells, analyzed by immunoprecipitation (IP) with HA-Tag antibody followed by immunoblot (IB) with anti–p-tyrosine (p-Tyr) and HA-Tag antibodies. Blot demonstrates reduced p-Tyr content in Lys650Asn, with none detectable in Phe867Leu.Representative immunoblot demonstrating binding of Eph-B4 constructs by Ras-GAP.

Ras-GAP protein was co-immunoprecipitated with Eph-B4 mutants. Ras-GAP binding to Lys650Asn and to Phe867 was markedly reduced and abrogated, respectively.

Figure 4. Damaging *EPHB4* mutations in choroidal VOGM

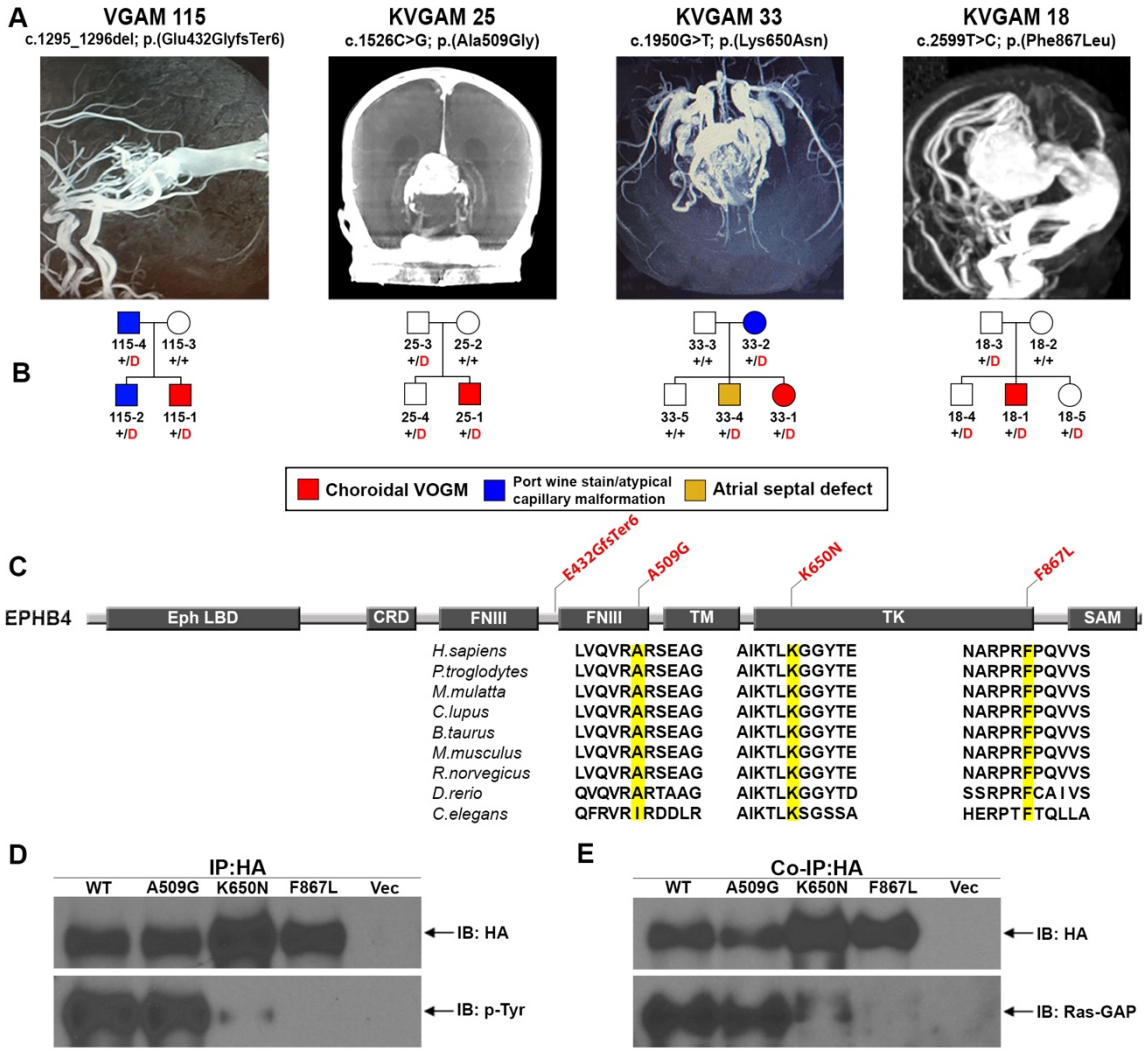

Figure 5. Damaging *CLDN14* mutations in VOGM

(A) Representative images from digital subtraction angiographies and magnetic resonance angiography demonstrating VOGMs of the probands.

(B) Pedigree structures indicating genotypes and phenotypes as described in Figure 2.

(C) Linear representation of Claudin-14 functional domains (dark rectangles) with location of VOGM mutations (in red). Conservation of the wild-type amino acid is shown. TM = Transmembrane domain; C = cytoplasmic loop; E = extracellular loop.

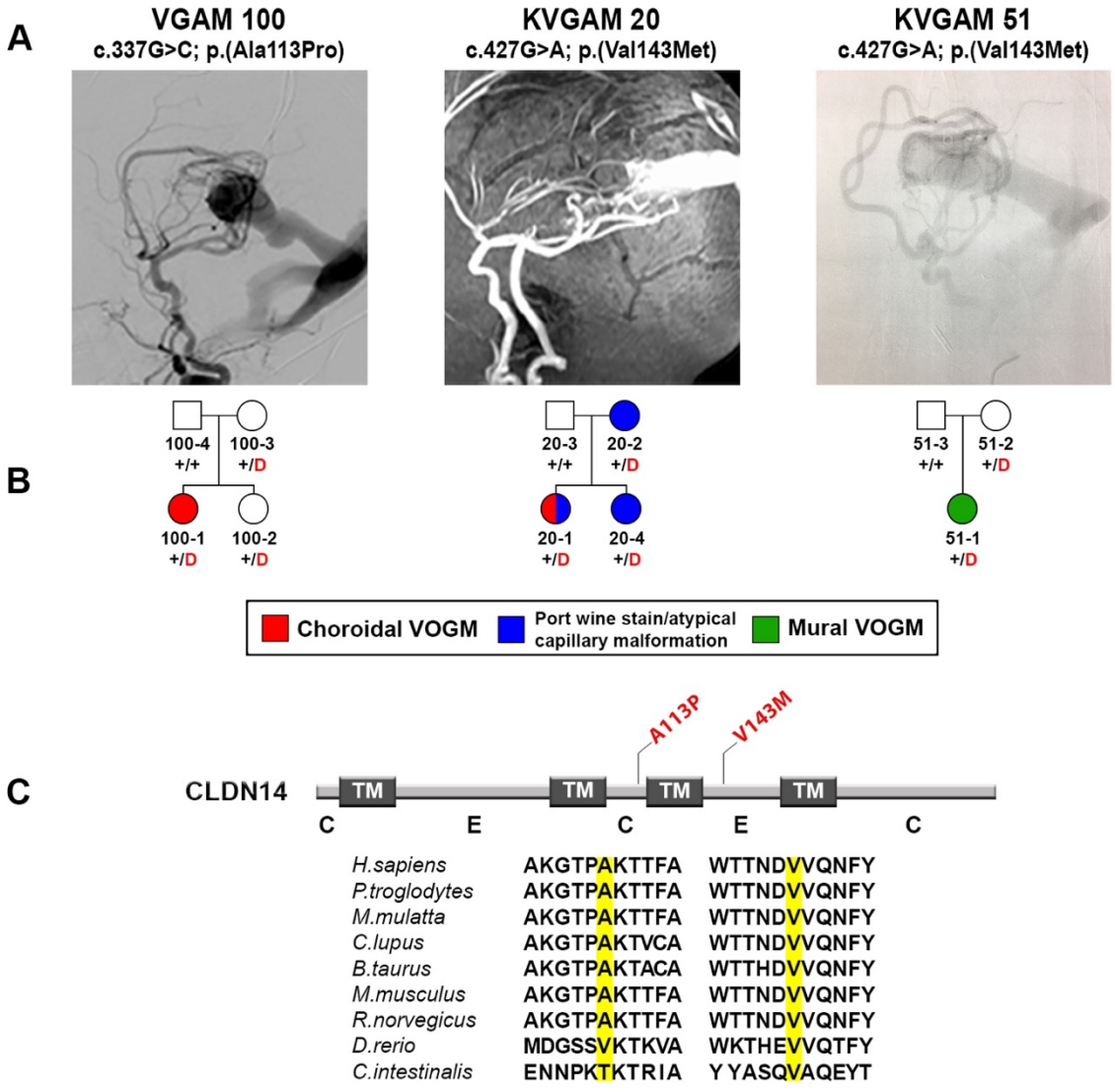

STAR*METHODS

REAGENT or RESOURCE	SOURCE	IDENTIFIER
Deposited Data		
Whole exome sequencing data of 52 VOGM trios and 3 singletons	This paper (Duran et al., 2018b)	Accession number phs000744.v4.p2 https://www.ncbi.nlm.nih.gov/projects/gap/cgi-bin/study.cgi?study_id=phs000744
Whole exome sequencing data of 1,789 control trios from the Simon Simplex Collection	(Iossifov et al., 2014)	NDAR: https://doi.org/10.15154/1149697https://ndar.nih.gov/study.html?id=352
Software and Algorithms		
Genome Analysis Tool Kit (GATK)	(DePristo et al., 2011; McKenna et al., 2010; Van der Auwera et al., 2013)	https://software.broadinstitute.org/gatk/best-practices/
BWA-mem	(Li and Durbin, 2010)	http://bio-bwa.sourceforge.net/
Annovar	(Wang et al., 2010a)	http://annovar.openbioinformatics.org/en/latest/
PLINK/SEQ	(Fromer and Purcell, 2014)	https://atgu.mgh.harvard.edu/plinkseq/
Antibodies		
Anti-Phosphotyrosine Monoclonal Antibody; P-Tyr-100	Cell Signaling Technology, Danvers, MA, USA	RRID: AB_331230
Anti-Ras GAP Monoclonal Antibody	Santa Cruz Biotechnology, Dallas, TX, USA	RRID: AB_628207
Anti-HA-Tag antibody	Cell Signaling Technology, Danvers, MA, USA	RRID: AB_10691311
Other		
1000 Genomes GRCh37 h19 genome build	1000 Genomes Project	http://ftp.1000genomes.ebi.ac.uk/vol1/ftp/technical/reference/human_g1k_v37.fasta.gz
RefSeq hg19 gene annotation	UCSC Genome Browser	http://genome.ucsc.edu/cgi-bin/hgTables?command=start
Intervals file for IDT xGen v1.0	Integrated DNA Technologies	http://www.idtdna.com/pages/products/next-generation-sequencing/hybridization-capture/lockdown-panels/xgen-exome-research-panel
ExAC Browser (Beta)	Exome Aggregation Consortium	http://exac.broadinstitute.org/
gnomAD Browser	genome Aggregation Database	http://gnomad-old.broadinstitute.org/

CONTACT FOR REAGENT AND RESOURCE SHARING

Further information and requests for resources and reagents should be directed to and will be fulfilled by the Lead Contact, Dr. Kristopher T. Kahle (kristopher.kahle@yale.edu).

EXPERIMENTAL MODEL AND SUBJECT DETAILS

Patient Subjects

All procedures in this study comply with Yale University's Human Investigation Committee (HIC) and are Human Research Protection Program. Written informed consent was obtained from all adult participants. Parent or legal guardian authorization was obtained in writing for sample collection of all minors in this study. Inclusion criteria included male or female patients with clearly defined mural or choroidal VOGMs, radiographically-confirmed by both a neurosurgeon and neuroradiologist from an angiogram or magnetic resonance angiogram, along with their family members. Fifty-five probands diagnosed with VOGM were included in this study, of which 52 were parent-offspring trios. Among these 55 VOGM probands, 65.5% were female, 76.4% were self-reported Europeans, and 56.4% had a family history of cutaneous vascular abnormalities. (**Supplementary Table 1**).

Controls consist of 1,789 unaffected siblings of autism cases and unaffected parents from the Simons Foundation Autism Research Initiative Simplex Collection (SSC)(Fischbach and Lord, 2010; Iossifov et al., 2014; Krumm et al., 2015; O'Roak et al., 2011; Sanders et

al., 2012). Only the unaffected siblings and parents, as designated by SSC, were included in the analysis and served as controls for this study. Permission to access to the genomic data in the SCC on the National Institute of Mental Health Data Repository was obtained. Written informed consent for all participants was provided by the Simons Foundation Autism Research Initiative.

Whole Exome Sequencing and Variant Calling

Exon capture was performed on genomic DNA samples derived from saliva or blood using Roche SeqCap EZ MedExome Target Enrichment kit or IDT xGen target capture kit followed by 99 base paired-end sequencing on the Illumina HiSeq 2500 platform. Sequence reads were aligned to the human reference genome GRCh37/hg19 using BWA-MEM (Li, 2014) and further processed to call variants following the GATK Best Practices workflow (McKenna et al., 2010). Variants were annotated with ANNOVAR (Wang et al., 2010a) and MetaSVM (Dong et al., 2015) was used to predict the deleteriousness of non-synonymous variants (herein referred to as D-mis). All variants covered by independent aligned sequencing reads with a depth of 8x or greater were visualized *in silico* to eliminate false positives.

De novo mutations were called using TrioDeNovo (Venugopal, 2014). Candidate *de novo* mutations were further filtered based on the following criteria: (1) exonic or splice-site variants; (2) read depth (DP) of 10 in the proband and both parents; (3) genotype quality (GQ) score ≥ 20; (4) minium proband alternative read depth of 5; (5) proband alternative allele ratio ≥ 28% if having < 10 alternative reads or ≥ 20% if having ≥ 10 alternative reads;

(6) alternative allele ratio in both parents ≤ 3.5%; (8) in-cohort allele frequency ≤ 4×10^{-4} for controls and MAF ≤ 4×10^{-4} in gnomAD for cases due to limited cohort size.

For rare transmitted dominant variants, only LoF mutations (stop-gains, stop-losses, canonical splice-sites, and frameshift indels) and D-mis mutations (missense mutations predicted deleterious by MetaSVM) were considered potentially damaging for subsequent one-tailed binomial analysis and filtered using the following criteria to reduce false positives: (1) GATK variant quality score recalibration (VQSR) of PASS, (2) MAF ≤ 2×10^{-5} in gnomAD (calculated based on combined dataset of WES and WGS data from gnomAD database, Lek et al. 2016), (3) DP ≥ 8 independent reads, and (4) GQ score ≥ 20. Transmitted recessive variants were filtered for rare (MAF ≤ 10^{-3} in gnomAD) homozygous and compound heterozygous variants using the same criteria described above.

Candidate mutations were confirmed by PCR amplification followed by Sanger sequencing (primer sequences available on request).

METHOD DETAILS

Kinship Analysis

Pairwise proband relatedness and pedigree information of trios were confirmed using KING (Manichaikul et al., 2010) by estimating kinship coefficient and calculating identity-by-descent (IBD). The shared pairwise IBD segments in 45 European probands were detected using Beagle v3.3.2 (Browning and Browning, 2011).

De Novo Mutation Expectation Model

We used a sequence context probability model to derive the per-gene probability of observing a *de novo* mutation by chance as previously described (Samocha et al., 2014). In brief, for each base in the exonic region, the probability of observing each of the three possible single nucleotide changes was determined. The coding consequence of each possible mutation was determined, and then these probabilities of mutations were summed for each variant functional class (synonymous, missense, nonsense, canonical splice site, frameshift, and stop-lost) to create a per-gene probability of mutations. The probability of a frameshift mutation was determined by multiplying the probability of a nonsense mutation by 1.25 as described previously (Samocha et al., 2014). In-frame insertions and deletions are not currently accounted for by this framework and were not included in the analysis. The per-gene probability for each functional class was adjusted to control for sequencing coverage. Due to the difference in exome capture kits, DNA sequencing platforms, and variable sequencing coverage between case and control cohorts, the expected number of *de novo* mutations was estimated by adjusting for sequencing depth in 52 case trios and 1,789 autism control trios separately.

De Novo Enrichment Analysis and Variant Stratification

Rather than using the variant calls in controls published in the SSC study (Krumm et al., 2015), we downloaded the bam files from the SSC, reanalyzed the data, and filtered the control vcf file using the same filtering criteria as what was used in our case cohort. A one-tail Poisson test was used to compare observed number of *de novo* mutations across each

variant class to expected number under the null hypothesis. R package 'denovolyzeR' (Ware et al., 2015) was used to perform the analyses. The Benjamini-Hochberg method was used to correct for multiple testing while taking into account all genes (N = 18,989) and calculate adjusted p-values. A gene was considered significant if Benjamini-Hochberg adjusted p-value is ≤ 0.05. All genes represented in this dataset were annotated with artery-specific and brain-specific expression values in a form of reads per kilobase transcript per million reads (RPKM) from the GTEx database (https://gtexportal.org/home/). Genes harboring *de novo* mutations were also annotated with human brain specific expression data obtained during the first four weeks of development (Gerrard et al., 2016) in the form of quantile rank based on transcript per kilobase million (TPM), indicating the relative rank of expression level within human genome. The final dataset was analyzed for recurrently affected genes, and all variants in genes affected by a single *de novo* mutation were stratified. LoF variants were ranked based on pLI (from highest to lowest).

QUANTIFICATION AND STATISTICAL ANALYSIS

Estimation of the Number of Damaging *De Novo* Mutations in LoF-intolerant Chromatin Modifiers

One million permutations were performed to derive the empirical distribution of the number of damaging *de novo* mutation in the LoF-intolerant chromatin modifier genes. For each permutation, the number of observed damaging *de novo* mutations in all genes (n = 19) was randomly distributed across the exome, weighted according to the *de novo* probabilities of damaging mutations. The empirical p-value is calculated as the proportion

of times that the number of damaging *de novo* mutations in the LoF-intolerant chromatin modifier genes is greater than or equal to the observed number (n = 4). The average number of damaging *de novo* mutations in the LoF-intolerant chromatin modifier genes is also calculated.

Binomial Analysis

Independent binomial tests were used to compare the expected and observed counts of rare variants in each gene. The expected number of rare damaging variants is determined by taking the fractional length of a gene (in base pairs) relative to the entire exome and multiplying this by the total number of rare damaging variants. This represents the expected occurrence of sporadic mutations in each gene without considering the influences of selection pressure or precedents of ethnic background. Inputs for this test were those with inferred pathogenicity, including missense mutations called deleterious per MetaSVM and inferred LoF mutations (stop-gains, stop-losses, frameshift insertions/deletions, or canonical splice site mutations). Binomial analysis for mutational enrichment did not include non-frameshift insertions or deletions. The Benjamini-Hochberg method was performed taking into account all genes (N = 18,989 for *CLDN14*) or all LoF-intolerant genes (N = 3,230 for *EPHB4* and *CAD*) as described above and the significance cutoff was 0.05. We reported genes that reached a more stringent Bonferroni multiple testing cutoff of 2.63×10^{-6} (= 0.05/18,989) or 1.55×10^{-5} for binomial testing of all genes or LoF-intolerant genes, respectively.

Pathway Analysis

Inputs for this analysis were LoF-intolerant genes (pLI ≥ 0.9) harboring damaging *de novo* mutations and/or rare (MAF ≤ 2×10^{-5}) damaging transmitted mutations, as well as genes with significant burden of *de novo* (*KEL*) or transmitted mutation (*EPHB4* and *CLDN14*) (n = 128 genes) into Ingenuity Pathway Analysis (IPA, Apr 2018). Core analysis using Ingenuity Knowledge Base (Gene Only) as the reference set was performed. P-value was calculated using a one-tailed Fisher's exact test reflecting the likelihood that the overlap between the input and a given gene set is due to random chance. In individual based case-control analysis, ethnicity-matched case and control samples were filtered using the same criteria. Individuals carrying variants of interest in case and control groups were tallied separately, and the p-value was obtained from a one-tailed Fisher's exact test. In binomial pathway analysis, the observed number of rare damaging variants in LoF-intolerant genes that belong to statistically significant canonical pathways of interest were compared to the expected number of mutations in each set using a one-tailed binomial test. Gene sets of canonical pathways were obtained from IPA. The expected number of mutations in a given gene set is calculated as the formula below:

$$\text{Expected number of mutations} = \text{N} \times \frac{\sum_{Gene\ Set} \text{Gene Length}}{\sum_{Intolerant\ Genes} \text{Gene Length}}$$

Where N denotes total number of rare damaging *de novo* and transmitted mutations in intolerant genes as well as genes with significant burden of *de novo* and transmitted mutations.

Interactome Construction

We input all genes contributing to the significantly enriched pathway to String (version 10.5) (Szklarczyk et al., 2015). For organism, *Homo sapiens* was selected. For each displayed interaction, active interaction sources were restricted to experiments, and the maximum number of interactors was limited to 50.

***In Silico* Modeling of Mutational Effects on Protein Structure**

The sequence for all available modeled human proteins was downloaded from Uniprot (Apweiler et al., 2004). The stereochemical parameters of VOGM-associated mutations were analyzed using PROCHECK (Laskowski et al., 1993) and PROSA (Wiederstein and Sippl, 2007), and the final models were chosen based on the lowest energy function score (Dope) within the modeling program. The mutations were constructed and the free energy of change calculated ($\Delta\Delta G$) in silico using the ICM mutagenesis (Abagyan et al., 1994).

Cell Culture

HEK 293T cells were passaged at 80-90% confluence on high glucose DMEM (Dulbecco's modified Eagle's medium, Gibco Life Technologies, Waltham MA, USA) supplemented with 10% fetal bovine serum (FBS, Gibco Life Technologies Waltham MA, USA), L-glutamine, and penicillin/streptomycin.

Mutagenesis of Eph-B4 and Plasmid Transfection

A wild-type mouse *EPHB4* cDNA was sub-cloned into the pShuttle-IRES-hrGFP-2 plasmid vector with HA-Tag sequence (Protack et al., 2017). The QuikChange II Site-

Directed Mutagenesis Kit (Aligent Technologies, Santa Clara CA, USA) was used to generate isolated single amino-acid changes within the *EPHB4* ORF (A509G, K650N, F867L). All mutant constructs were sequenced to confirm successful mutagenesis. The wild-type *EPHB4*, the mutant constructs, and empty vector were individually transiently transfected into HEK 293T cells using Lipofectamine 2000 transfection reagent (Invitrogen, Carlsbad, CA, USA) according to its standard protocol. DNA complexes were removed after 5 h and replaced with fresh complete medium. After 48 hours, the medium was aspirated and the cells starved for 18 h in serum-free conditions.

Co-immunoprecipitation and Western Blotting

Cell lysates were prepared using NP40 lysis buffer (50 mM Tris, pH7.5; 1% Nonidet P-40; 150 mM NaCl; 10% Glycerol) containing protease and phosphatase inhibitor cocktail (Roche, Basel, Switzerland). Protein concentrations were measured with DC Protein Assay Reagents (Bio-Rad, Hercules CA, USA). For immunoprecipitation, equal amounts of cell lysates were incubated with Sepharose beads linked to anti-HA-Tag antibody (Cell Signaling Technology, Danvers, MA, USA) overnight at 4 °C. Immunoprecipitated protein complexes were separated on SDS-PAGE gel and analyzed by Western blotting using following antibodies: anti-phosphotyrosine P-Tyr-100, anti-HA-Tag, (Cell Signaling Technology, Danvers MA, USA), anti-Ras GAP (Santa Cruz Biotechnology, Dallas TX, USA). Band intensities were quantified using ImageJ software (Schneider et al., 2012). Statistical analyses were performed using Prism 7 software (GraphPad Software, La Jolla CA, USA).

Attribution of work

Dr. Kristopher T. Kahle posted to social media site information pertaining to the genetics study and potential participants reached out by email. Jonathan R. Gaillard assisted Dr. Daniel Duran with the management of the secure Yale email address and were responsible for the recruitment of subjects to the genetics study, obtaining consent, information, and cheek swabs. Participant information was stored in a HIPAA compliant manner in a RedCap database. DNA was extracted from cheek swabs by Carol Nelson-Williams. Dr. Duran and JRG prepared extracted DNA for sequencing at Yale Center for Genomic Analysis. Exome analysis was performed by Jungmin Choi, Peter Jin, and Xue Zheng, from Dr. Richard Lifton's lab, to select candidate genes with input from Daniel Duran, JRG, and Dr. Kahle. Cell work and western blotting was performed by Bogdan Yatsula, Alan Dardic, and Jinwei Zhang. All figures and supplementary figures were made by JRG.

Our Yale based collaborators, Michael L. DiLuna, Charles C. Matouk, Murat Gunnel, referred cases seen at Yale. The many members of the Kahle, Gunel, and Lifton labs including Charuta Furey, August Allocco, Ava Hunt, Sierra Conine, Jason K. Karimy, Qiongshi Lu, Andrew T. Timberlake, Mark Youngblood, and Weilai Dong also contributed their feedback, insights, and assistance with recruitment and genetic analysis.

Many collaborators contributed their efforts by alerting patients to our study and providing input and feedback of the manuscript including Michelle A. Sorscher, Shrikant Mane, Irina R. Tikhonova, Christopher Castaldi, Francesc López-Giráldez, James Knight, Shozeb

Haider, Mariya Soban, Seth L. Alper, Masaki Komiyama, Andrew F. Ducruet, Joseph M. Zabramski, Brian P. Walcott, Christopher J. Stapleton, Beverly Aagaard-Kienitz, Georges Rodesch, Eric Jackson, Edward R. Smith, Darren B. Orbach, Erin Loring, Jennifer Klein, Alejandro Berenstein, Kaya Bilguvar, and Miikka Vikkula.

SUPPLEMENTARY FIGURES

Supplementary figure 1. VOGM type and representative imaging for probands, Related to Table 2

Representative images of 3-Tesla time-of-flight magnetic resonance angiography or digital subtraction angiography for all patients with available imaging, with patient codes and VOGM subtype. In cases for which imaging was not available, VOGM subtype was ascertained from detailed transcripts of angiographies during or before endovascular treatment of VOGM.

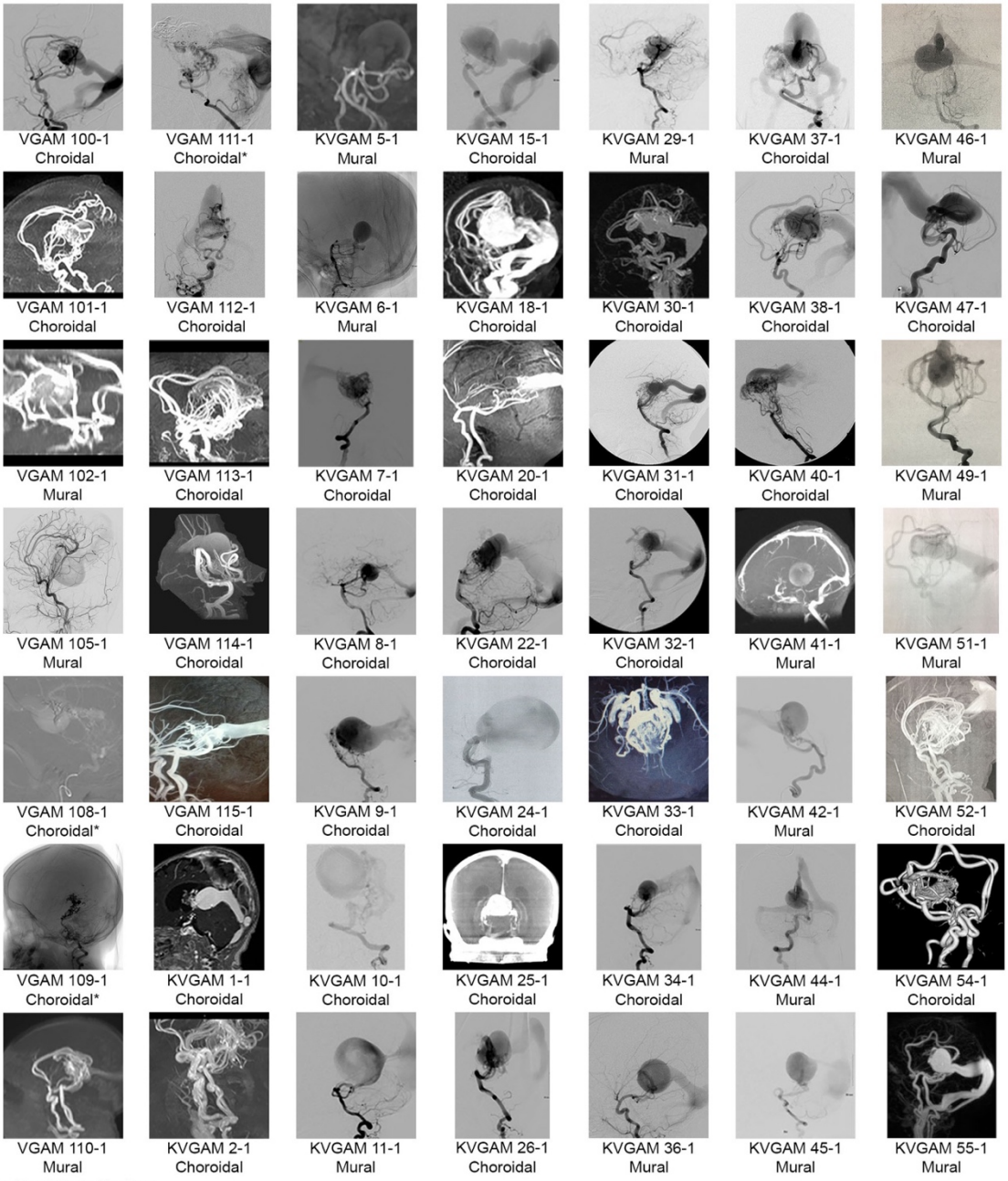

*** = Post Embolization**

Per Detailed Angiogram Report: VGAM 104-1: Choroidal; VGAM 107-1: Choroidal; KVGAM 3-1: Mural; KVGAM 4-1: Choroidal; KVGAM 35-1: Choroidal; KVGAM 43-1: Mural.

Supplementary figure 2. Chromatogram alignments and segregation of select candidate variants, Related to Table 2 and Figure 2, 4, and 5

Mutations identified by exome sequencing were confirmed by direct PCR amplification with custom primers followed by Sanger sequencing.

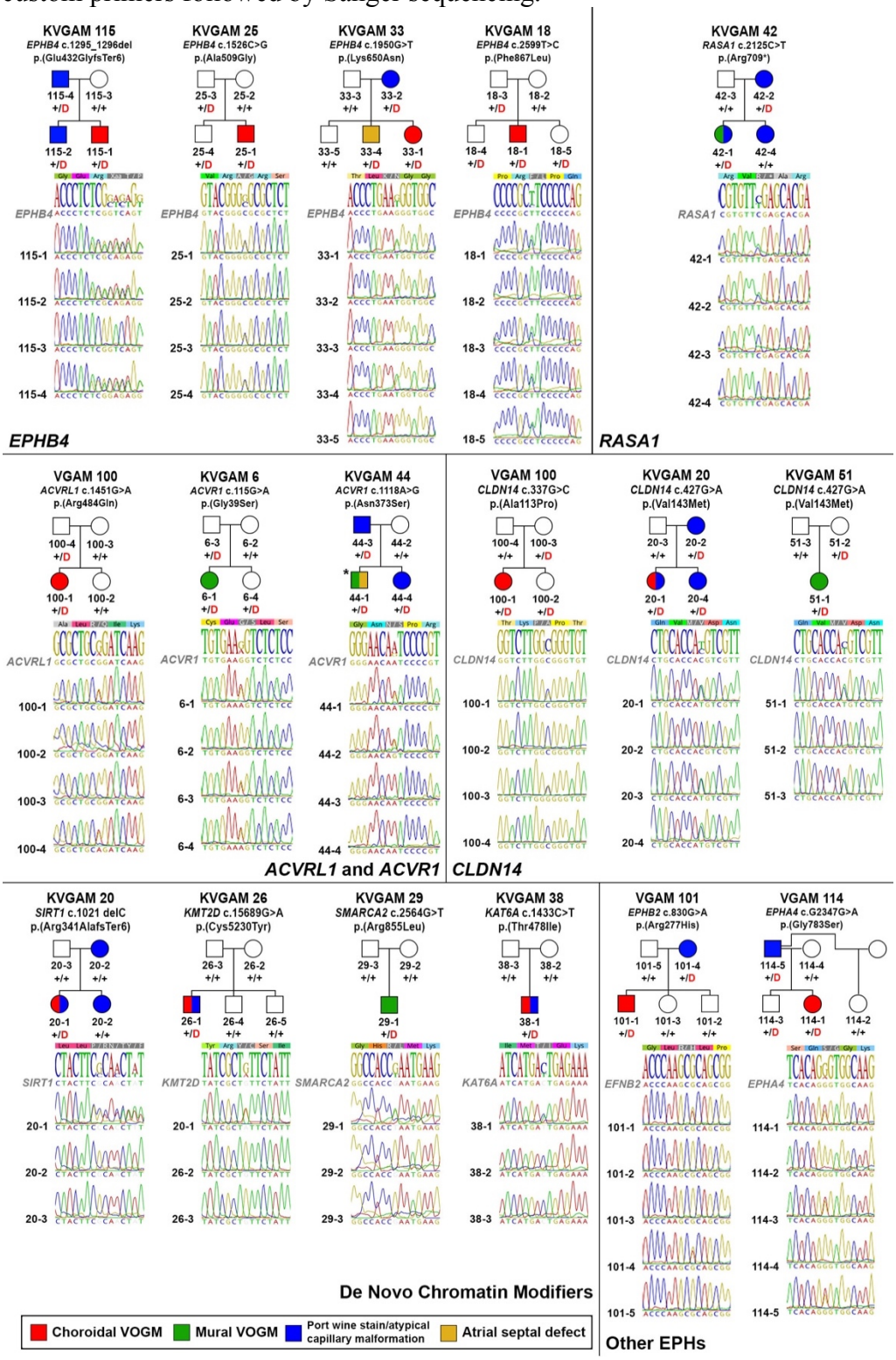

Supplementary figure 3. Cutaneous manifestations in VOGM probands and family members, Related to Figure 4 and 5

Atypical capillary malformation on the posterolateral aspect of the distal third of the thigh (A) and left cheek (B) of VGAM115-2. Panel C demonstrates an atypical capillary malformation on left flank of VGAM115-4 – both individuals depicted in panels A-C carry EPHB4 c.1295_1296del; p.Glu432fs. Atypical capillary malformations on the angle of the jaw and superior right thorax of KVGAM42-1 (D) and KVGAM42-2 (E). Both individuals depicted in panels DE carry RASA1 c.2125C>T; p.Arg708*. (F). Atypical capillary malformation on the posterolateral aspect of the forearm in VGAM114-5, carrier of EPHA4 c.2347G>A; p.Gly783Ser. (G). Nuccal atypical capillary malformation in a proband harboring CLDN14 p.(Val143Met) (H). Lumbar atypical capillary malformation in the same proband depicted in panel G. (I). Nuccal atypical capillary malformation in the sister of the proband depicted in panels G and H, also harboring CLDN14 p.Val143Met. (J). Atypical capillary malformation in the thigh of the mother of individuals depicted in panels G-I, carrying and transmitting CLDN14 p.Val143Met.

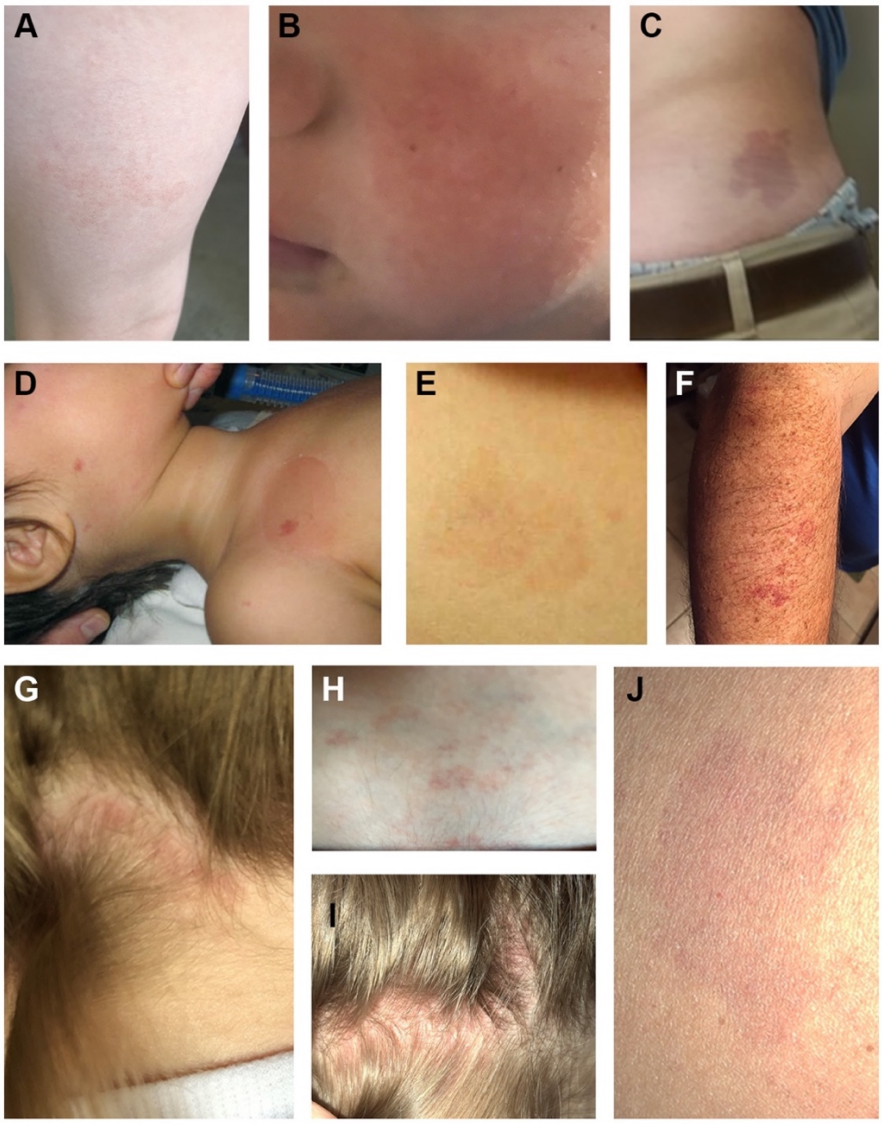

Supplementary figure 4. In silico modeling of CLDN14 mutations, Related to Figure 5

(A) In silico modeling of p.Ala113Pro. Ala113 is the first residue of Helix-3 and lies between P112 and K114 at the interface of Claudin-14 and the cytoplasmic side of the lipid bilayer. Just preceding helix-3 is the loop that connects helix-2 and -3, on which posttranslational modification sites are present, including for palmitoylation. The presence of Proline in an alpha helix can result in helix distortion since it lacks the backbone NH to establish the hydrogen bonding necessary to complete the H-bond chain. Additionally the steric or rotamer effects prevent Proline from adopting helical geometry. The two adjacent Proline residues 112 and 113 likely influence the conformation of the helix 2-3 connector loop and destabilize the initial portion of helix-3. Calculated ΔΔG of A113P is 1.08 Kcal/mol.

(B) In silico modeling of p.Val143Met located towards the end of helix-3 at the outer leaflet of the lipid bilayer. The Valine side chain is tightly packed against b sheets, being surrounded by the hydrophobic side chains of L164, I160 and V144. The V143M mutation (ΔΔG = 0.6 Kcal/mol) results in steric clash of the larger Methionine side chain with the beta sheets.

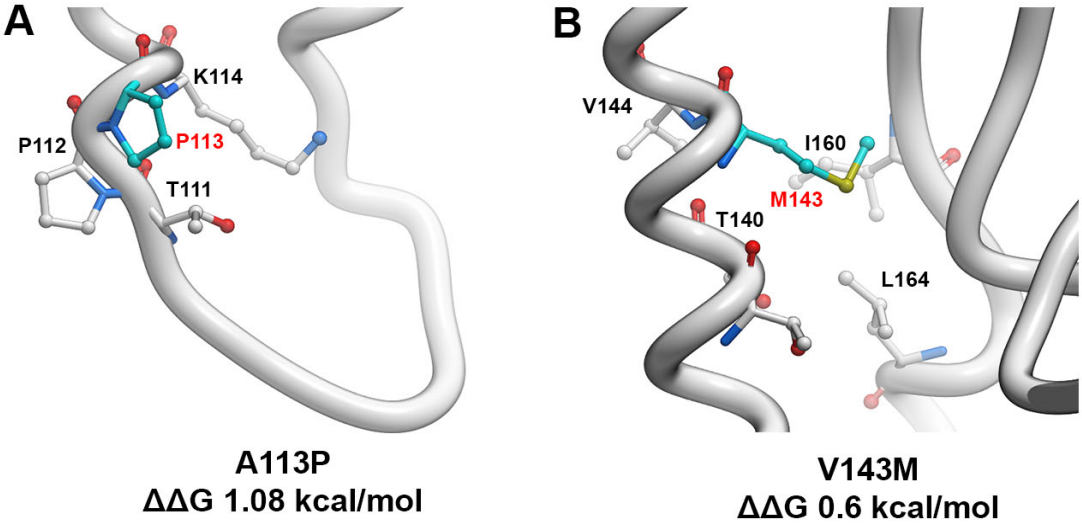

Supplementary figure 5. Mutations affecting other members of the Ephrin family in VOGM patients displaying CM-AVM-like cutaneous manifestations, Related to Figure 3

(A) Representative magnetic resonance angiography and digital subtraction angiography images demonstrating choroidal Vein of Galen malformations in probands.

(B) Pedigrees depicting kindred structure and phenotypic variance. Note the presence of atypical capillary malformations represented by blue symbols in both parents transmitting EFNB2 and EPHB4 mutations in families VGAM101 and VGAM114. Red 'D' denotes damaging mutation, '+' denotes wild type sequence.

(C) Linear representation of affected Ephrin polypeptides. Functional domains are represented by dark rectangles. Amino acid modifications are mapped on the protein structure in red lettering. Conservation of the wild-type amino acid substituted by the four deleterious missense mutations is depicted on the right of each molecule schematic. LB = ligand binding domain; CRD = Cysteine-rich domain; FNIII = Fibronectin III domain; TM = Transmembrane domain; TK = Tyrosine kinase domain; SAM = Sterile alpha motif.

(D) In silico modelling of the repercussion of Eph-A4 p.Gly783Ser. Gly783 lies at the base of a flexible loop in Eph-A4.

(E) The Gly-to-Ser substitution at this position (ΔΔG 0.6Kcal/mol) is predicted to affect loop stability.

Supplementary figure 5. Mutations affecting other members of the Ephrin family in VOGM patients displaying CM-AVM-like cutaneous manifestations, Related to Figure 3

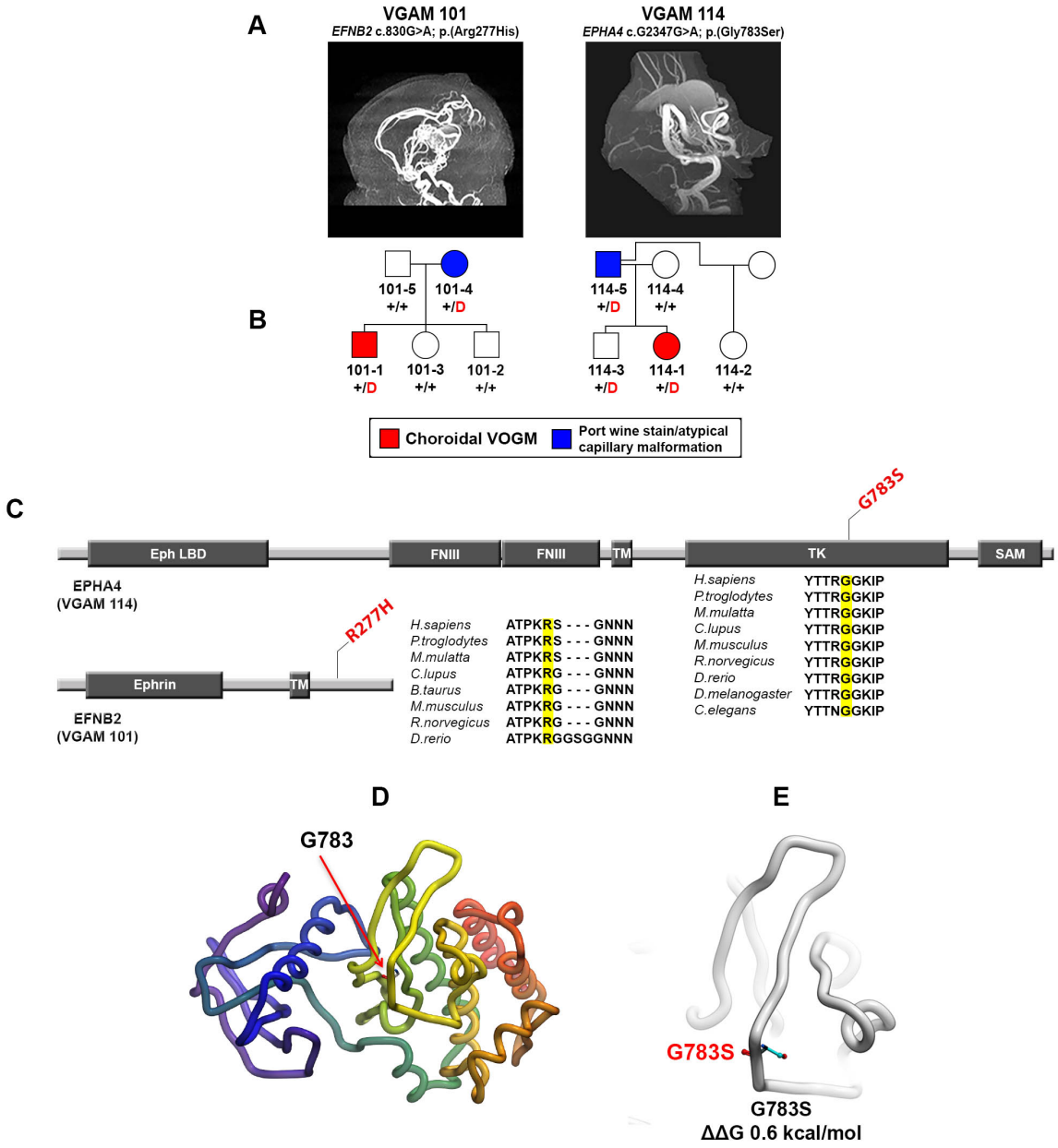

Supplementary figure 6. Damaging ACVR1 mutations in mural Vein of Galen malformation, Related to Figure 3

(A) Representative images from digital subtraction angiographies demonstrating mural Vein of Galen Malformations in probands.

(B) Pedigrees depicting kindred structure and phenotypic variance. Blue symbols represent atypical capillary malformations in individuals harboring the c.1118A>G; p.Asn373Ser mutation. Yellow coloring of half the symbol denotes concomitant presence of an atrial septal defect and (asterisk) partial anomalous pulmonary venous return in the proband of family KVGAM44. Red 'D' denotes damaging mutation, '+' denotes wild type sequence.

(C) Linear representation of the ACVR1 polypeptide, with functional domains represented as dark rectangles. Amino acid modifications are mapped (in red) on the protein structure. Conservation of the wild-type amino acid substituted by the two deleterious missense mutations is depicted below each. AR = activin receptor; TM = Transmembrane domain; KD = Kinase domain

(D) In silico modelling of p.Asn373Ser. Asn373 in a 3D model of ACVR1.

(E) Predicted energetically costly (ΔΔG 2.9Kcal/mol) loss of hydrogen bond formation between the Asn373 side chain and backbone atoms of Gly356, Lys243, Arg375 and the side chain of Ser244 caused by Asn373 substitution to serine.

Supplementary figure 6. Damaging ACVR1 mutations in mural Vein of Galen malformation, Related to Figure 3

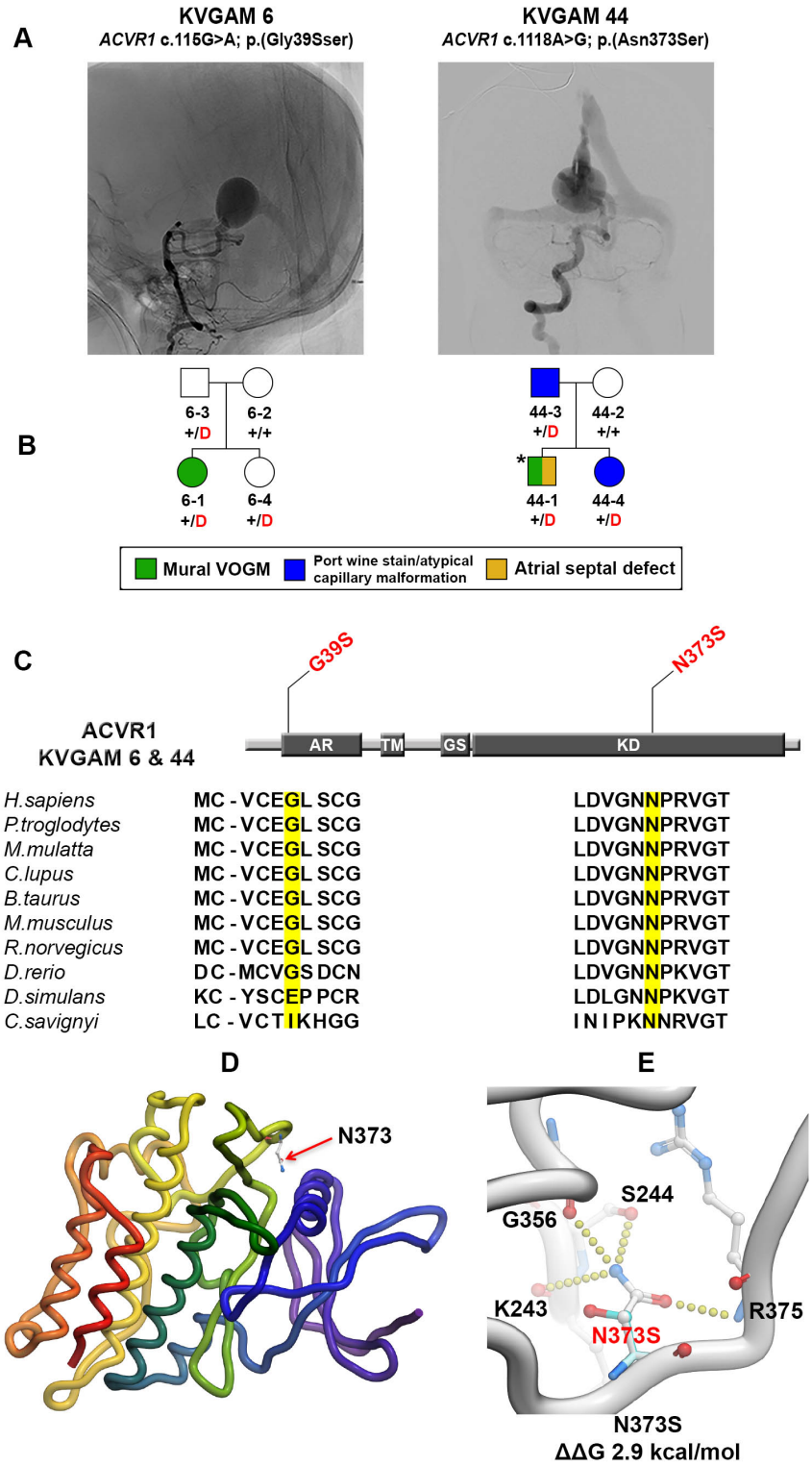

Supplementary figure 7. Interactome of mutated Ephrin receptor signaling genes in VOGM, Related to Table 2 and Figure 3

All 7 genes (highlighted) contributing to the significant result of the Ephrin receptor signaling pathway in IPA pathway analysis were input into String. These 7 genes are mapped into a single experimentally supported STRING interactome.

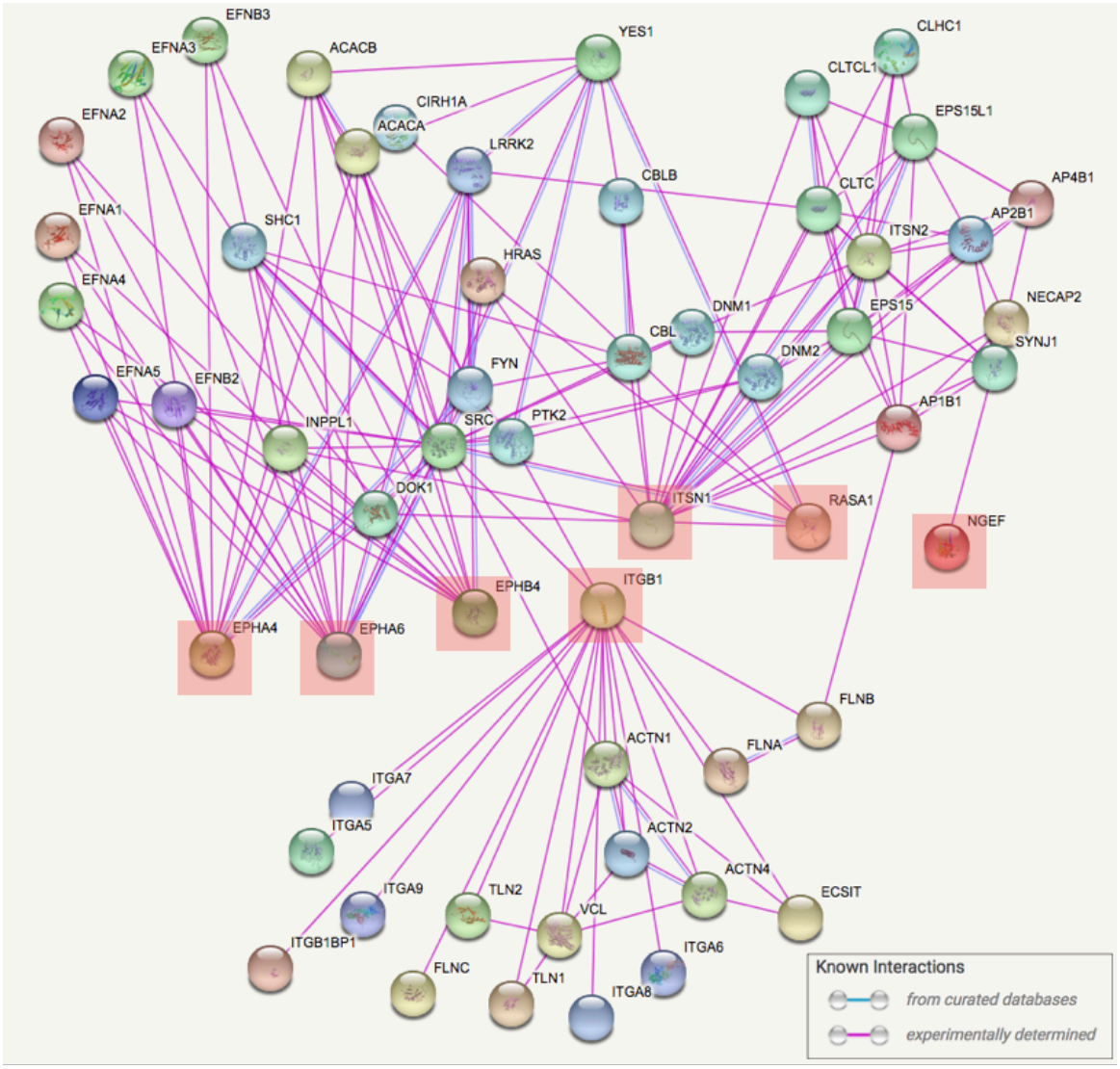

Supplementary figure 8. The genomic landscape of VOGM, Related to Figure 3
Schematic representation of signaling between two primitive endothelial cells showing contact-mediated interaction between the membrane-bound ligand Ephrin-B2 in the upper cell and its receptor, Eph-B4, in the lower cell. The figure depicts crosstalk between Eph-B4, its effector and binding partner RASA1, and activin type 1 receptors mediated by non-canonical TGF-b signaling. Mutations discovered in our cohort affecting EPHB4, EFNB2, and ACVR1 are shown in red, and previously reported mutations in RASA1, EPHB4, and ENG in VOGM patients are indicated in black. RASA1 p.Arg709* (highlighted in yellow) is the sole RASA1 mutation detected in our cohort.

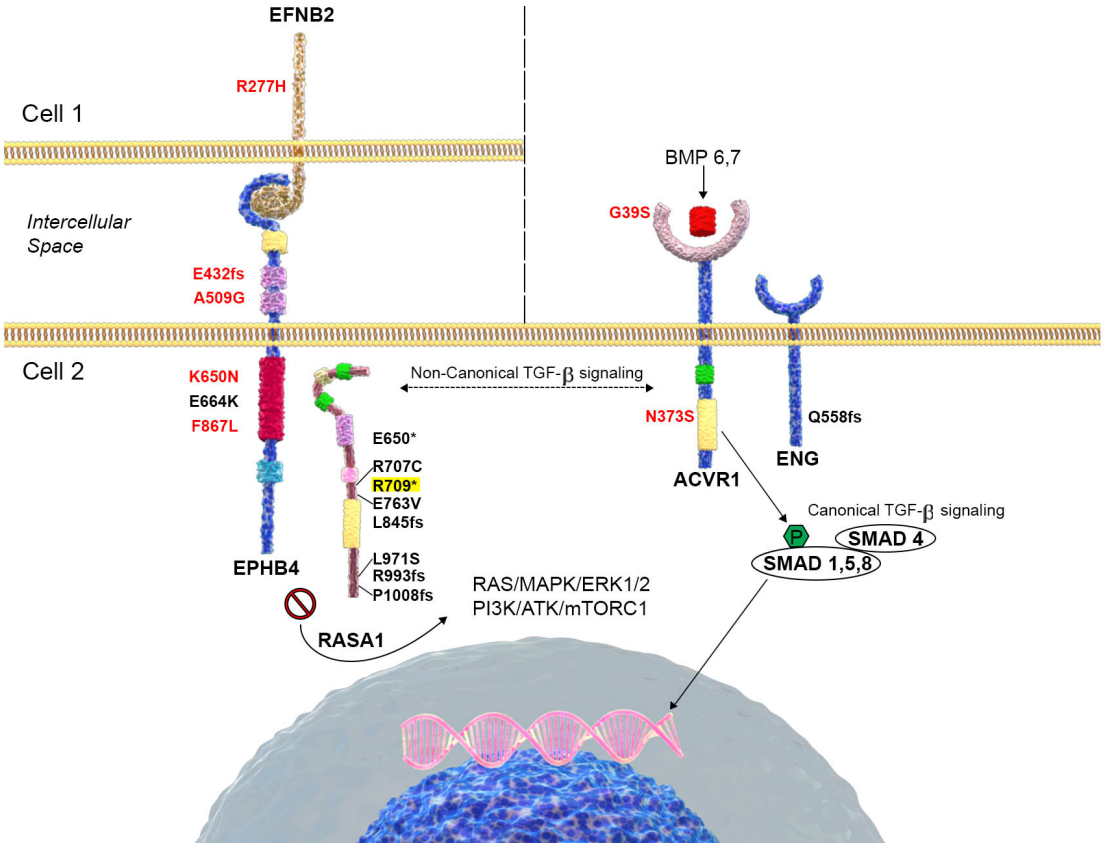

SUPPLEMENTARY TABLES

Supplementary Table 1. VOGM patient clinical and demographic characteristics, Related to STAR Methods

Variable			Type of VOGM *Choroidal (%)* 37 (67.27)	*Mural (%)* 18 (32.73)	Grand Total (%) 55 (100.00)
Gender					
	Female		11 (29.73)	8 (44.44)	19 (34.55)
	Male		26 (70.27)	10 (55.56)	36 (65.45)
		Total	37 (100.00)	18 (100.00)	55 (100.00)
Age at diagnosis					
	Prenatal		15 (40.54)	7 (38.89)	22 (40.00)
		Neonate (0-30 days)	12 (32.43)	0 (0.00)	12 (21.82)
		Infant (1 month-2 years)	9 (24.32)	10 (55.56)	19 (34.55)
	Postnatal	Young child (3-6 years)	0 (0.00)	0 (0.00)	0 (0.00)
		Child (7-12 years)	1 (2.70)	0 (0.00)	1 (1.82)
		Adolescent (13-17 years)	0 (0.00)	0 (0.00)	0 (0.00)
	Unknown		0 (0.00)	1 (5.56)	1 (1.82)
		Total	37 (100.00)	18 (100.00)	55 (100.00)
Term vs. preterm delivery					
	Term (≥ 37 wks)		32 (86.49)	13 (72.22)	45 (81.82)
	Preterm		4 (10.81)	4 (22.22)	8 (14.55)
	Unknown		1 (2.70)	1 (5.56)	2 (3.64)
		Total	37 (100.00)	18 (100.00)	55 (100.00)
Family history of cutaneous vascular abnormalities*					
	Yes		23 (62.16)	8 (44.44)	31 (56.36)
	No		7 (18.92)	7 (38.89)	14 (25.45)
	Unknown		7 (18.92)	3 (16.67)	10 (18.18)
		Total	37 (100.00)	18 (100.00)	55 (100.00)
Self-reported ethnicity					
	European		29 (78.38)	13 (72.22)	42 (76.36)
		European/Asian	3 (8.11)	1 (5.56)	4 (7.27)
	Mixed	European/Hispanic	1 (2.70)	1 (5.56)	2 (3.64)
		Latin American/African American	1 (2.70)	0 (0.00)	1 (1.82)
	Asian		1 (2.70)	0 (0.00)	1 (1.82)
	African		0 (0.00)	2 (11.11)	2 (3.64)
	Ashkenazi Jewish		0 (0.00)	1 (5.56)	1 (1.82)
	Unknown		2 (5.41)	0 (0.00)	2 (3.64)
		Total	37 (100.00)	18 (100.00)	55 (100.00)
Associated conditions					**Total**
	High output cardiac failure		23 (62.16)	1 (5.56)	24 (43.64)
	Progressive macrocephaly		22 (59.46)	13 (72.22)	35 (63.64)
	Hydrocephalus		24 (64.86)	9 (50.00)	33 (60.00)
	Prominent facial or scalp vasculature		18 (48.65)	9 (50.00)	27 (49.09)
	Structural cardiac abnormalities†		4 (10.81)	1 (5.56)	5 (9.09)

*History of vascular birthmarks was self-reported in most cases, including first and second-degree relatives.

†Structural cardiac abnormalities include atrial septal defects, congenital valvular insufficiency, partial anomalous pulmonary venous return, patent foramen ovale, patent ductus arteriosus, and congenital pulmonary artery stenosis.

Supplementary Table 2. Summary sequencing statistics for the VOGM cases and control cohorts, Related to START Methods			
Category	Cases*	Cases*	Controls
	(xGen; N=88)	(MedExome; N=71)	(Roche V2; N=5,367)
Read length (bp)	99	99	50-94
# of reads per sample (M)	48.9	53.7	99.7
Median coverage at each targeted base (X)	54.4	37.2	67
Mean coverage at each targeted base (X)	59.4	43.8	79.1
% of all reads that map to target	60.70%	48.30%	57.60%
% of all bases that map to target	46.10%	39.10%	49.00%
% of targeted bases read at least 8x	98.40%	96.30%	94.60%
% of targeted bases read at least 10x	98.00%	95.00%	93.40%
% of targeted bases read at least 15x	96.30%	89.80%	89.90%
% Mean error rate	0.30%	0.30%	0.40%

*88 VOGM samples were sequenced using the xGen Exome Research Panel v1.0 capture reagent (IDT). The remaining cases were sequenced using the MedExome capture reagent. 8X, 10X and 15X were comparable across the platforms.

Supplementary Table 3. Enrichment of *de novo* variant types in 52 VOGM and 1,789 control trios, Related to Table 1

	Cases, N = 52						Controls, N = 1,789					
	Observed		Expected		Enrichment	p-value	Observed		Expected		Enrichment	p-value
	N	Rate	N	Rate			N	Rate	N	Rate		
All Genes												
Total	63	1.21	58.10	1.12	1.08	0.28	1830	1.02	1949.9	1.09	0.94	1.00
Syn	15	0.29	16.50	0.32	0.91	0.68	484	0.27	549.6	0.31	0.88	1.00
D-Mis	14	0.27	6.80	0.13	2.05	0.01	222	0.12	232.8	0.13	0.95	0.77
T-Mis	29	0.56	29.70	0.57	0.98	0.58	974	0.54	993.3	0.56	0.98	0.73
LoF	5	0.10	5.10	0.10	0.98	0.58	150	0.08	174.3	0.10	0.86	0.97
Damaging	19	0.37	12.00	0.23	1.59	0.04	372	0.21	407.1	0.23	0.91	0.96

Syn = Synonymous single nucleotide variant; D-Mis = Missense variants with "D" annotation per MetaSVM; T-Mis = Missense variants with "T" or "." annotation per MetaSVM; LoF = Predicted loss-of-function variants (canonical splice site, frameshift indels, stop gains, and stop losses); Damaging = D-mis and/or LoF.

Supplementary Table 4. *De novo* burden analysis comparing cases to controls, Related to Table 1						
	# of *de novo* mutations		# of *de novo* mutations per subject			
	Cases N=52	Controls[&] N=1,789	Cases N=52	Controls[&] N=1,789	Binomial P-value*	Odds ratio (95% CI)[#]
LoF-intolerant genes (n = 3,230)						
Total	14	597.9	0.27	0.33	0.5	NA
Syn	2	150.7	0.04	0.08	0.38	NA
Mis	11	402.1	0.21	0.22	0.96	2.06 (0.45 - 9.41)
D-Mis	6	75.9	0.12	0.04	0.03	5.96 (1.17 - 30.22)
LoF	1	45.1	0.02	0.03	1	1.67 (0.15 - 18.85)
Damaging	7	121.0	0.13	0.07	0.12	4.36 (0.89 - 21.37)
All chromatin genes (n = 547)						
Total	4	77.1	0.08	0.04	0.42	NA
Syn	0	14.2	0.00	0.01	1	NA
Mis	3	55.8	0.06	0.03	0.51	NA
D-Mis	3	14.2	0.06	0.01	$3.4x10^{-3}$	NA
LoF	1	7.1	0.02	0.00	0.57	NA
Damaging	4	21.4	0.08	0.01	$8.6x10^{-4}$	NA
LoF-intolerant chromatin genes (n = 272)						
Total	4	55.8	0.08	0.03	0.16	NA
Syn	0	10.7	0.00	0.01	1	NA
Mis	3	41.5	0.06	0.02	0.26	NA
D-Mis	3	8.3	0.06	0.00	$9.0x10^{-5}$	NA
LoF	1	3.6	0.02	0.00	0.3	NA
Damaging	4	11.9	0.08	0.01	$3.9x10^{-6}$	NA

[&] Due to the difference in the *de novo* mutation rates between cases and controls, we adjusted the *de novo* mutation rate in controls to match the per-person rate by dividing the original rate per control by 0.84 (=1.02/1.21).

***** The p-values compare the number of *de novo* mutations between 52 case trios and 1,789 control trios using a two-tailed binomial exact test as shown previously (Sanders et al. 2012 Nature; Zaidi et al. 2013 Nature).

[#] The odds ratio calculates the proportion of *de novo* mutations in a specific category to synonymous *de novo* mutations and then compare these ratios in case trios versus control trios. NA, not applicable.

Supplementary Table 5. Damaging *de novo* mutation in loss-of-function intolerant chromatin modifier genes in 55 cases, Related to Table 1

Salient genetic information												Salient clinical and segregation information					
Proband code	**Gene**	**Coordinate (hg19)**	**Ethnicity**	**Inheritance**	**AA Change**	**gnomAD combined MAF****	**pLI**	**Missense Z-score**	**OMIM phenotype**	**CADD**	**MetaSVM**	**Type of VOGM**	**Cutaneous manifestations or non CNS AVMs in kindred?**	**Vascular cutaneous manifestations on proband?**	**Vascular Birthmarks/ AVMs on mother**	**Vascular Birthmarks/AVMs on father**	**Concordance with mutation type**
KVGAM38	*KAT6A*	8:41832271:G:A	Mexican	*De novo*	p.Thr478Ile	< 4.11E-06	1.00	2.14	Mental retardation (AD)	24.2	D	Choroidal	y	y	n	n	y
KVGAM26	*KMT2D*	12:49420060:C:T	European	*De novo*	p.Cys5230Tyr	< 4.06E-06	1.00	3.10	Kabuki syndrome (AD)	22.4	D	Choroidal	y	y	n	n	y
KVGAM20*	*SIRT1*	10:69666624:TC:T	European	*De novo*	p.Arg341fs5	< 3.63E-06	0.95	0.58	None	.	N/A	Choroidal	y	y	y	n	n
KVGAM29	*SMARCA2*	9:2086866:G:T	European	*De novo*	p.Arg855Leu	< 4.06E-06	1.00	5.57	Nicolaides-Baraitser syndrome (AD)	26.5	D	Mural	n	n	n	n	N/A

* This subject also carried a p.Val143Met mutation in CLDN14 transmitted from mother
** For variants not observed in public databases, their minor allele frequency is calculated as less than 1 out of total number of alleles sampled at the closest locus with allele number available

Supplementary Table 6a. Case-control analysis of gene burden of damaging variants in all probands versus 3,578 Autism parental controls, Related to Figure 3						
	Case		Control			
Gene	# mutant allele	# ref allele	# mutant allele	# ref allele	Fisher p value	Odds ratio
EPHB4	4	106	3	7,153	1.68E-06	89.97
MYH7	3	107	0	7,156	3.38E-06	Inf
AOC2	3	107	0	7,156	3.38E-06	Inf
CLDN14	3	107	0	7,156	3.38E-06	Inf
OTOG	2	108	0	7,156	2.27E-04	Inf
NALCN	2	108	0	7,156	2.27E-04	Inf
LTBP2	2	108	0	7,156	2.27E-04	Inf
MLH3	2	108	0	7,156	2.27E-04	Inf
PKM	2	108	0	7,156	2.27E-04	Inf
TPSG1	2	108	0	7,156	2.27E-04	Inf

Supplementary Table 6b. Case-control analysis of gene burden of damaging variants in all probands versus ExAC controls, Related to Figure 3						
	Case		Control			
Gene	# mutant allele	# ref allele	# mutant allele	# ref allele	Fisher p value	Odds ratio
EPHB4	4	106	92	121,318	1.98E-06	49.76
AOC2	3	107	39	121,373	8.07E-06	87.26
CLDN14	3	107	50	120,946	1.65E-05	67.82
MPST	2	108	17	116,829	1.48E-04	127.26
DNAH12	2	108	37	121,367	5.89E-04	60.74
EMILIN3	2	108	40	121,192	6.85E-04	56.11
ABHD17A	2	108	42	118,070	7.91E-04	52.06
PRKDC	1	109	0	121,412	9.05E-04	Inf
SEPT1	1	109	0	121,412	9.05E-04	Inf
ADGRL4	2	108	50	120,618	1.06E-03	44.67

Supplementary Table 7. Significant pathways in Ingenuity ® Pathway Analysis including intolerant genes harboring damaging de novo mutations, damaging rare transmitted mutations, and significantly mutated genes (*KEL*, *EPHB4*, *CLDN14*) (n = 128), Related to Table 1 and Figure 3

Rank	Ingenuity Canonical Pathways	P-value	Corrected P-value	Ratio	Genes
1	**Axonal Guidance Signaling**	**6.61E-08**	**1.33E-05**	**0.03**	***SLIT3, ITGB1, SHH, EPHB4, NGEF, ITSN1, EPHA4, KEL, SLIT2, ADAMTS2, MET, EPHA6, SHANK2, RASA1, NRP1***
2	nNOS Signaling in Skeletal Muscle Cells	1.32E-07	2.64E-05	0.15	*CACNA1G, CACNG2, CACNA1B, RYR2, CACNA2D3, CACNA1A*
3	GABA Receptor Signaling	1.41E-06	2.81E-04	0.07	*CACNA1G, CACNG2, CACNA1B, GABRB1, KCNH2, CACNA2D3, CACNA1A*
4	Netrin Signaling	2.19E-06	4.34E-04	0.09	*CACNA1G, CACNG2, CACNA1B, RYR2, CACNA2D3, CACNA1A*
5	FcγRIIB Signaling in B Lymphocytes	6.92E-06	1.36E-03	0.08	*CACNA1G, CACNG2, CD79B, CACNA1B, CACNA2D3, CACNA1A*
6	Corticotropin Releasing Hormone Signaling	1.74E-05	3.41E-03	0.05	*CACNA1G, CACNG2, SHH, CACNA1B, KRT1, CACNA2D3, CACNA1A*
7	G Beta Gamma Signaling	5.62E-05	0.01	0.05	*CACNA1G, CACNG2, CACNA1B, CACNA2D3, CACNA1A, DNM2*
8	Synaptic Long Term Depression	7.41E-05	0.01	0.04	*CACNA1G, CACNG2, CACNA1B, RYR2, PPP2R2B, CACNA2D3, CACNA1A*
9	**Ephrin Receptor Signaling**	**7.59E-05**	**0.01**	**0.04**	***ITGB1, EPHA6, NGEF, EPHB4, ITSN1, EPHA4, RASA1***
10	Androgen Signaling	1.55E-04	0.03	0.04	*CACNA1G, CACNG2, CACNA1B, POLR2H, CACNA2D3, CACNA1A*
11	CCR5 Signaling in Macrophages	2.40E-04	0.05	0.05	*CACNA1G,CACNG2,CACNA1B,CACNA2D3,CACNA1A*

Supplementary Table 8. Mutation burden in cases compared to European ethnicity-matched controls in IPA-determined significant pathways, Related to Table 1 and Figure 3

Control_Group	Pathway (# of intolerant genes)	Case_Carrier	Case_NonCarrier	CaseTotal	Control_Carrier*	Control_NonCarrier	ControlTotal	Enrichment	Confident_Interval	p-value
Autism	nNOS Signaling in Skeletal Muscle Cells (n = 18)	4	41	45	196	2,690	2,886	1.34	[0.43, Inf)	0.37
Autism	**Axonal Guidance Signaling (n = 161)**	**14**	**31**	**45**	**279**	**2,607**	**2,886**	**4.22**	**[2.29, Inf)**	**6.94E-05**
Autism	**Ephrin Receptor Signaling (n = 73)**	**8**	**37**	**45**	**127**	**2,759**	**2,886**	**4.69**	**[2.15, Inf)**	**8.36E-04**
Autism	Androgen Signaling (n = 55)	4	41	45	193	2,693	2,886	1.36	[0.44, Inf)	0.36
Autism	CCR5 Signaling in Macrophages (n = 31)	3	42	45	138	2,748	2,886	1.42	[0.37, Inf)	0.37
Autism	Corticotropin Releasing Hormone Signaling (n = 57)	5	40	45	244	2,642	2,886	1.35	[0.5, Inf)	0.33
Autism	FcγRIIB Signaling in B Lymphocytes (n = 36)	3	42	45	149	2,737	2,886	1.31	[0.34, Inf)	0.42
Autism	G Beta Gamma Signaling (n = 53)	4	41	45	189	2,697	2,886	1.39	[0.45, Inf)	0.34
Autism	GABA Receptor Signaling (n = 45)	6	39	45	175	2,711	2,886	2.38	[0.97, Inf)	0.06
Autism	Netrin Signaling (n = 32)	4	41	45	212	2,674	2,886	1.23	[0.4, Inf)	0.43
Autism	Synaptic Long Term Depression (n = 65)	5	40	45	289	2,597	2,886	1.12	[0.42, Inf)	0.48
ExAC	nNOS Signaling in Skeletal Muscle Cells (n = 18)	4	41	45	3,145	33,532	36,677	1.04	[0.34, Inf)	0.55
ExAC	**Axonal Guidance Signaling (n = 161)**	**14**	**31**	**45**	**3,878**	**32,799**	**36,677**	**3.82**	**[2.1, Inf)**	**1.52E-04**
ExAC	**Ephrin Receptor Signaling (n = 73)**	**8**	**37**	**45**	**1,621**	**35,056**	**36,677**	**4.68**	**[2.18, Inf)**	**7.33E-04**
ExAC	Androgen Signaling (n = 55)	4	41	45	4,718	31,959	36,677	0.66	[0.22, Inf)	0.85
ExAC	CCR5 Signaling in Macrophages (n = 31)	3	42	45	2,138	34,539	36,677	1.15	[0.3, Inf)	0.49
ExAC	Corticotropin Releasing Hormone Signaling (n = 57)	5	40	45	3,466	33,211	36,677	1.20	[0.45, Inf)	0.42
ExAC	FcγRIIB Signaling in B Lymphocytes (n = 36)	3	42	45	2,321	34,356	36,677	1.06	[0.28, Inf)	0.55
ExAC	G Beta Gamma Signaling (n = 53)	4	41	45	2,726	33,951	36,677	1.22	[0.4, Inf)	0.43
ExAC	GABA Receptor Signaling (n = 45)	6	39	45	2,995	33,682	36,677	1.73	[0.71, Inf)	0.16
ExAC	Netrin Signaling (n = 32)	4	41	45	3,361	33,316	36,677	0.97	[0.32, Inf)	0.60
ExAC	Synaptic Long Term Depression (n = 65)	5	40	45	4,494	32,183	36,677	0.89	[0.34, Inf)	0.66

P values were calculated using the one-tailed Fisher's Exact Test. Values in red bold are P values exceeding the Bonferroni multiple-testing cutoff (0.05/(2x11) = 2.27E-03)

* ExAC database does not provide individual level information, number of damaging mutations in each gene set carried by each individual was assumed to be 1.

Supplementary Table 9. Gene burden in cases compared to expectation for axonal guidance and Ephrin receptor signaling pathways, Related to Table 1 and Figure 3

Axon guidance signaling					Ephrin receptor signaling				
LoF-intolerant genes with damaging mutations in VOGM cases	**Observed**	**Expected**	**Enrichment**	**p-value**	**LoF-intolerant genes with damaging mutations in VOGM cases**	**Observed**	**Expected**	**Enrichment**	**p-value**
	18	7.14	2.52	**3.02E-04**		10	2.90	3.45	**7.28E-04**
LoF-intolerant genes with synonymous mutations in VOGM cases	**Observed**	**Expected**	**Enrichment**	**p-value**	**LoF-intolerant genes with synonymous mutations in VOGM cases**	**Observed**	**Expected**	**Enrichment**	**p-value**
	21	20.12	1.04	0.45		4	8.17	0.49	0.96
LoF-intolerant genes with damaging mutations in autism controls	**Observed**	**Expected**	**Enrichment**	**p-value**	**LoF-intolerant genes with damaging mutations in autism controls**	**Observed**	**Expected**	**Enrichment**	**p-value**
	372	348.77	1.07	0.11		166	141.56	1.17	0.02
LoF-intolerant genes with damaging mutations in ExAC controls	**Observed**	**Expected**	**Enrichment**	**p-value**	**LoF-intolerant genes with damaging mutations in ExAC controls**	**Observed**	**Expected**	**Enrichment**	**p-value**
	3878	3967.08	0.98	0.93		1621	1611.57	1.01	0.41

P values were calculated using the one-tailed binomial test comparing observed number of variants in LoF-intolerant genes that belong to statistically significant canonical pathways of interest to the expected number of mutations in each set (see Methods). Values in bold red are P values exceeding the Bonferroni multiple-testing cutoff (0.05/(2x3) = 0.008)

Supplementary table 10a. Gene burden in cases compared to expectation for axonal guidance pathway after removing genes in the ephrin signaling pathway, Related to Table 1 and Figure 3				
LoF-intolerant genes with damaging mutations in VOGM cases	**Observed**	**Expected**	**Enrichment**	**p-value**
	8	6.66	1.2	0.35

P values were calculated using the one-tailed binomial test comparing observed number of variants in LoF-intolerant genes that belong to statistically significant canonical pathways of interest to the expected number of mutations in each set (see Methods).

Supplementary Table 10b. Mutation burden in cases compared to European ethnicity-matched controls for axonal guidance pathway after removing genes in the ephrin signaling pathway, Related to Table 1 and Figure 3										
Control_Sample	**Pathway**	**Case_Carrier**	**Case_NonCarrier**	**CaseTotal**	**Control_Carrier***	**control_NonCarrier**	**ControlTotal**	**Enrichment**	**Confident_Interval**	**p-value**
Autism	Axonal Guidance Signaling (n = 161)	6	39	45	197	2,689	2,886	2.10	[0.86,Inf)	0.09
ExAC	Axonal Guidance Signaling (n = 161)	6	39	45	2,726	33,951	36,677	1.92	[0.79,Inf)	0.11

P values were calculated using the one-tailed Fisher's Exact Test. Bonferroni multiple-testing cutoff for this test is 0.05/2 = 0.025

* ExAC database does not provide individual level information, number of damaging mutations in each gene set carried by each individual was assumed to be 1.

Supplementary Table 11. Mutations in genes in the Ephrin receptor signaling pathway, Related to Table 1 and Figure 3

Proband code	Inheritance	Mutation Type	Gene	Coordinate (hg19)	Coding sequence variant	AA Modification	ExAC MAF*	gnomAD combined MAF*	pLI	Missense Z-score	OMIM phenotype	CADD	Meta SVM
VGAM105	Transmitted	LoF	*ITGB1*	chr10:33196073	N/A	Splice site	< 8.27E-06	< 4.15E-06	0.91	3.47	None	20.9	N/A
VGAM115	Transmitted	LoF	*EPHB4*	chr7:100417179	c.1295_1296del	p.Glu432fs1	< 9.06E-06	< 4.76E-06	0.99	2.84	Non-immune hydrops fetails with/without atrial septal defect	.	D
KVGAM25	Transmitted	D-mis		chr7:100414876	c.1526C>G	p.Ala509Gly	3.30E-05	1.13E-05				25	D
KVGAM33	Transmitted	D-mis		chr7:100410537	c.1950G>T	p.Lys650Asn	< 8.24E-06	< 4.06E-06				29.9	D
KVGAM18	Transmitted	D-mis		chr7:100403202	c.2599T>C	p.Phe867Leu	< 9.03E-06	< 5.17E-06				31	D
KVGAM55	Transmitted	D-mis	*NGEF*	chr2:233745889	c.1909G>A	p.Asp637Asn	2.83E-05	1.22E-05	0.95	2.18	None	34	D
KVGAM7	Transmitted	D-mis	*ITSN1*	chr21:35260471	c.5033C>T	p.Thr1678Met	1.89E-05	8.13E-06	1.00	3.44	None	34	D
VGAM114	Transmitted	D-mis	*EPHA4*	chr2:222299011	c.G2347G>A	p.Gly783Ser	< 8.28E-06	< 4.07E-06	1.00	3.15	None	34	D
KVGAM45	Transmitted	D-mis	*EPHA6*	chr3:96706498	c.775C>T	p.Arg259Cys	< 8.38E-06	< 3.23E-05	0.95	0.93	None	34	D
KVGAM42	Transmitted	LoF	*RASA1*	chr5:86672323	c.2125C>T	p.Arg709*	< 8.26E-06	< 3.23E-05	1.00	2.96	CM-AVM1; Parkes Weber Syndrome; Somatic basal cell carcinoma	40	N/A

* For variants not observed in public databases, their minor allele frequency is calculated as less than 1 out of total number of alleles sampled at the closest locus with allele number available

Supplementary Table 12. Transmitted VOGM mutations in Mendelian AVM genes, Related to Figure 3

Family	Type of VOGM	Ethnicity	Gene	Mutation	Domain affected	ExAC MAF*	gnomAD MAF*	pLI	MetaSVM	CADD
KVGAM6	Mural	European	*ACVR1*[&]	p.(G39S)	Activin receptor	< 8.24E-06	3.24E-05	0.96	D	24.8
KVGAM44	Mural	European	*ACVR1*[&]	p.(N373S)	Kinase domain	< 8.26E-06	< 4.07E-06	0.96	T	24.1
VGAM100	Choroidal	Mexican	*ACVRL1*	p.(R484Q)	Kinase domain	< 8.28E-06	< 3.24E-05	0.01	D	33

[&] *ACVR1* is a paralog of *ACVRL1*

* For variants not observed in public databases, their minor allele frequency is calculated as less than 1 out of total number of alleles sampled at the closest locus with allele number available

Supplementary Table 13. Distribution of highly pathogenic mutations in VOGM patients with different subphenotypes, Related to Table 1, Figure 3, and STAR Methods

Proband Code	Gender	Ethnicity	Sub-Phenotype at Diagnosis	Fetal Age (weeks)	Postnatal Age at Diagnosis	Gene	Amino Acid Change	Type	Transmission	Proband with Capillary Malformation	Relatives with Capillary Malformation	Other phenotypes
KVGAM1	M	European	Choroidal		*7 mo.*					n	n	Neurodevelopmental delay
KVGAM10	M	European	Choroidal	*34*		*KEL*	p.Gln321*	stopgain	*De novo*	n	y	Pulmonary hypertension, neurodevelopmental delay
KVGAM15	M	European	Choroidal		*3 d.*					n	y	Patent ductus arteriosis, neurodevelopmental delay
KVGAM18	M	European	Choroidal	*40*		*EPHB4*	p.Phe867Leu	Dmis	Transmitted	n	y	Cryptorchidism, strabismus, cerebral palsy
KVGAM2	M	Undetermined	Choroidal	*33*						n	n	n
KVGAM20	F	European	Choroidal		*6 mo.*	*CLDN14* *SIRT1*	p.Val143Met p.Arg341fs5	Dmis Frameshift deletion	Transmitted *De novo*	y	y	n
KVGAM22	F	European	Choroidal		*5 mo.*					n	n	n
KVGAM24	M	European	Choroidal		*8 yr.*					n	n	Recurrent epistaxis
KVGAM25	M	European	Choroidal		*19 d.*	*EPHB4*	p.Ala509Gly	Dmis	Transmitted	n	n	Pectus excavatum
KVGAM26	M	European	Choroidal		*1 d.*	*KMT2D*	p.Cys5230Tyr	Dmis	*De novo*	n	n	Hypothyroidism, low set ears, long and everted palpebral fissures, neurodevelopmental delay, seizures
KVGAM30	M	European	Choroidal		*5 d.*					n	y	Neurodevelopmental delay, seizures
KVGAM31	F	European	Choroidal		*11 mo.*					n	n	Neurodevelopmental delay
KVGAM32	M	European	Choroidal		*7 d.*					n	y	n
KVGAM33	F	Mexican	Choroidal		*1 d.*	*EPHB4*	p.Lys650Asn	Dmis	Transmitted	n	y	Neurodevelopmental delay
KVGAM34	M	European	Choroidal	*35*						n	n	Neurodevelopmental delay, attention deficit hyperactivity disorder
KVGAM35	M	European	Choroidal	*37*						n	n	n
KVGAM37	M	European	Choroidal	*36*						n	y	Neurodevelopmental delay
KVGAM38	M	Mexican	Choroidal		*6 d.*	*KAT6A*	p.Thr478Ile	Dmis	*De novo*	y	n	Neurodevelopmental delay, seizures
KVGAM4	M	Undetermined	Choroidal		*2 d.*					n	n	n
KVGAM40	M	European	Choroidal		*3 mo.*					n	y	Cerebral palsy, hip dysplasia, visual impairment, gastroesaphageal reflux disease, neurodevelopmental delay, seizures
KVGAM52	F	European	Choroidal	*32*						n	n	n
KVGAM54	F	European	Choroidal	*38*						n	y	n
KVGAM55	F	European	Mural	*20*		*NGEF*	p.Asp637Asn	Dmis	Transmitted	n	n	n
KVGAM7	F	European	Choroidal		*1 yr.*	*ITSN1*	p.Thr1678Met	Dmis	Transmitted	n	y	Pulmonary valve stenosis, neurodevelopmental delay
KVGAM8	M	European	Choroidal	*39*						n	y	Neurodevelopmental delay, seizures
KVGAM9	F	European	Choroidal	*38*						n	n	Patent ductus arteriosis, patent foramen ovale, seizures
VGAM100	F	Mexican	Choroidal	*34*		*ACVRL1* *CLDN14*	p.R484Q p.Ala113Pro	Dmis Dmis	Transmitted Transmitted	n	n	Strabismus
VGAM101	M	European	Choroidal	*36*		*EFNB2*	p.Arg277His	Dmis	Transmitted	y	y	Hip dysplasia, neurodevelopmental delay, seizures
VGAM104	M	European	Choroidal		*3 d.*					y	n	Cerebral palsy, neurodevelopmental delay
VGAM107	F	European	Choroidal		*4 d.*					n	n	Medulloblastoma, seizures
VGAM108	M	European	Choroidal		*2 mo.*					n	y	Asthma
VGAM109	M	Mexican	Choroidal		*3 d.*					y	y	Cerebral palsy, neurodevelopmental delay, seizures
VGAM111	M	European	Choroidal	*31*						n	n	Cerebral palsy, gastroesophageal reflux disease, renal agenesis, precocious puberty, mitral insufficiency, neurodevelopmental delay, seizures
VGAM112	M	European	Choroidal	*36*						n	n	n
VGAM113	M	European	Choroidal		*2 d.*					n	n	Chiari Type I malformation
VGAM114	F	European	Choroidal		*11 mo.*	*EPHA4*	p.Gly783Ser	Dmis	Transmitted	y	y	n
VGAM115	M	European	Choroidal		*3 mo.*	*EPHB4*	p.Glu432fs1	Frameshift deletion	Transmitted	n	y	Neurodevelopmental delay, seizures
VGAM47	M	European	Choroidal	*29*						n	n	Hypospadias
KVGAM11	M	European	Mural		*6 mo.*					n	y	n
KVGAM29	M	European	Mural	*38*		*SMARCA2*	p.Arg855Leu	Dmis	*De novo*	n	n	Seizures
KVGAM3	F	European	Mural	*31*						n	n	n
KVGAM36	F	European	Mural		*3 mo.*					n	y	n
KVGAM41	M	European	Mural		*14 mo.*					n	y	Major depressive disorder with psychotic features, attention deficit hyperactivity disorder, hydrocephalus, migraines
KVGAM42	F	Mexican	Mural		*6 mo.*	*RASA1*	p.Arg709*	stopgain	Transmitted	y	y	Cerebral palsy, seizures
KVGAM43	M	African	Mural		*14 mo.*					n	y	n
KVGAM44	M	European	Mural		*9 mo.*	*ACVR1*	p.Asn373Ser	T-mis (high CADD = 24.1)	Transmitted	n	y	Atrial septal defect, partial anomalous pulmonary venous return
KVGAM45	F	European	Mural		*6 mo.*	*EPHA6* *KEL*	p.Arg259Cys p.Gly202Ser	Dmis T-mis (high CADD = 22.6)	Transmitted *De novo*	n	n	Neurodevelopmental delay, seizures
KVGAM49	M	Undetermined	Mural		*16 mo.*					n	n	n
KVGAM5	M	Mexican	Mural	*28*						n	n	Cystic fibrosis
KVGAM51	F	European	Mural	*31*		*CLDN14*	p.Val143Met	Dmis	Transmitted	n	n	n
KVGAM6	F	European	Mural	*35*		*ACVR1*	p.Gly39Ser	Dmis	Transmitted	n	n	n
VGAM102	M	European	Mural		*3 d.*					n	n	Attention deficit hyperactivity disorder, recurrent epistaxis
VGAM105	M	European	Mural		*2 mo.*	*ITGB1*	Splice site	splice site	Transmitted	n	n	Chiari Type I malformation
VGAM110	F	European	Mural	*39*						y	n	n
VGAM46	M	European	Mural		*1 yr.*					n	n	n

Gender M = Male, F = Female; Dmis = Missense variants with 'D' annotation per MetaSVM; T-mis = Missense variants with 'T' or '.' annotation per MetaSVM; y = Yes; n = No

VII. CLDN14 Knockdown Impairs Vasculogenesis and Brain Vasculature in *Xenopus tropicalis*

VI. CLDN14 Knockdown Impairs Vasculogenesis and Brain Vasculature in *Xenopus tropicalis*

INTRODUCTION

Recent advances have revealed whole exome wide significant mutations in *EPHB4* (Duran et al., 2018b; Vivanti et al., 2018), de novo chromatin modifying genes, and *CLDN14* (Duran et al., 2018b) in patients with Vein of Galen Malformation. It has been proposed that Vein of Galen Malformation is a phenotypically variable condition with a possible second hit causing vascular malformations throughout the body, typically capillary malformations (Duran et al., 2018b). The need for functional validation of whole exome wide significant findings in genetic studies to determine disease causality is growing (Neveling et al., 2013). *Xenopus tropicalis* offer a rapid and easy solution to functional validation of reported variants. *Xenopus* lay thousands of eggs which can be easily manipulated with microinjections of mRNA or CRISPR/Cas9, mature within several days, and can easily be screened, all at low cost compared to mice (Bhattacharya et al., 2015).

The APJ receptor, also known as *msr,* is important for both vasculogenesis including the intersegmental vessels and tail veins (Cox et al., 2006; Devic et al., 1996) and has been used as an in situ hybridization marker for drug screens testing drugs that effect vasculature (Cha et al., 2012; Kalin et al., 2009). *EPHB4* is a venous vascular marker an important receptor in determining arterio-venous specification (Wang et al., 1998), the disruption of which causes arteriovenous malformations in developing animals (Adams et al., 1999) and

VOGM in humans (Duran et al., 2018b; Vivanti et al., 2018). Helbling and colleagues demonstrated the *EPHB4* and EphrinB2 expression pattern in *Xenopus*. *EPHB4* was determined to be in the forebrain, midbrain-hindbrain boundary, posterior cardinal vein, intersomitic veins throughout development with its ligand Ephrin-B2 located in the hindbrain, somites, and visceral arches (Helbling et al., 1999). A dominant negative, truncated *EPHB4* resulted in abnormal venous vasculature developing into, rather than between, the somites (Helbling et al. 2000) and recapitulated the phenotypes of *Ephrinb2* KO mice (Wang et al., 1998) and *Rasa1* mutant mice (Henkemeyer et al., 1995). Less is known about *CLDN14* in *Xenopus*. **Raciti and colleagues** found that CLDN14 was expressed at stage 34 in *Xenopus laevis*, cousin to *X. tropicalis*, in the intermediate and distal duct as well as the head (Raciti et al., 2008).

Xenopus embryos are transparent which allows direct visualization of blood vessels, especially in the tail which is thin, yet difficult in other regions and organs particularly in the brain. One of the early attempts to delineate the blood vessels of the brain involved observing the optic tectum to see the blood vessels and use flowing red blood cells to confirm their location (Rovainen and Kakarala, 1989). The use of intracardiac FITC dextran allowed better visualization of patent vessels but it did not allow visualization of the deeper vasculature (Tiedeken and Rovainen, 1991). The FITC dextran did however allow researchers to observe the effects of drugs such as adenosine and their antagonists (Jen and Rovainen, 1994). Levine and colleagues (Levine et al., 2003)created the technique of intracadiac Dil-Acl-LDL and used their technique to visualize the developing vasculature from stages 33-46. This technique has been refined and elaborated on by others

(Ohk and Jung, 2017). Dil-Acl-LDL improved the visualization of deeper vasculature but it was still limited to relatively superficial vessels that were patent. The creation of *Xflk-1*:GFP transgenic *X. laevis* (Doherty et al., 2007) allowed direct visualization not only of patent vessels but the stages of angiogenesis from endothelial cell migration and sprouting to lumenization. This has greatly improved the ability to live image and study *in vivo* vasculogenesis and angiogenesis. However, as embryos develop, it becomes difficult to visualize deeper vessel structures.

In this thesis, I demonstrate the application and modification of established clearing techniques (Hama et al., 2015) to improve visualization of the full thickness of the *Xenopus* brain vasculature, using the zebrafish vascular map (Isogai et al., 2001) and previous studies on the optic tectum in *Xenopus* (Rovainen and Kakarala, 1989; Tiedeken and Rovainen, 1991) as guides. We generate an *in situ* probe of *CLDN14* for *X. tropicalis* examining expression in the whole embryo (Raciti et al., 2008) and in the brain at different stages of development. Using this new clearing application, we compare the expression of *in situ* marker *msr* as well as the brain vasculature of embryos injected with sgRNA targeted against *RASA1, EPHB4,* and *CLDN14*. Finally, we rescue the *CLDN14* CRISPR/Cas9 injected animals with wild type (WT) human *CLDN14* compared to the recurrent patient mutation (Mut) *CLDN14* p.V143M(Duran et al., 2018b).

RESULTS

EPHB4 and CLDN14 co-immunoprecipitate *in vitro*

Before beginning our investigation into the effects of knockdown on individual genes in *Xenopus*, we wanted to ascertain the relationship between *EPHB4* and *CLDN14 in vivo*. Human *CLDN14* Flag tagged constructs were created, both WT and one with the recurrent mutation p.Val143Met from Duran and colleagues (Duran et al., 2018b)(**see methods**). Combinations of wild type HA-Tag *EPHB4* constructs and wild-type vs. mutant *CLDN14* constructs were transfected simultaneously into COS-7 cells and immunoprecipitation was performed (**see methods**). Both wild type and mutant CLDN14 co-immunoprecipitated with EPHB4 (**Fig. 1**).

CRISPR/Cas9 KD of CLDN14 decreased *msr* expression

CRISPR sgRNAs were synthesized and confirmed to cause double strand cutting (**see methods**). Embryos injected with confirmed Cas 9 and CRISPR sgRNAs against RASA1, EPHB4, and CLDN14 were collected at stage 34 and fixed. *In situ* hybridization was performed using in situ marker *msr* (**Fig. 2A**). Embryos were scored for normal expression (ISAs and un-interrupted posterior cardinal vein, **Fig. 2B**), abnormal (interrupted PCV or absent/diminished ISAs, **Fig. 2C**), or absent (lack of any PCV or ISAs, **Fig. 2D**), and percentages of all embryos were compared to one another (**Fig. 2E**). Two-way ANOVA revealed significant differences in normal, abnormal, and absent expression across conditions ($p<0.0001$). Further examination revealed significant decrease in normal expression of Uninjected Controls (UICs) compared to RASA1 ($p=0.0002$), EPHB4

($p<0.0001$), and CLDN14 ($p<0.0001$). There was also significant increase in abnormal expression of UICs compared to *RASA1* ($p=0.0015$), *EPHB4* ($p=0.0028$), and *CLDN14* ($p=0.0001$) (**Fig. 2E**) CRISPR/Cas9 injected embryos. There was no significant difference amongst any conditions with absent expression, and no significant difference amongst *RASA1*, *EPHB4*, and *CLDN14* CRISPR/Cas9 injected embryos in either normal or abnormal expression of *msr*.

Xenopus brain vasculature

The neural tube of *Xenopus tropicalis* closes around stages 19-20 and continues to develop further, becoming a more complex structure with recognizable telencephalon, mesencephalon, and rhombencephalon structures in the *Xenopus* after developmental stage 38. The skin is covered by melanocytes (**Fig. 3A**), which limit the visualization of the superficial, and most dorsal vasculature, of the brain (**Fig. B**) preventing direct observation of the vasculature. The clearing of the animal (Hama et al., 2015)(**Hama et al. 2015**) and extraction of the brain allows visualization of the deeper vasculature to the most ventral side of the brain (**Fig. C**).

CRISPR/Cas9 KD of VOGM genes causes decreased posterior venous plexus area

Xflk-1:GFP embryos injected with CRISPR/Cas9 against *RASA 1*, *EPHB4*, and *CLDN14* were collected at stage 47, fixed, cleared, and brains were extracted for confocal microscopy (**see methods**). The posterior venous plexus (PVP) develops from the Dorsal longitudinal vein, the evolutionary precursor to the Median Prosencephalic Vein (Aurboonyawat et al., 2007). The dorsal most layer of the brain vasculature was analyzed,

specifically the PVP area (**Fig. 4C**), and ANOVA one-way test between conditions was significant ($F(6,69) = 4.828$, $p=0.0004$). Further analysis revealed that *RASA1* CRISPR/Cas9 injected animals showed significant increase in the PVP area compared to UICs ($p= 0.0160$), Cas9 only injected animals ($p=0.0223$), and CLDN14 CRISPR/Cas9 injected animals ($p=0.0357$) (**Fig. 4E**). There were no other significant differences between conditions. Attempts at rescue the PVP area with wild type (WT) vs. mutant V143M (Mut) human CLDN14 mRNA were not successful, with no significant differences either compared to UIC, Cas9, CRISPR/Cas9 of CLDN14, or compared to each other.

CRISPR/Cas9 KD of VOGM genes causes decreased Mesencephalic Vein Length

The Mesencephalic Vein (MSV) makes up part of the deep venous drainage system in mammals, and helps drain blood from the VOGM in affected patients. The MSV lengths (**Fig. 4 B**) of CRISPR/Cas9 injected animals were compared and ANOVA one-way test between conditions was significant ($F= 16.76$, $p<0.0001$). Further analysis demonstrated significance of conditions for *RASA1*, *EPHBB4*, and *CLDN14* CRISPR/Cas9 injected animals compared to both UIC (RASA1 $p<0.0001$; EPHB4 $p<0.0001$; CLDN14 $p=0.0006$) as well as Cas9 only (RASA1 $p<0.0001$; EPHB4 $p<0.0001$; CLDN14 $p=0.001$) (**Fig. 4D**). There was no significant difference between UIC ($p=0.5377$), nor Cas9 only ($p=0.5307$), compared to CLDN14 CRISPR/Cas9 + WT mRNA. However, the same was true for CLDN14 CRISPR/Cas9 + Mut mRNA, and there was no significant difference either between the WT mRNA or Mut mRNA injected conditions, nor *CLDN14* CRISPR/Cas9 alone compared to CLDN14 CRISPR/Cas9 + WT vs. Mut mRNA. No other significant differences between conditions

DISCUSSION

This work suggests an interconnection between *EPHB4* and *CLDN14* and the similar impact they each have on developmental vasculature, strengthening their implication in VOGM. When compared to the known gene, *RASA1*, both *EPHB4* and *CLDN14* demonstrated similar effects on abnormal vasculogenesis as measured by in situ marker *msr*. However, it remains unclear whether or not they are acting along the same pathway or mechanism, or if they are completely independent pathways.

Previous work using EPHB4 morpholino in zebrafish noted abnormalities in both the dorsal longitudinal vein, with duplication or increased size/area, and the MSVs with either narrowing, absence, or duplication (Vivanti et al., 2018). Although we observed differences of UIC and Cas9 compared to CRISPR/Cas9 injected animals (not shown), namely more deranged vasculature in CRISPR/Cas9 injected animals, in this work we attempted a more quantitative rather than observational approach. Additionally, CRISPR/Cas9 injection of *EPHB4* and *CLDN14* also decreased MSV length in a similar fashion to *RASA1*. However, there was no significant difference between CRISPR/Cas9 injections of EPHB4 or CLDN14 compared to UIC or Cas9 only for the PVP, which is the more relevant as the evolutionary precursor to the Median Prosencephalic Vein which is associated with VOGM (Aurboonyawat et al., 2007). On the contrary, *RASA1* CRISPR/Cas9 injected animals had significantly increased PVP area, compared to UIC, Cas9, and *CLDN14* CRISPR/Cas9 injected animals, suggesting increased angiogenesis and abnormal vasculature.

Coinjection of CLDN14 CRISPR/Cas9 with either WT or Mut mRNA failed to rescue the PVP area or MSV length when compared to CLDN14 CRISPR/Cas9 only injected embryos. This is likely due to insufficient data to make meaningful comparisons and analyses. Future investigation will continue to compare the brain vasculature, and perhaps the vasculogenesis using in situ hybridization as well.

The lack of significant findings may be due to the limitations of the *Xenopus* model and difficulties extracting and imaging the brains (see below) which contributed to the low number of replicates for all *CLDN14* conditions, with or without mRNA, with ranges of n=1-8 for all conditions in examining the MSV lengths and PVP area. Although CRISPR/Cas9 successfully causes double strand breaks and subsequent knockout of candidate genes using the methods applied here, the cutting efficiency is not 100% throughout all cells and is instead mosaic (Bhattacharya et al., 2015). This may contribute to the range of findings in CRISPR/Cas9 injected animals' PVP area as the CRISPR/Cas9 double stranded break is not always certain to occur in cells in vascular and endothelial lineages.

Evidence of EPHB4 and CLDN14 interactions

Claudins have been shown to be associated with and interact with various ephrins and Ephs. Both claudin-1 and claudin-4 are co-localized with ephrin-B2 and EphB2 on the cell surface of adhering epithelial cells which come into contact in the midline (Dravis and Henkemeyer, 2011). This interaction was impaired in ephrin-B2-Beta-gal fusion

suggesting a possible extracellular (Dravis and Henkemeyer, 2011). EPHA2 has been shown to associate with Claudin-4 extracellularly which allows EPHA2 to phosphorylate Claudin 4 intracellularly at Tyr-208, thereby increasing paracellular permeability (Tanaka et al., 2005a). Furthermore, binding of claudins to cause cell-cell interactions has also been associated with the interaction between claudins as well as induction of EPH phosphorylation (Tanaka et al., 2005b).

Our findings contribute to the growing evidence of a connection between EPHB4 and RASA1. The co-immunoprecipitation of WT EPHB4 and both WT and Mut CLDN14 suggest some yet unknown interaction. The significant findings of abnormal vasculogenesis and MSV length further lend to this connection. CLDN11 was recently found to interact only with EphrinB2 on osteoclasts but was found to only interact with EPHB4 on osteoblasts (Baek et al., 2018). While the various motifs and mechanisms that allow the specific interaction between CLDN14 and EPHB4/ Ephrin B2, is not well known, our results from co-IP indicate that this interaction is possible and merits further investigation.

Limitations of the *Xenopus* model

We found that the use of the zebrafish brain vascular map served as a useful guide for studying the brain vasculature of *Xenopus tropicalis* (Isogai et al., 2001). There were however still difficulties with assuring the identity of the different vessels. *Xenopus* offer several difficulties in observing brain vasculature: 1) melanocytes which overly the brain, 2) auto-fluorescence, 3) extraction of brains, and 4) mounting. Melanocytes which overly

the brain vasculature are the foremost problem in observing the brain vasculature. The melanocytes are more concentrated over the brain and early spinal cord, blocking direct observation of vessels *in vivo*. While melanocytes could be removed with other methods including PTU (Milos and Dingle, 1978), or direct light exposure on a light box for 4 hours (direct observation made by lab colleague), however these might cause unknown consequences on the brain vasculature or reduce the GFP signal.

The high background fluorescence generated in *Xenopus* (Lee and Bezanilla, 2019), though more prominent in the tailbud stages, still remains slightly during stages 46-47 when our observations were made. The green fluorescent background, in combination with the proteins and cellular contents, prevented visualization of deeper vasculature structures in vivo. The use of clearing techniques (Hama et al., 2015)) removed the fluorescent background without effecting the GFP signal and thereby allowed visualization of the full thickness of the brain and all the brain's vasculature. Due to the round head of dorsal aspect of the *Xenopus* embryo, we extracted brains from fixed embryos at stages 46-47. However, with extraction of the brain, the tissue of skin would often fuse to the brain tissue overlying the 4^{th} ventricle which also contained the vessels. Removal of the brains would often incidentally de-roof the 4^{th} ventricle thereby destroying the vessels of interest in the process. Finally, to observe all levels of the brain vasculature, dorsal to ventral, we mounted brains between two coverslips using Dow Corning high vacuum grease so as not to completely flatten the brains and still visualize the 3D structure. However, there was no way to standardize this approach and so some brains may have been more compressed than others.

We attempted the use of optical coherence tomography (OCT) to observe vessels in vivo both in the tail and in the brain. OCT can provide resolutions similar to histology but in a fraction of the time or effort (Huang et al., 2015). While standard Doppler allowed good visualization of the heart, outflow tract, and dorsal artery and both dorsal and ventral veins of the tail, it did not allow adequate visualization of the remaining smaller tail vessels. Vessels on the dorsal aspect of the brain were also unable to be visualized due to the small caliber, thinness as they overly the comparatively vast 4th ventricle of the brain. Though we did not attempt it in this study, OCT may be better suited at assessing the downstream impact of candidate gene knockout on blood flow to the brain by examining changes in the size of ventricles and the parenchyma itself as has been done by our group studying candidate hydrocephalus genes in *Xenopus tropicalis* (data not yet published).

Future work studying the vasculature of brain below the most dorsal aspect necessitates further techniques. The use of a combined *flk1:GFP* and albino model may solve the issue of melanocytes but will not address the issue of auto-fluorescence preventing the observation of deeper structures. Future work may also benefit from a mammalian model to more specifically address the effects on the vein of Galen proper in heterozygous animals, as many patients presented with inherited mutations (Duran et al., 2018b) rather complete knockdown with CRISPR/Cas9,

MATERIALS AND METHODS

CRISPR/Cas9 design and creation

CRISPRs will be designed as previously described (Deniz et al., 2018). CRISPRs are designed by a combination of CRISPRscan.org (Doench et al., 2016; Moreno-Mateos et al., 2015) and UCSC genome browser (Kent et al., 2002) by selecting a CRISPR with a high score (>60), targets an early exon, few off targets by All (Hsu et al., 2013) or Seed (Cong et al., 2013), and a low CFD (Doench et al., 2016). The final CRISPR sequence created is 5'-CTAGCTAATACGACTCACTATAGG - n(18) target sequence - GTTTAGAGCTAGAAATAGCAAG-3'as previously described (Bhattacharya et al., 2015). CRISPR sgRNA primers can be seen in **Table 1**. The CRISPR is created by following the protocol of the EnGen sgRNA synthesis kit (NEB). RNA is purified using the Zymo RNA Clean and Concentrator kit. The CRISPR concentration is measured by NanoDrop, diluted, and stored at -80C. Cas9 Protein was ordered from PNA-Bio (Item #CP01) and eluted to stock concentration of 2 ng/nL. We inject Cas9 protein at a concentration of 1.6ng/ embryo.

Constructs

Human CLDN14 was obtained from the hORFeome v8.1 (HsCD00512723) (Yang et al., 2011). Plasmids were transformed into XL10 gold cells. A miniprep was performed from the cultured colonies using the Qiagen miniprep kit and then sequenced using T7 and Sp6. Gateway cloning was performed using standard procedures using Gateway LR Clonase II

Enzyme mix (Invitrogen) into pDEST vectors, with or without mCherry. Sequence was confirmed by Sanger sequencing.

Patient mutations were created using the Q5 Site-directed mutagenesis kit and primers designed using the NEB Base Changer online tool http://nebasechanger.neb.com/. Primers can be found in **Table 1**. Point mutations were confirmed by sequencing. WT and mutant mRNA was created from the WT and point mutated vectors respectively using the mMessage mMachine kit (Ambion), nanodroped, diluted, and stored at -80C in aliquots for injection. Vectors were transformed into XL10 gold cells. Selected colonies were further grown overnight before DNA extraction using the Qiagen miniprep kit, purified, and sequenced to confirm point mutation.

Animal Husbandry and In Vitro Fertilization

X. tropicalis were housed and cared for in our aquatics facility according to established protocols that were approved by our local IACUC (Bhattacharya et al., 2015). In vitro fertilization was performed as previously described (del Viso and Khokha, 2012).

Microinjection

Reaction mix, composed of CRISPR, Cas9 protein, and tracer, is prepared as previously described and 2nL is injected per embryo (Deniz et al., 2018). Total CRISPR sgRNA dose is titrated per gene targeted to be between 50ng to 500ng (Blitz et al., 2013; Guo et al., 2014; Nakayama et al., 2013). Injected embryos were kept at 28C for 2 hours after injection to ensure CRISPR/Cas9 efficiency before being raised at 25 C until desired stages.

Similarly, mRNA and tracer reaction mix is prepared to also inject 2nL per embryo at the 1 cell stage. mRNA is also titrated for rescue up to 500ng total per embryo. Rescue experiments had embryos injected with 2nL of CRISPR/Cas9 mix followed by 2nL of mRNA mix. Embryos were examined for tracer 4-12 hours after injection. Embryos that did not display the tracer were euthanized and discarded.

In situ hybridization probes

A CS107 plasmid containing *msr*, originally from the sanger library (clone ID# Tneu054M15) was transformed into XL10 gold cells (Agilent Technologies). A miniprep was performed from the cultured colonies using the Qiagen miniprep kit. Minipreps were sequenced using the Sp6 and T3 reverse. After sequence confirmation, plasmid was linearized with restriction enzymes, flanking the inserted *msr* sequence, for at least 2h at 37C. DNA was cleaned using RNAse free Qiagen PCR Purification kit. Anti-sense rna probe was created using the HiScribe T7 High Yield RNA synthesis kit (NewEngland Biolabs). RNA was purified with Zymo Clean and Concentrator kit. Anti-sense RNA probe concentration was determined by nanodrop before dilution and storage at -80C in aliquoted concentration.

CLDN14 probe was created *de novo* for *X. tropicalis*. *X. tropicalis* cDNA was obtained using the SuperScript III kit (ThermoFischer). Primers for CLDN14 were created (see **Table 1**) using the Primer BLAST (NIH website). CLDN14 sequence was amplified by PCR using the Phusion High Fidelity DNA Polymerase (M030, NEB) and PCR product

was run on a 1.6% agrose gel to confirm sequence amplification. CLDN14 sequence was cloned using the Zero Blunt TOPO Blunt End kit (ThermoFischer). Colonies were amplified, minipreped, sequenced, and probe was created as detailed above.

Whole Mount In situ hybridization

Embryos were fixed in Memfa solution and then dehydrated with 100% ethanol and stored at -20C until in situ hybridization was performed. *In Situ* hybridization was performed on embryos as previously described (Khokha et al., 2002). In situ hybridization was performed by a semi-automated process using the Biolane HT1 16V machine (Intavis Bioanalytical Instruments). Embryos were developed in BM Purple at 4C or room temperature until signal was adequately visible. When mature, the *in situ* hybridization was stopped with 1x Maleic Acid Buffer washing for 5 minutes, followed by fixation with Bouin's Solution for 1 hour, washed with 1x Standard Saline Citrate (SSC) until the yellow staining was removed. Embryos were then bleached in a solution containing 1% hydrogen peroxide, 5% formamide, 1x SSC on a light box for 1 hour to remove pigments. Bleaching was stopped by washing in 1x SSC twice.

Confirming CRISPR cut T7 endonuclease reaction

CRISPR/Cas9 injected and uninjected control (UIC) embryos were collected at stage 40. DNA was extracted using the Qiagen Blood and Tissue kit and stored. Gene targets were amplified by PCR using primers flanking the targeted cut site and Phusion High Fidelity DNA Polymerase kit (M030, NEB). The T7 endonuclease reaction was performed as previously described (Guschin et al., 2010), to ascertain CRISPR/Cas9 cutting.

Clearing of Embryos

Embryos were collected at stage 47 and fixed in 4%PFA. Fixed embryos were washed twice with 1x PBS and then placed in Scale-S4 (Hama et al., 2015) for 2 days at 4°C on a rocker. This cleared the embryo of pigments without degrading the fluorescent signal. After clearing, embryos were washed with 1xPBS twice and stored at 4°C until dissection and mounting for microscopy.

Confocal Imaging

Brains were extracted from cleared embryos, placed on a coverslip slide. Prolong antifate gold reagent (Invitrogen) was used to prevent degeneration of GFP signal. Dow Corning high vacuum grease was placed at the corners of the coverslip slide before placing onto the slide to prevent complete squashing of the dissected brain.

Confocal microscopy was performed using the AireScan microscope. Full thickness Z-stack images were obtained of extracted brains. Images were processed to adjust brightness and contrast, and analyzed for their posterior venous plexus area and mesencephalic vein length.

ImageJ was used to stitch and analyze images.

Cell Culture

COS-7 cells Cos-7 (COS) cells were passaged at 80–90% confluence on high glucose DMEM (Dulbecco's modified Eagle's medium, Gibco Life Technologies) supplemented

with 10% fetal bovine serum (FBS, Gibco Life Technologies), L-glutamine, and penicillin/streptomycin.

Mutagenesis of CLDN14 and Plasmid Transfection

A wild-type human *CLDN14* cDNA was sub-cloned into pShuttle-IRES-hrGFP-2 plasmid vector with Flag-Tag sequence. The QuikChange II Site-Directed Mutagenesis Kit (Aligent Technologies, Santa Clara CA, USA) was used to generate isolated single amino-acid changes within the *CLDN14* ORF (Val143Met). All mutant constructs were sequenced to confirm successful mutagenesis. The wild-type *EPHB4* construct used previously (Duran et al., 2018b) and either wild-type *CLDN14*, mutant construct, or empty vector were both transiently transfected into COS-7 cells using Lipofectamine 2000 transfection reagent (Invitrogen, Carlsbad, CA, USA) according to its standard protocol. DNA complexes were removed after 5 h and replaced with fresh complete medium. After 48 hours, the medium was aspirated and the cells starved for 18 h in serum-free conditions.

Co-immunoprecipitation and Western Blotting

Cell lysates were prepared using NP40 lysis buffer (50 mM Tris, pH7.5; 1% Nonidet P-40; 150 mM NaCl; 10% Glycerol) containing protease and phosphatase inhibitor cocktail (Roche, Basel, Switzerland). Protein concentrations were measured with DC Protein Assay Reagents (Bio-Rad, Hercules CA, USA). For immunoprecipitation, equal amounts of cell lysates were incubated with Sepharose beads linked to anti-HA-Tag antibody (Cell Signaling Technology, Danvers, MA, USA) overnight at 4 °C. Immunoprecipitated protein complexes were separated on SDS-PAGE gel and analyzed by Western blotting using anti-

HA-Tag and anti-Flag-Tag (Cell Signaling Technology, Danvers MA, USA), anti-Ras GAP (Santa Cruz Biotechnology, Dallas TX, USA). Band intensities were quantified using ImageJ software (Schneider et al., 2012). Statistical analyses were performed using Prism 7 software (GraphPad Software, La Jolla CA, USA).

Statistics

Statistical analyses were performed using Prism 7 software (GraphPad Software, La Jolla CA, USA).

Attribution of work

Jonathan R. Gaillard was trained in and performed *Xenopus tropicalis* IVF, CRISPR sgRNA design, creation, and confirmation using the T7 endonuclease reaction in the labs of Dr. Mustafa Khokha and Dr. Engin Deniz. JRG generated in situ hybridization probes and performed in situ hybridization experiments, injected embryos with CRISPR/Cas9 with or without mRNA, fixed and cleared embryos, extracted brains, and mounted them for imaging with the help of Dr. Deniz. JRG and Dr. Deniz performed the confocal imaging of the brains.

Cell work and western blotting was performed by Bogdan Yatsula, Alan Dardic, and Jinwei Zhang.

FIGURES

Figure 1. Co-Immunoprecipitation reveals interaction between EPHB4 and CLDN14
Representative immunoblot showing effects of Ala509Gly, Lys650Asn, and Phe867Leu mutations on WT EPHB4 and CLDN14 in Cos-7 cells, analyzed by immunoprecipitation (IP) with HA-Tag antibody followed by immunoblot (IB) with HA-Tag and Flag-Tag antibodies. Blot demonstrates EPHB4 co-immunoprecipitation with both wild type and mutant Val143Met CLDN14

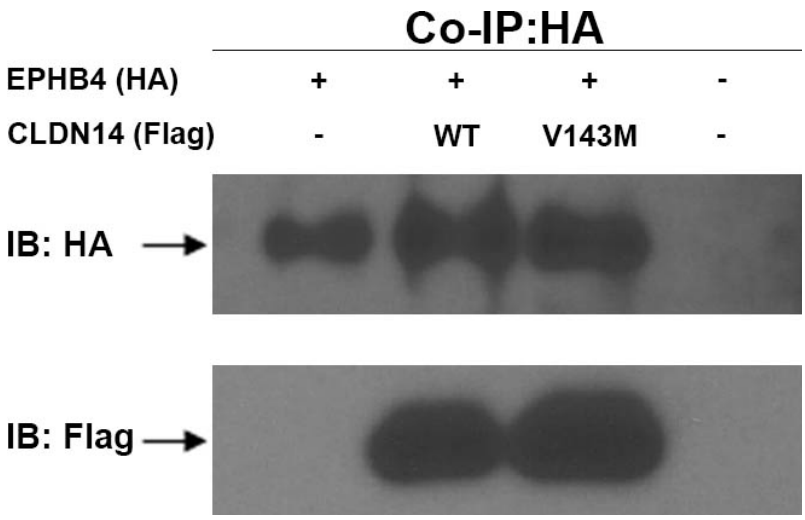

Figure 2. msr expression is decreased in CRISPR/Cas9 injected embryos
In situ hybridization was performed using marker *msr* on Uninjected Control (UIC) and embryos with Cas9 and CRISPR sgRNA targeted against RASA1, EPHB4, and CLDN14, that were raised to stage 34. (**A**) *msr* is localized to the developing endothelium and vasculature and allows the visualization of the Viteline Vein Network (VVN), where early hematopoiesis is located, the Posterior Cardinal Vein (PCV, arrows), and sprouting and growth of the Intersegmental Arteries (ISA, arrow heads). For the purposes of scoring only the head and the VVN were not used, and only the tail and body were used (dashed box). Embryos were scored as (**B**) normal expression with ISAs formed or sprouting (arrow head) and un-interrupted PCV (arrow), (**C**) abnormal with interrupted PCV (arrow) or absent/diminished ISAs (arrow head), or (**D**) absent with lack of any PCV(arrow) or ISAs (arrow head). (**E**) Embryos were scored data collected for the percentage of embryos displaying normal, abnormal, or absent expression and found to be significant by two-way ANOVA comparing both expression (normal, abnormal, and absent) and conditions (UIC, RASA1, EPHB4, CLDN14), with $p<0.0001$. Significant findings for **abnormal** expression UIC and CRISPR/Cas9 are noted (E). **: $p\leq0.01$; ***: $p\leq0.001$

Figure 2. msr expression is decreased in CRISPR/Cas9 injected embryos

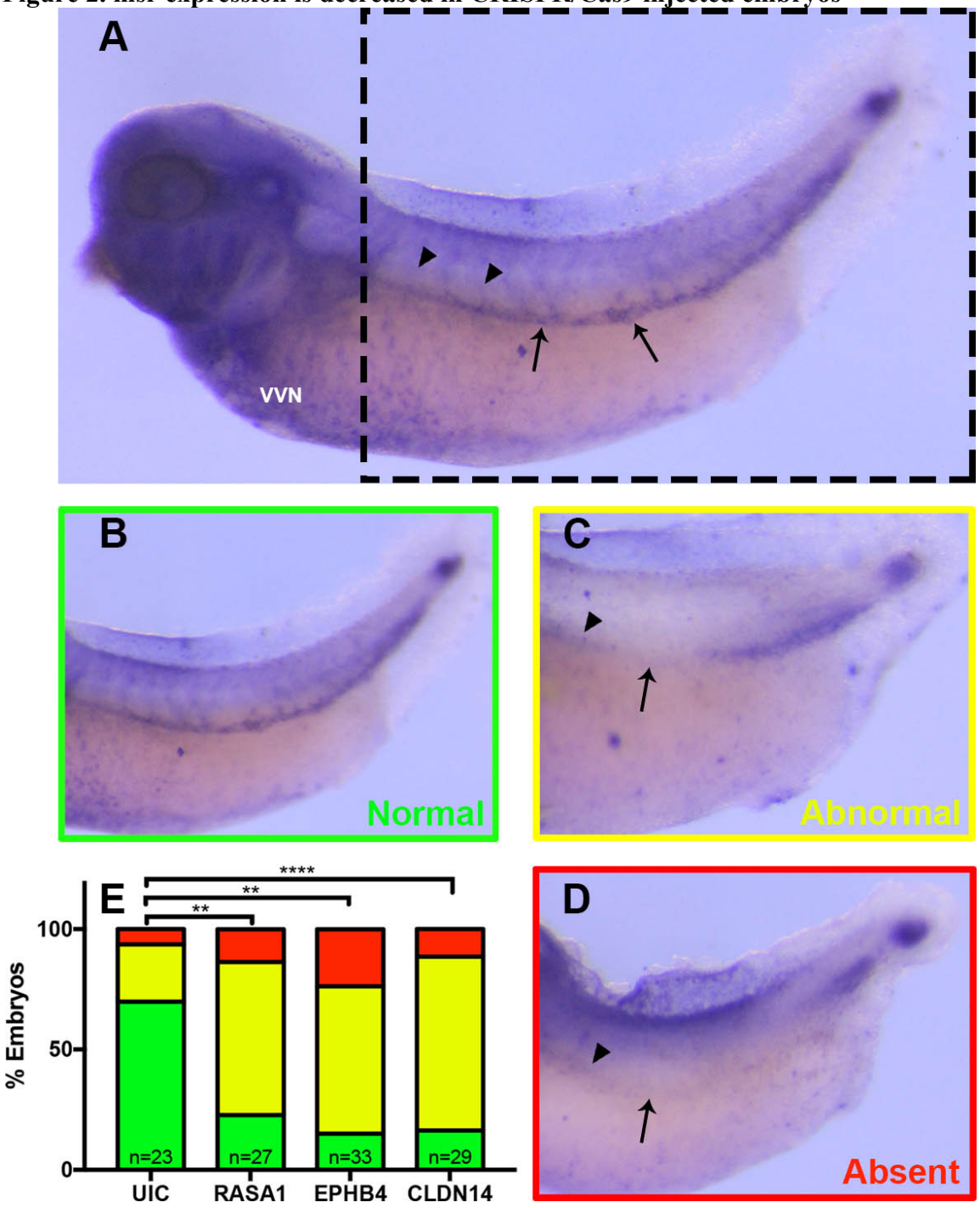

Figure 3. Clearing allows visualization of full thickness brain vasculature
(**A**) The stage 47 *Xenopus tropicalis* embryo has prominent melanocytes covering the dorsal aspect of the animal from anterior to posterior, including the head (red oval). (**B**) In *Xflk1:GFP* embryos, melanocytes obstruct the view of the dorsal vasculature of the brain. Additionally, deep vasculature is unable to be visualized. (**C**) Clearing of the animal and subsequent extraction of the brain allows full visualization of the entire thickness of the brain vasculature, here presented with three z-stacks of the dorsal most vessels, the middle vessels, and the ventral vessels.

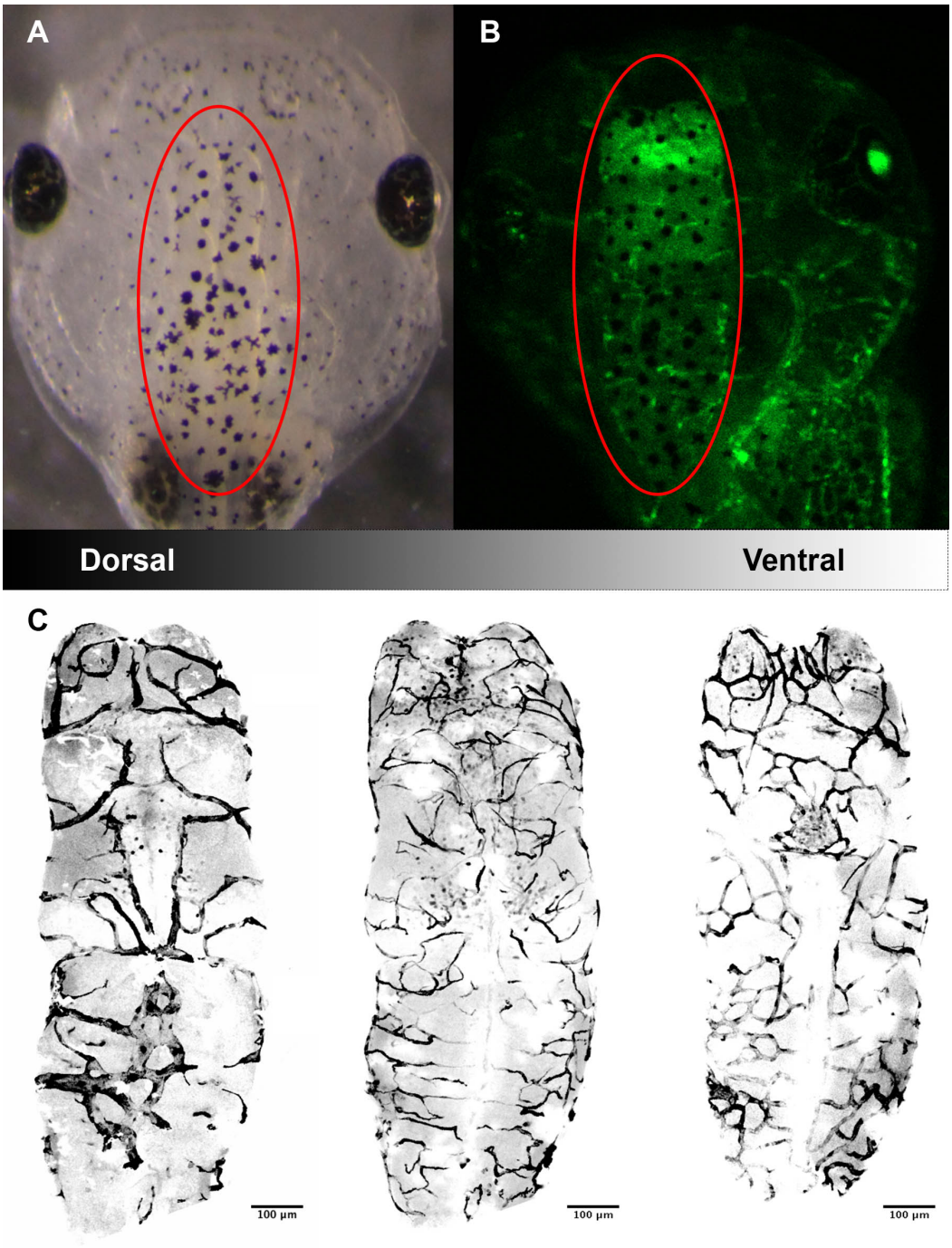

Figure 4. CRISPR/Cas9 KD decreases Mesencephalic Vein length and Posterior Vascular Plexus area

(**A**) Stage 47 *Xflk1:GFP* embryos for uninjected control (UIC), Cas9 only, CRISPR/Cas9 against *RASA1*, *EPHB4,* and CLDN14, and coinjected CLDN14 CRISPR/Cas9 and wild type (WT) vs. mutant (Mut) were collected, fixed, and cleared. Brain were removed and mounted for confocal microscopy imaging. (**B**) The Mesencephalic Vein (MSV, green line) and the (**C**) Posterior venous plexus (PVP, red area) were measured and compared across conditions using ImageJ. (**D**) One-way ANOVA demonstrated significance across conditions for MSV length ($F= 16.76$, $p<0.0001$). Further analysis demonstrated significance between *RASA1*, *EPHBB4*, and *CLDN14* CRISPR/Cas9 injected animals compared to both UIC, as well as Cas9 only. (**E**) Similarly, one-way ANOVA demonstrated significance across conditions for PVP area ($F(6,69) = 4.828$, $p=0.0004$). Further analysis revealed that *RASA1* CRISPR/Cas9 injected animals showed significant increase in the PVP area compared to UICs ($p= 0.0160$), Cas9 only injected animals ($p=0.0223$), and CLDN14 CRISPR/Cas9 injected animals ($p=0.0357$).

Figure 4. CRISPR/Cas9 KD decreases Mesencephalic Vein length and Posterior Vascular Plexus area

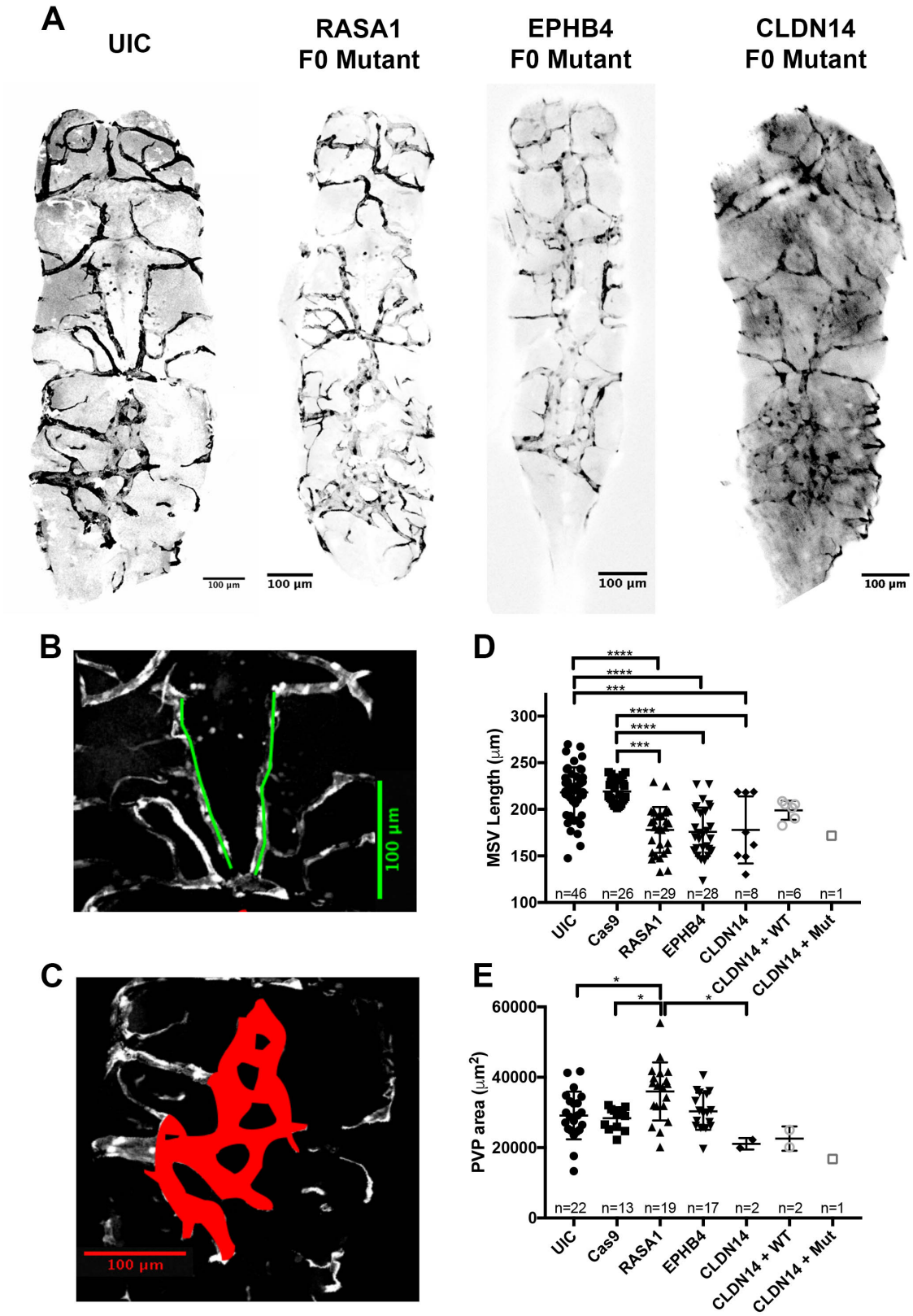

SUPPLEMENTARY FIGURES AND TABLES

Supplementary Figure 1. T7 endonuclease confirms cutting by sgRNAs
Embryos that were uninjected controls (UIC) or injected with sgRNA/Cas9 for RASA1, CLDN14, and EPHB4, and PCR amplified around the target region of the sgRNA. Application of T7 endonuclease reveals additional bands in sgRNA/Cas9 injected animals but not in uninjected control animals.

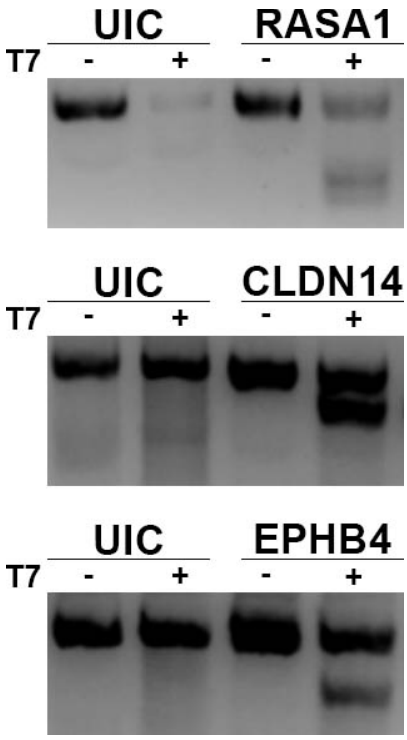

Supplementary Table 1. Nucleotide sequences used

sgRNA design for CRISPR/Cas9		
Gene	**Sequence**	
RASA1	taatacgactcactataGGGAGGTGGCGAGGCGACATgttttagagctagaa	
EPHB4	taatacgactcactataGGGAGAATGGGCCAAACCGGgttttagagctagaa	
CLDN14	taatacgactcactataGGGGGGCTATCGGTGATCGGgttttagagctagaa	
Primers used for T7 fragment analysis		
Gene	**Forward Sequence**	**Reverse Sequence**
RASA1	CGGAAGCTGCCACTGATCTAA	TGTTTGGGACCCGGGATAAG
EPHB4	TGGCTTCTACTTGGCGTTCC	AGTCAGACAACCACACCACC
CLDN14	CCTCATTGGCTTCATCGGGA	TGCTTTTGTTGACGGGCTG
Primers used for Q5 site directed mutagenesis		
Gene	**Forward Sequence**	**Reverse Sequence**
CLDN14	CACCAACGACaTGGTGCAGAACTTC	GTCCAGGAGACGGCCACC
Primers used to design *Xenopus* tropicalis in situ probe		
Gene	**Forward Sequence**	**Reverse Sequence**
CLDN14	TGGCATACATGAAGGGCCTG	TTGCTTTTGTTGACGGGCTG

VIII. References

Abagyan, R., Totrov, M., and Kuznetsov, D. (1994). Icm - a New Method for Protein Modeling and Design - Applications to Docking and Structure Prediction from the Distorted Native Conformation. J Comput Chem *15*, 488-506.

Abdalla, S.A., Geisthoff, U.W., Bonneau, D., Plauchu, H., McDonald, J., Kennedy, S., Faughnan, M.E., and Letarte, M. (2003). Visceral manifestations in hereditary haemorrhagic telangiectasia type 2. J Med Genet *40*, 494-502.

Abdalla, S.A., Pece-Barbara, N., Vera, S., Tapia, E., Paez, E., Bernabeu, C., and Letarte, M. (2000). Analysis of ALK-1 and endoglin in newborns from families with hereditary hemorrhagic telangiectasia type 2. Hum Mol Genet *9*, 1227-1237.

Adams, R.H., and Eichmann, A. (2010). Axon guidance molecules in vascular patterning. Cold Spring Harb Perspect Biol *2*, a001875.

Adams, R.H., Wilkinson, G.A., Weiss, C., Diella, F., Gale, N.W., Deutsch, U., Risau, W., and Klein, R. (1999). Roles of ephrinB ligands and EphB receptors in cardiovascular development: demarcation of arterial/venous domains, vascular morphogenesis, and sprouting angiogenesis. Genes Dev *13*, 295-306.

Altschul, D., Paramasivam, S., Ortega-Gutierrez, S., Fifi, J.T., and Berenstein, A. (2014). Safety and efficacy using a detachable tip microcatheter in the embolization of pediatric arteriovenous malformations. Childs Nerv Syst *30*, 1099-1107.

Amacher, A.L., and Shillito, J., Jr. (1973). The syndromes and surgical treatment of aneurysms of the great vein of Galen. J Neurosurg *39*, 89-98.

Amyere, M., Revencu, N., Helaers, R., Pairet, E., Baselga, E., Cordisco, M., Chung, W., Dubois, J., Lacour, J.P., Martorell, L.*, et al.* (2017). Germline Loss-of-Function Mutations in EPHB4 Cause a Second Form of Capillary Malformation-Arteriovenous Malformation (CM-AVM2) Deregulating RAS-MAPK Signaling. Circulation *136*, 1037-1048.

Apweiler, R., Bairoch, A., Wu, C.H., Barker, W.C., Boeckmann, B., Ferro, S., Gasteiger, E., Huang, H., Lopez, R., Magrane, M.*, et al.* (2004). UniProt: the Universal Protein knowledgebase. Nucleic Acids Res *32*, D115-119.

Arboleda, Valerie A., Lee, H., Dorrani, N., Zadeh, N., Willis, M., Macmurdo, Colleen F., Manning, Melanie A., Kwan, A., Hudgins, L., Barthelemy, F.*, et al.* (2015). De Novo Nonsense Mutations in KAT6A, a Lysine Acetyl-Transferase Gene, Cause a Syndrome Including Microcephaly and Global Developmental Delay. The American Journal of Human Genetics *96*, 498-506.

Aurboonyawat, T., Suthipongchai, S., Pereira, V., Ozanne, A., and Lasjaunias, P. (2007). Patterns of cranial venous system from the comparative anatomy in vertebrates. Part I, introduction and the dorsal venous system. Interventional neuroradiology : journal of peritherapeutic neuroradiology, surgical procedures and related neurosciences *13*, 335-344.

Baek, J.M., Cheon, Y.H., Kwak, S.C., Jun, H.Y., Yoon, K.H., Lee, M.S., and Kim, J.Y. (2018). Claudin 11 regulates bone homeostasis via bidirectional EphB4-EphrinB2 signaling. Experimental & molecular medicine *50*, 50.

Baker, M., Reynolds, L.E., Robinson, S.D., Lees, D.M., Parsons, M., Elia, G., and Hodivala-Dilke, K. (2013). Stromal Claudin14-heterozygosity, but not deletion, increases tumour blood leakage without affecting tumour growth. PloS one *8*, e62516.

Barak, T., Kwan, K.Y., Louvi, A., Demirbilek, V., Saygi, S., Tuysuz, B., Choi, M., Boyaci, H., Doerschner, K., Zhu, Y*., et al.* (2011). Recessive LAMC3 mutations cause malformations of occipital cortical development. Nature genetics *43*, 590-594.
Barbara, N.P., Wrana, J.L., and Letarte, M. (1999). Endoglin is an accessory protein that interacts with the signaling receptor complex of multiple members of the transforming growth factor-beta superfamily. The Journal of biological chemistry *274*, 584-594.
Bayrak-Toydemir, P., McDonald, J., Markewitz, B., Lewin, S., Miller, F., Chou, L., Bayrak-Toydemir, P., McDonald, J., Markewitz, B., Lewin, S*., et al.* (2006). Genotype-phenotype correlation in hereditary hemorrhagic telangiectasia: mutations and manifestations. Am J Med Genet A *140*, 463-470.
Berenstein, A., Fifi, J., Niimi, Y., Presti, S., Ortiz, R., Ghatan, S., Berenstein, A., Fifi, J., Niimi, Y., Presti, S*., et al.* (2012). Vein of Galen malformations in neonates: new management paradigms for improving outcomes. Neurosurgery *70*, 1207-1214.
Besse, W., Dong, K., Choi, J., Punia, S., Fedeles, S.V., Choi, M., Gallagher, A.R., Huang, E.B., Gulati, A., Knight, J*., et al.* (2017). Isolated polycystic liver disease genes define effectors of polycystin-1 function. J Clin Invest *127*, 1772-1785.
Bhattacharya, D., Marfo, C.A., Li, D., Lane, M., and Khokha, M.K. (2015). CRISPR/Cas9: An inexpensive, efficient loss of function tool to screen human disease genes in Xenopus. Dev Biol *408*, 196-204.
Bhattacharya, J.J., and Thammaroj, J. (2003). Vein of galen malformations. Journal of neurology, neurosurgery, and psychiatry *74 Suppl 1*, i42-44.
Bilguvar, K., Ozturk, A.K., Louvi, A., Kwan, K.Y., Choi, M., Tatli, B., Yalnizoglu, D., Tuysuz, B., Caglayan, A.O., Gokben, S*., et al.* (2010). Whole-exome sequencing identifies recessive WDR62 mutations in severe brain malformations. Nature *467*, 207-210.
Blitz, I.L., Biesinger, J., Xie, X., and Cho, K.W. (2013). Biallelic genome modification in F(0) Xenopus tropicalis embryos using the CRISPR/Cas system. Genesis (New York, NY : 2000) *51*, 827-834.
Boon, L., Mulliken, J., Vikkula, M., Boon, L., Mulliken, J., and Vikkula, M. (2005). RASA1: variable phenotype with capillary and arteriovenous malformations. Curr Opin Genet Dev *15*, 265-269.
Breysem, L., Bosmans, H., Dymarkowski, S., Schoubroeck, D.V., Witters, I., Deprest, J., Demaerel, P., Vanbeckevoort, D., Vanhole, C., Casaer, P*., et al.* (2003). The value of fast MR imaging as an adjunct to ultrasound in prenatal diagnosis. Eur Radiol *13*, 1538-1548.
Brouillard, P., Boon, L.M., Mulliken, J.B., Enjolras, O., Ghassibe, M., Warman, M.L., Tan, O.T., Olsen, B.R., and Vikkula, M. (2002). Mutations in a novel factor, glomulin, are responsible for glomuvenous malformations ("glomangiomas"). American journal of human genetics *70*, 866-874.
Brouillard, P., and Vikkula, M. (2007). Genetic causes of vascular malformations. Human molecular genetics *16 Spec No. 2*, R140-149.
Browning, B.L., and Browning, S.R. (2011). A fast, powerful method for detecting identity by descent. American journal of human genetics *88*, 173-182.
Brunelle, F. (1997). Arteriovenous malformation of the vein of Galen in children. Pediatric radiology *27*, 501-513.

Casasco, A., Lylyk, P., Hodes, J.E., Kohan, G., Aymard, A., and Merland, J.J. (1991). Percutaneous transvenous catheterization and embolization of vein of galen aneurysms. Neurosurgery *28*, 260-266.
Cha, H.J., Byrom, M., Mead, P.E., Ellington, A.D., Wallingford, J.B., and Marcotte, E.M. (2012). Evolutionarily repurposed networks reveal the well-known antifungal drug thiabendazole to be a novel vascular disrupting agent. PLoS biology *10*, e1001379.
Chen, Y.G., Hata, A., Lo, R.S., Wotton, D., Shi, Y., Pavletich, N., and Massague, J. (1998). Determinants of specificity in TGF-beta signal transduction. Genes Dev *12*, 2144-2152.
Chida, A., Shintani, M., Wakamatsu, H., Tsutsumi, Y., Iizuka, Y., Kawaguchi, N., Furutani, Y., Inai, K., Nonoyama, S., and Nakanishi, T. (2013). ACVRL1 gene variant in a patient with vein of Galen aneurysmal malformation.
Ciricillo, S.F., Edwards, M.S., Schmidt, K.G., Hieshima, G.B., Silverman, N.H., Higashida, R.T., and Halbach, V.V. (1990). Interventional neuroradiological management of vein of Galen malformations in the neonate. Neurosurgery *27*, 22-27; discussion 27-28.
Cong, L., Ran, F.A., Cox, D., Lin, S., Barretto, R., Habib, N., Hsu, P.D., Wu, X., Jiang, W., Marraffini, L.A.*, et al.* (2013). Multiplex genome engineering using CRISPR/Cas systems. Science *339*, 819-823.
Cox, C.M., D'Agostino, S.L., Miller, M.K., Heimark, R.L., and Krieg, P.A. (2006). Apelin, the ligand for the endothelial G-protein-coupled receptor, APJ, is a potent angiogenic factor required for normal vascular development of the frog embryo. Dev Biol *296*, 177-189.
de Koning, T.J., Gooskens, R., Veenhoven, R., Meijboom, E.J., Jansen, G.H., Lasjaunias, P., and de Vries, L.S. (1997). Arteriovenous malformation of the vein of Galen in three neonates: emphasis on associated early ischaemic brain damage. Eur J Pediatr *156*, 228-229.
de Ligt, J., Willemsen, M.H., van Bon, B.W., Kleefstra, T., Yntema, H.G., Kroes, T., Vulto-van Silfhout, A.T., Koolen, D.A., de Vries, P., Gilissen, C.*, et al.* (2012). Diagnostic exome sequencing in persons with severe intellectual disability. The New England journal of medicine *367*, 1921-1929.
De Rubeis, S., He, X., Goldberg, A.P., Poultney, C.S., Samocha, K., Cicek, A.E., Kou, Y., Liu, L., Fromer, M., Walker, S.*, et al.* (2014). Synaptic, transcriptional and chromatin genes disrupted in autism. Nature *515*, 209-215.
del Viso, F., and Khokha, M. (2012). Generating diploid embryos from Xenopus tropicalis. Methods in molecular biology (Clifton, NJ) *917*, 33-41.
Deloison, B., Chalouhi, G.E., Sonigo, P., Zerah, M., Millischer, A.E., Dumez, Y., Brunelle, F., Ville, Y., and Salomon, L.J. (2012). Hidden mortality of prenatally diagnosed vein of Galen aneurysmal malformation: retrospective study and review of the literature. Ultrasound Obstet Gynecol *40*, 652-658.
Deniz, E., Mis, E.K., Lane, M., and Khokha, M.K. (2018). CRISPR/Cas9 F0 Screening of Congenital Heart Disease Genes in Xenopus tropicalis. Methods in molecular biology (Clifton, NJ) *1865*, 163-174.
Dentici, M.L., Di Pede, A., Lepri, F.R., Gnazzo, M., Lombardi, M.H., Auriti, C., Petrocchi, S., Pisaneschi, E., Bellacchio, E., Capolino, R.*, et al.* (2015). Kabuki

syndrome: clinical and molecular diagnosis in the first year of life. Archives of Disease in Childhood *100*, 158-164.
DePristo, M.A., Banks, E., Poplin, R., Garimella, K.V., Maguire, J.R., Hartl, C., Philippakis, A.A., del Angel, G., Rivas, M.A., Hanna, M.*, et al.* (2011). A framework for variation discovery and genotyping using next-generation DNA sequencing data. Nature Genetics *43*, 491.
Devic, E., Paquereau, L., Vernier, P., Knibiehler, B., and Audigier, Y. (1996). Expression of a new G protein-coupled receptor X-msr is associated with an endothelial lineage in Xenopus laevis. Mechanisms of development *59*, 129-140.
Doench, J.G., Fusi, N., Sullender, M., Hegde, M., Vaimberg, E.W., Donovan, K.F., Smith, I., Tothova, Z., Wilen, C., Orchard, R.*, et al.* (2016). Optimized sgRNA design to maximize activity and minimize off-target effects of CRISPR-Cas9. Nature biotechnology *34*, 184-191.
Doherty, J.R., Johnson Hamlet, M.R., Kuliyev, E., and Mead, P.E. (2007). A flk-1 promoter/enhancer reporter transgenic Xenopus laevis generated using the Sleeping Beauty transposon system: an in vivo model for vascular studies. Dev Dyn *236*, 2808-2817.
Dong, C., Wei, P., Jian, X., Gibbs, R., Boerwinkle, E., Wang, K., and Liu, X. (2015). Comparison and integration of deleteriousness prediction methods for nonsynonymous SNVs in whole exome sequencing studies. Human molecular genetics *24*, 2125-2137.
Doren, M., Tercanli, S., and Holzgreve, W. (1995). Prenatal sonographic diagnosis of a vein of Galen aneurysm: relevance of associated malformations for timing and mode of delivery. Ultrasound Obstet Gynecol *6*, 287-289.
Dravis, C., and Henkemeyer, M. (2011). Ephrin-B reverse signaling controls septation events at the embryonic midline through separate tyrosine phosphorylation-independent signaling avenues. Dev Biol *355*, 138-151.
Duran, D., Karschnia, P., Gaillard, J.R., Karimy, J.K., Youngblood, M.W., DiLuna, M.L., Matouk, C.C., Aagaard-Kienitz, B., Smith, E.R., Orbach, D.B.*, et al.* (2018a). Human genetics and molecular mechanisms of vein of Galen malformation. J Neurosurg Pediatr *21*, 367-374.
Duran, D., Zeng, X., Jin, S.C., Choi, J., Nelson-Williams, C., Yatsula, B., Gaillard, J., Furey, C.G., Lu, Q., Timberlake, A.T.*, et al.* (2018b). Mutations in Chromatin Modifier and Ephrin Signaling Genes in Vein of Galen Malformation. Neuron.
Epi, K.C., Epilepsy Phenome/Genome, P., Allen, A.S., Berkovic, S.F., Cossette, P., Delanty, N., Dlugos, D., Eichler, E.E., Epstein, M.P., Glauser, T.*, et al.* (2013). De novo mutations in epileptic encephalopathies. Nature *501*, 217-221.
Feinberg, A.P. (2018). The Key Role of Epigenetics in Human Disease Prevention and Mitigation. The New England journal of medicine *378*, 1323-1334.
Ferguson, B.D., Tan, Y.H., Kanteti, R.S., Liu, R., Gayed, M.J., Vokes, E.E., Ferguson, M.K., Iafrate, A.J., Gill, P.S., and Salgia, R. (2015). Novel EPHB4 Receptor Tyrosine Kinase Mutations and Kinomic Pathway Analysis in Lung Cancer. Sci Rep *5*, 10641.
Fischbach, G.D., and Lord, C. (2010). The Simons Simplex Collection: a resource for identification of autism genetic risk factors. Neuron *68*, 192-195.
Fish, J.E., and Wythe, J.D. (2015). The molecular regulation of arteriovenous specification and maintenance. Dev Dyn *244*, 391-409.

Friedman, D., Madrid, M., Berenstein, A., Choi, I., Wisoff, J., Friedman, D., Madrid, M., Berenstein, A., Choi, I., and Wisoff, J. (1991). Neonatal vein of Galen malformations: experience in developing a multidisciplinary approach using an embolization treatment protocol. Clin Pediatr (Phila) *30*, 621-629.
Fromer, M., and Purcell, S.M. (2014). Using XHMM Software to Detect Copy Number Variation in Whole-Exome Sequencing Data. Current Protocols in Human Genetics *81*, 7.23.21-27.23.21.
Furey, C.G., Zeng, X., Dong, W., Jin, S.C., Choi, J., Timberlake, A.T., Dunbar, A.M., Allocco, A.A., Gunel, M., Lifton, R.P.*, et al.* (2018). Human Genetics and Molecular Mechanisms of Congenital Hydrocephalus. World Neurosurg *119*, 441-443.
Gabriel, R.A., Kim, H., Sidney, S., McCulloch, C.E., Singh, V., Johnston, S.C., Ko, N.U., Achrol, A.S., Zaroff, J.G., and Young, W.L. (2010). Ten-year detection rate of brain arteriovenous malformations in a large, multiethnic, defined population. Stroke *41*, 21-26.
Gentsch, G.E., Spruce, T., Monteiro, R.S., Owens, N.D.L., Martin, S.R., and Smith, J.C. (2018). Innate Immune Response and Off-Target Mis-splicing Are Common Morpholino-Induced Side Effects in Xenopus. Developmental cell *44*, 597-610.e510.
Gerety, S.S., Wang, H.U., Chen, Z.F., and Anderson, D.J. (1999). Symmetrical mutant phenotypes of the receptor EphB4 and its specific transmembrane ligand ephrin-B2 in cardiovascular development. Molecular cell *4*, 403-414.
Gerrard, D.T., Berry, A.A., Jennings, R.E., Piper Hanley, K., Bobola, N., and Hanley, N.A. (2016). An integrative transcriptomic atlas of organogenesis in human embryos. Elife *5*.
Gold, A., Ransohoff, J., and Carter, S. (1964). Vein of Galen Malformation. Acta Neurol Scand Suppl *40*, SUPPL 11:11-31.
Gonzalez-Mariscal, L., Lechuga, S., and Garay, E. (2007). Role of tight junctions in cell proliferation and cancer. Prog Histochem Cytochem *42*, 1-57.
Griffin, C.T., Brennan, J., and Magnuson, T. (2008). The chromatin-remodeling enzyme BRG1 plays an essential role in primitive erythropoiesis and vascular development. Development *135*, 493-500.
Guo, S., Zhou, Y., Xing, C., Lok, J., Som, A.T., Ning, M., Ji, X., and Lo, E.H. (2012). The vasculome of the mouse brain. PloS one *7*, e52665.
Guo, X., Zhang, T., Hu, Z., Zhang, Y., Shi, Z., Wang, Q., Cui, Y., Wang, F., Zhao, H., and Chen, Y. (2014). Efficient RNA/Cas9-mediated genome editing in Xenopus tropicalis. Development *141*, 707-714.
Guschin, D.Y., Waite, A.J., Katibah, G.E., Miller, J.C., Holmes, M.C., and Rebar, E.J. (2010). A rapid and general assay for monitoring endogenous gene modification. Methods in molecular biology (Clifton, NJ) *649*, 247-256.
Halbach, V.V., Dowd, C.F., Higashida, R.T., Balousek, P.A., Ciricillo, S.F., and Edwards, M.S. (1998). Endovascular treatment of mural-type vein of Galen malformations. J Neurosurg *89*, 74-80.
Hama, H., Hioki, H., Namiki, K., Hoshida, T., Kurokawa, H., Ishidate, F., Kaneko, T., Akagi, T., Saito, T., Saido, T.*, et al.* (2015). ScaleS: an optical clearing palette for biological imaging. Nature neuroscience *18*, 1518-1529.

Harrison, R.E., Berger, R., Haworth, S.G., Tulloh, R., Mache, C.J., Morrell, N.W., Aldred, M.A., and Trembath, R.C. (2005). Transforming growth factor-beta receptor mutations and pulmonary arterial hypertension in childhood. Circulation *111*, 435-441.
Helbling, P.M., Saulnier, D.M., Robinson, V., Christiansen, J.H., Wilkinson, D.G., and Brandli, A.W. (1999). Comparative analysis of embryonic gene expression defines potential interaction sites for Xenopus EphB4 receptors with ephrin-B ligands. Dev Dyn *216*, 361-373.
Henkemeyer, M., Rossi, D.J., Holmyard, D.P., Puri, M.C., Mbamalu, G., Harpal, K., Shih, T.S., Jacks, T., and Pawson, T. (1995). Vascular system defects and neuronal apoptosis in mice lacking ras GTPase-activating protein. Nature *377*, 695-701.
Heuchan, A., Joss, S., Berg, J., Suri, M., Bhattacharya, J., Heuchan, A., Joss, S., Berg, J., Suri, M., and Bhattacharya, J. (2013). RASA1 mutations and vein of Galen arterial malformations. Arch Dis Child *98*, A16-A17.
Hirsch, N., Zimmerman, L.B., and Grainger, R.M. (2002). Xenopus, the next generation: X. tropicalis genetics and genomics. Dev Dyn *225*, 422-433.
Hoffman, H.J., Chuang, S., Hendrick, E.B., and Humphreys, R.P. (1982). Aneurysms of the vein of Galen. Experience at The Hospital for Sick Children, Toronto. J Neurosurg *57*, 316-322.
Homsy, J., Zaidi, S., Shen, Y., Ware, J.S., Samocha, K.E., Karczewski, K.J., DePalma, S.R., McKean, D., Wakimoto, H., Gorham, J*., et al.* (2015). De novo mutations in congenital heart disease with neurodevelopmental and other congenital anomalies. Science *350*, 1262-1266.
Hsu, P.D., Scott, D.A., Weinstein, J.A., Ran, F.A., Konermann, S., Agarwala, V., Li, Y., Fine, E.J., Wu, X., Shalem, O*., et al.* (2013). DNA targeting specificity of RNA-guided Cas9 nucleases. Nature biotechnology *31*, 827-832.
Huang, B.K., Gamm, U.A., Jonas, S., Khokha, M.K., and Choma, M.A. (2015). Quantitative optical coherence tomography imaging of intermediate flow defect phenotypes in ciliary physiology and pathophysiology. J Biomed Opt *20*, 030502.
Huisman, T.A., Wisser, J., Martin, E., Kubik-Huch, R., and Marincek, B. (2002). Fetal magnetic resonance imaging of the central nervous system: a pictorial essay. Eur Radiol *12*, 1952-1961.
Iossifov, I., O'Roak, B.J., Sanders, S.J., Ronemus, M., Krumm, N., Levy, D., Stessman, H.A., Witherspoon, K.T., Vives, L., Patterson, K.E*., et al.* (2014). The contribution of de novo coding mutations to autism spectrum disorder. Nature *515*, 216.
Iossifov, I., Ronemus, M., Levy, D., Wang, Z., Hakker, I., Rosenbaum, J., Yamrom, B., Lee, Y.H., Narzisi, G., Leotta, A*., et al.* (2012). De novo gene disruptions in children on the autistic spectrum. Neuron *74*, 285-299.
Isogai, S., Horiguchi, M., and Weinstein, B.M. (2001). The vascular anatomy of the developing zebrafish: an atlas of embryonic and early larval development. Dev Biol *230*, 278-301.
Jaeger, J.R., Forbes, R.P., and Dandy, W.E. (1937). Bilateral congenital cerebral arteriovenous communication aneurysm. Transactions of the American Neurological Association, 173–176.
Jen, S.C., and Rovainen, C.M. (1994). An adenosine agonist increases blood flow and density of capillary branches in the optic tectum of Xenopus laevis tadpoles. Microcirculation (New York, NY : 1994) *1*, 59-66.

Jin, S.C., Homsy, J., Zaidi, S., Lu, Q., Morton, S., DePalma, S.R., Zeng, X., Qi, H., Chang, W., Sierant, M.C.*, et al.* (2017). Contribution of rare inherited and de novo variants in 2,871 congenital heart disease probands. Nature Genetics *49*, 1593.
Johnston, I.H., Whittle, I.R., Besser, M., and Morgan, M.K. (1987). Vein of Galen malformation: diagnosis and management. Neurosurgery *20*, 747-758.
Jones, B.V., Ball, W.S., Tomsick, T.A., Millard, J., and Crone, K.R. (2002). Vein of Galen aneurysmal malformation: diagnosis and treatment of 13 children with extended clinical follow-up. AJNR Am J Neuroradiol *23*, 1717-1724.
Kalin, R.E., Banziger-Tobler, N.E., Detmar, M., and Brandli, A.W. (2009). An in vivo chemical library screen in Xenopus tadpoles reveals novel pathways involved in angiogenesis and lymphangiogenesis. Blood *114*, 1110-1122.
Kawasaki, J., Aegerter, S., Fevurly, R.D., Mammoto, A., Mammoto, T., Sahin, M., Mably, J.D., Fishman, S.J., and Chan, J. (2014). RASA1 functions in EPHB4 signaling pathway to suppress endothelial mTORC1 activity. The Journal of clinical investigation *124*, 2774-2784.
Kent, W.J., Sugnet, C.W., Furey, T.S., Roskin, K.M., Pringle, T.H., Zahler, A.M., and Haussler, D. (2002). The human genome browser at UCSC. Genome Res *12*, 996-1006.
Khokha, M.K., Chung, C., Bustamante, E.L., Gaw, L.W., Trott, K.A., Yeh, J., Lim, N., Lin, J.C., Taverner, N., Amaya, E.*, et al.* (2002). Techniques and probes for the study of Xenopus tropicalis development. Dev Dyn *225*, 499-510.
Khullar, D., Andeejani, A., Bulsara, K., Khullar, D., Andeejani, A., and Bulsara, K. (2010). Evolution of treatment options for vein of Galen malformations. J Neurosurg Pediatr *6*, 444-451.
Kim, I., Ryu, Y.S., Kwak, H.J., Ahn, S.Y., Oh, J.L., Yancopoulos, G.D., Gale, N.W., and Koh, G.Y. (2002). EphB ligand, ephrinB2, suppresses the VEGF- and angiopoietin 1-induced Ras/mitogen-activated protein kinase pathway in venous endothelial cells. FASEB J *16*, 1126-1128.
Kim, J.H., Peacock, M.R., George, S.C., and Hughes, C.C. (2012). BMP9 induces EphrinB2 expression in endothelial cells through an Alk1-BMPRII/ActRII-ID1/ID3-dependent pathway: implications for hereditary hemorrhagic telangiectasia type II. Angiogenesis *15*, 497-509.
Klagsbrun, M., and Eichmann, A. (2005). A role for axon guidance receptors and ligands in blood vessel development and tumor angiogenesis. Cytokine Growth Factor Rev *16*, 535-548.
Kniesel, U., and Wolburg, H. (2000). Tight junctions of the blood-brain barrier. Cell Mol Neurobiol *20*, 57-76.
Kramer, A., Green, J., Pollard, J., Jr., and Tugendreich, S. (2014). Causal analysis approaches in Ingenuity Pathway Analysis. Bioinformatics *30*, 523-530.
Krumm, N., Turner, T.N., Baker, C., Vives, L., Mohajeri, K., Witherspoon, K., Raja, A., Coe, B.P., Stessman, H.A., He, Z.X.*, et al.* (2015). Excess of rare, inherited truncating mutations in autism. Nat Genet *47*, 582-588.
Lasjaunias, P. (1997). Vein of Galen Aneurysmal Malformation. In Vascular Diseases in Neonates, Infants and Children: Interventional Neuroradiology Management (Berlin, Heidelberg: Springer Berlin Heidelberg), pp. 67-202.

Lasjaunias, P., Garcia-Monaco, R., Rodesch, G., Ter Brugge, K., Zerah, M., Tardieu, M., and de Victor, D. (1991). Vein of Galen malformation. Endovascular management of 43 cases. Childs Nerv Syst *7*, 360-367.
Lasjaunias, P., Hui, F., Zerah, M., Garcia-Monaco, R., Malherbe, V., Rodesch, G., Tanaka, A., and Alvarez, H. (1995). Cerebral arteriovenous malformations in children. Management of 179 consecutive cases and review of the literature. Childs Nerv Syst *11*, 66-79; discussion 79.
Lasjaunias, P., Rodesch, G., Terbrugge, K., Pruvost, P., Devictor, D., Comoy, J., and Landrieu, P. (1989). Vein of Galen aneurysmal malformations. Report of 36 cases managed between 1982 and 1988. Acta Neurochir (Wien) *99*, 26-37.
Lasjaunias, P., Terbrugge, K., Piske, R., Lopez Ibor, L., and Manelfe, C. (1987). [Dilatation of the vein of Galen. Anatomoclinical forms and endovascular treatment apropos of 14 cases explored and/or treated between 1983 and 1986]. Neuro-Chirurgie *33*, 315-333.
Lasjaunias, P.L. (2003). Brain and Spine AVMs, Vein of Galen Malformation. Treatments and Embryological Considerations. Interventional neuroradiology : journal of peritherapeutic neuroradiology, surgical procedures and related neurosciences *9*, 263-272.
Lasjaunias, P.L., Chng, S.M., Sachet, M., Alvarez, H., Rodesch, G., and Garcia-Monaco, R. (2006). The management of vein of Galen aneurysmal malformations. Neurosurgery *59*, S184-194; discussion S183-113.
Laskowski, R.A., Macarthur, M.W., Moss, D.S., and Thornton, J.M. (1993). Procheck - a Program to Check the Stereochemical Quality of Protein Structures. J Appl Crystallogr *26*, 283-291.
Lee, E.E.L., and Bezanilla, F. (2019). Methodological improvements for fluorescence recordings in Xenopus laevis oocytes. The Journal of General Physiology, jgp.201812189.
Lee, S., Lin, M., Mele, A., Cao, Y., Farmar, J., Russo, D., and Redman, C. (1999). Proteolytic processing of big endothelin-3 by the kell blood group protein. Blood *94*, 1440-1450.
Lek, M., Karczewski, K.J., Minikel, E.V., Samocha, K.E., Banks, E., Fennell, T., O'Donnell-Luria, A.H., Ware, J.S., Hill, A.J., Cummings, B.B.*, et al.* (2016). Analysis of protein-coding genetic variation in 60,706 humans. Nature *536*, 285-291.
Levine, A.J., Munoz-Sanjuan, I., Bell, E., North, A.J., and Brivanlou, A.H. (2003). Fluorescent labeling of endothelial cells allows in vivo, continuous characterization of the vascular development of Xenopus laevis. Dev Biol *254*, 50-67.
Li, A.H., Armstrong, D., and terBrugge, K.G. (2011). Endovascular treatment of vein of Galen aneurysmal malformation: management strategy and 21-year experience in Toronto. J Neurosurg Pediatr *7*, 3-10.
Li, H. (2014). Toward better understanding of artifacts in variant calling from high-coverage samples. Bioinformatics *30*, 2843-2851.
Li, H., and Durbin, R. (2010). Fast and accurate long-read alignment with Burrows–Wheeler transform. Bioinformatics *26*, 589-595.
Lisabeth, E.M., Falivelli, G., and Pasquale, E.B. (2013). Eph receptor signaling and ephrins. Cold Spring Harb Perspect Biol *5*.

Long, D., Seljeskog, E., Chou, S., French, L., Long, D., Seljeskog, E., Chou, S., and French, L. (1974). Giant arteriovenous malformations of infancy and childhood. J Neurosurg *40*, 304-312.
Lylyk, P., Vinuela, F., Dion, J.E., Duckwiler, G., Guglielmi, G., Peacock, W., and Martin, N. (1993). Therapeutic alternatives for vein of Galen vascular malformations. J Neurosurg *78*, 438-445.
Machida, Y., Murai, K., Miyake, K., and Iijima, S. (2001). Expression of chromatin remodeling factors during neural differentiation. J Biochem *129*, 43-49.
Maher, C., Piepgras, D., Brown, R., Friedman, J., Pollock, B., Maher, C., Piepgras, D., Brown, R., Friedman, J., and Pollock, B. (2001). Cerebrovascular manifestations in 321 cases of hereditary hemorrhagic telangiectasia. Stroke *32*, 877-882.
Makita, T., Sucov, H.M., Gariepy, C.E., Yanagisawa, M., and Ginty, D.D. (2008). Endothelins are vascular-derived axonal guidance cues for developing sympathetic neurons. Nature *452*, 759-763.
Manichaikul, A., Mychaleckyj, J.C., Rich, S.S., Daly, K., Sale, M., and Chen, W.M. (2010). Robust relationship inference in genome-wide association studies. Bioinformatics *26*, 2867-2873.
Martin-Almedina, S., Martinez-Corral, I., Holdhus, R., Vicente, A., Fotiou, E., Lin, S., Petersen, K., Simpson, M.A., Hoischen, A., Gilissen, C.*, et al.* (2016). EPHB4 kinase-inactivating mutations cause autosomal dominant lymphatic-related hydrops fetalis. J Clin Invest *126*, 3080-3088.
McAllister, K., Grogg, K., Johnson, D., Gallione, C., Baldwin, M., Jackson, C., McAllister, K., Grogg, K., Johnson, D., Gallione, C.*, et al.* (1994). Endoglin, a TGF-β binding protein of endothelial cells, is the gene for hereditary haemorrhagic telangiectasia type 1. Nat Genet *8*, 345-351.
McElhinney, D.B., Halbach, V.V., Silverman, N.H., Dowd, C.F., and Hanley, F.L. (1998). Congenital cardiac anomalies with vein of Galen malformations in infants. Arch Dis Child *78*, 548-551.
McKenna, A., Hanna, M., Banks, E., Sivachenko, A., Cibulskis, K., Kernytsky, A., Garimella, K., Altshuler, D., Gabriel, S., Daly, M.*, et al.* (2010). The Genome Analysis Toolkit: a MapReduce framework for analyzing next-generation DNA sequencing data. Genome Res *20*, 1297-1303.
Meyers, P.M., Halbach, V.V., Phatouros, C.P., Dowd, C.F., Malek, A.M., Lempert, T.E., Lefler, J.E., and Higashida, R.T. (2000). Hemorrhagic complications in vein of Galen malformations. Ann Neurol *47*, 748-755.
Mickle, J.P., Quisling, R., and Ryan, P. (1994). Transtorcular approach to vein of Galen aneurysms. 1985. Pediatr Neurosurg *20*, 163-168.
Mills, K.R., Kruep, D., and Saha, M.S. (1999). Elucidating the origins of the vascular system: a fate map of the vascular endothelial and red blood cell lineages in Xenopus laevis. Dev Biol *209*, 352-368.
Milos, N., and Dingle, A.D. (1978). Dynamics of pigment pattern formation in the zebrafish, Brachydanio rerio. I. Establishment and regulation of the lateral line melanophore stripe during the first eight days of development. Journal of Experimental Zoology *205*, 205-216.
Mishra-Gorur, K., Caglayan, A.O., Schaffer, A.E., Chabu, C., Henegariu, O., Vonhoff, F., Akgumus, G.T., Nishimura, S., Han, W., Tu, S.*, et al.* (2014). Mutations in KATNB1

cause complex cerebral malformations by disrupting asymmetrically dividing neural progenitors. Neuron *84*, 1226-1239.
Mitchell, P.J., Rosenfeld, J.V., Dargaville, P., Loughnan, P., Ditchfield, M.R., Frawley, G., and Tress, B.M. (2001). Endovascular management of vein of Galen aneurysmal malformations presenting in the neonatal period. AJNR Am J Neuroradiol *22*, 1403-1409.
Mollat, P., Fournier, A., Yang, C., Alsat, E., Zhang, Y., Evain-Brion, D., Mollat, P., Fournier, A., Yang, C., Alsat, E.*, et al.* (1994). Species specificity and organ, cellular and subcellular localization of the 100 kDa Ras GTPase activating protein. J Cell Sci *107*, 427-435.
Moreno-Mateos, M.A., Vejnar, C.E., Beaudoin, J.D., Fernandez, J.P., Mis, E.K., Khokha, M.K., and Giraldez, A.J. (2015). CRISPRscan: designing highly efficient sgRNAs for CRISPR-Cas9 targeting in vivo. Nature methods *12*, 982-988.
Morin (2003). Nicolaides-Baraitser syndrome: confirmatory report of a syndrome with sparse hair, mental retardation, and short stature and metacarpals. Clinical dysmorphology *12*, 237-240.
Morita, K., Sasaki, H., Furuse, M., and Tsukita, S. (1999). Endothelial claudin: claudin-5/TMVCF constitutes tight junction strands in endothelial cells. J Cell Biol *147*, 185-194.
Mosch, B., Reissenweber, B., Neuber, C., and Pietzsch, J. (2010). Eph receptors and ephrin ligands: important players in angiogenesis and tumor angiogenesis. J Oncol *2010*, 135285.
Nakayama, T., Fish, M.B., Fisher, M., Oomen-Hajagos, J., Thomsen, G.H., and Grainger, R.M. (2013). Simple and efficient CRISPR/Cas9-mediated targeted mutagenesis in Xenopus tropicalis. Genesis (New York, NY : 2000) *51*, 835-843.
Neale, B.M., Kou, Y., Liu, L., Ma'ayan, A., Samocha, K.E., Sabo, A., Lin, C.F., Stevens, C., Wang, L.S., Makarov, V.*, et al.* (2012). Patterns and rates of exonic de novo mutations in autism spectrum disorders. Nature *485*, 242-245.
Neveling, K., Feenstra, I., Gilissen, C., Hoefsloot, L.H., Kamsteeg, E.J., Mensenkamp, A.R., Rodenburg, R.J., Yntema, H.G., Spruijt, L., Vermeer, S.*, et al.* (2013). A post-hoc comparison of the utility of sanger sequencing and exome sequencing for the diagnosis of heterogeneous diseases. Hum Mutat *34*, 1721-1726.
Nikolaev, S.I., Vetiska, S., Bonilla, X., Boudreau, E., Jauhiainen, S., Rezai Jahromi, B., Khyzha, N., DiStefano, P.V., Suutarinen, S., Kiehl, T.R.*, et al.* (2018). Somatic Activating KRAS Mutations in Arteriovenous Malformations of the Brain. The New England journal of medicine *378*, 250-261.
O'Roak, B.J., Deriziotis, P., Lee, C., Vives, L., Schwartz, J.J., Girirajan, S., Karakoc, E., Mackenzie, A.P., Ng, S.B., Baker, C.*, et al.* (2011). Exome sequencing in sporadic autism spectrum disorders identifies severe de novo mutations. Nat Genet *43*, 585-589.
O'Roak, B.J., Vives, L., Girirajan, S., Karakoc, E., Krumm, N., Coe, B.P., Levy, R., Ko, A., Lee, C., Smith, J.D.*, et al.* (2012). Sporadic autism exomes reveal a highly interconnected protein network of de novo mutations. Nature *485*, 246-250.
Ogawa, T., Wakai, C., Saito, T., Murayama, A., Mimura, Y., Youfu, S., Nakamachi, T., Kuwagata, M., Satoh, K., and Shioda, S. (2011). Distribution of the longevity gene product, SIRT1, in developing mouse organs. Congenit Anom (Kyoto) *51*, 70-79.
Ohk, J., and Jung, H. (2017). Visualization and Quantitative Analysis of Embryonic Angiogenesis in Xenopus tropicalis. J Vis Exp.

Pagenstecher, A., Stahl, S., Sure, U., Felbor, U., Pagenstecher, A., Stahl, S., Sure, U., and Felbor, U. (2009). A two-hit mechanism causes cerebral cavernous malformations: complete inactivation of CCM1, CCM2 or CCM3 in affected endothelial cells. Hum Mol Genet *18*, 911-918.
Pawson, T., and Scott, J.D. (1997). Signaling through scaffold, anchoring, and adaptor proteins. Science *278*, 2075-2080.
Pollen, A.A., Nowakowski, T.J., Chen, J., Retallack, H., Sandoval-Espinosa, C., Nicholas, C.R., Shuga, J., Liu, S.J., Oldham, M.C., Diaz, A.*, et al.* (2015). Molecular identity of human outer radial glia during cortical development. Cell *163*, 55-67.
Potente, M., Ghaeni, L., Baldessari, D., Mostoslavsky, R., Rossig, L., Dequiedt, F., Haendeler, J., Mione, M., Dejana, E., Alt, F.W.*, et al.* (2007). SIRT1 controls endothelial angiogenic functions during vascular growth. Genes Dev *21*, 2644-2658.
Protack, C.D., Foster, T.R., Hashimoto, T., Yamamoto, K., Lee, M.Y., Kraehling, J.R., Bai, H., Hu, H., Isaji, T., Santana, J.M.*, et al.* (2017). Eph-B4 regulates adaptive venous remodeling to improve arteriovenous fistula patency. Sci Rep *7*, 15386.
Raciti, D., Reggiani, L., Geffers, L., Jiang, Q., Bacchion, F., Subrizi, A.E., Clements, D., Tindal, C., Davidson, D.R., Kaissling, B.*, et al.* (2008). Organization of the pronephric kidney revealed by large-scale gene expression mapping. Genome biology *9*, R84.
Rauch, A., Wieczorek, D., Graf, E., Wieland, T., Endele, S., Schwarzmayr, T., Albrecht, B., Bartholdi, D., Beygo, J., Di Donato, N.*, et al.* (2012). Range of genetic mutations associated with severe non-syndromic sporadic intellectual disability: an exome sequencing study. Lancet *380*, 1674-1682.
Raybaud, C.A., Strother, C.M., and Hald, J.K. (1989). Aneurysms of the vein of Galen: embryonic considerations and anatomical features relating to the pathogenesis of the malformation. Neuroradiology *31*, 109-128.
Recinos, P.F., Rahmathulla, G., Pearl, M., Recinos, V.R., Jallo, G.I., Gailloud, P., and Ahn, E.S. (2012). Vein of Galen malformations: epidemiology, clinical presentations, management. Neurosurg Clin N Am *23*, 165-177.
Revencu, N., Boon, L., Mendola, A., Cordisco, M., Dubois, J., Clapuyt, P., Revencu, N., Boon, L., Mendola, A., Cordisco, M.*, et al.* (2013). RASA1 mutations and associated phenotypes in 68 families with capillary malformation-arteriovenous malformation. Hum Mutat *34*, 1632-1641.
Revencu, N., Boon, L.M., Mulliken, J.B., Enjolras, O., Cordisco, M.R., Burrows, P.E., Clapuyt, P., Hammer, F., Dubois, J., Baselga, E.*, et al.* (2008). Parkes Weber syndrome, vein of Galen aneurysmal malformation, and other fast-flow vascular anomalies are caused by RASA1 mutations. Hum Mutat *29*, 959-965.
Rodesch, G., Hui, F., Alvarez, H., Tanaka, A., and Lasjaunias, P. (1994). Prognosis of antenatally diagnosed vein of Galen aneurysmal malformations. Childs Nerv Syst *10*, 79-83.
Roman, B.L., and Hinck, A.P. (2017). ALK1 signaling in development and disease: new paradigms. Cell Mol Life Sci *74*, 4539-4560.
Roth Flach, R.J., Guo, C.A., Danai, L.V., Yawe, J.C., Gujja, S., Edwards, Y.J., and Czech, M.P. (2016). Endothelial Mitogen-Activated Protein Kinase Kinase Kinase Kinase 4 Is Critical for Lymphatic Vascular Development and Function. Mol Cell Biol *36*, 1740-1749.

Rovainen, C.M., and Kakarala, M.H. (1989). Angiogenesis on the optic tectum of albino Xenopus laevis tadpoles. Brain research Developmental brain research *48*, 197-213.
Salaita, K., and Groves, J.T. (2010). Roles of the cytoskeleton in regulating EphA2 signals. Commun Integr Biol *3*, 454-457.
Samocha, K.E., Robinson, E.B., Sanders, S.J., Stevens, C., Sabo, A., McGrath, L.M., Kosmicki, J.A., Rehnstrom, K., Mallick, S., Kirby, A.*, et al.* (2014). A framework for the interpretation of de novo mutation in human disease. Nat Genet *46*, 944-950.
Sanders, S.J., Murtha, M.T., Gupta, A.R., Murdoch, J.D., Raubeson, M.J., Willsey, A.J., Ercan-Sencicek, A.G., DiLullo, N.M., Parikshak, N.N., Stein, J.L.*, et al.* (2012). De novo mutations revealed by whole-exome sequencing are strongly associated with autism. Nature *485*, 237-241.
Scheffzek, K., Lautwein, A., Kabsch, W., Ahmadian, M., Wittinghofer, A., Scheffzek, K., Lautwein, A., Kabsch, W., Ahmadian, M., and Wittinghofer, A. (1996). Crystal structure of the GTPase-activating domain of human p120GAP and implications for the interaction with Ras. Nature *384*, 591-596.
Schneider, C.A., Rasband, W.S., and Eliceiri, K.W. (2012). NIH Image to ImageJ: 25 years of image analysis. Nature methods *9*, 671-675.
Shulman, L.P., Elias, S., Phillips, O.P., Grevengood, C., Dungan, J.S., and Simpson, J.L. (1994). Amniocentesis performed at 14 weeks' gestation or earlier: comparison with first-trimester transabdominal chorionic villus sampling. Obstet Gynecol *83*, 543-548.
Stuart, B.D., Choi, J., Zaidi, S., Xing, C., Holohan, B., Chen, R., Choi, M., Dharwadkar, P., Torres, F., Girod, C.E.*, et al.* (2015). Exome sequencing links mutations in PARN and RTEL1 with familial pulmonary fibrosis and telomere shortening. Nature Genetics *47*, 512.
Suh, D.C., Alvarez, H., Bhattacharya, J.J., Rodesch, G., and Lasjaunias, P.L. (2001). Intracranial haemorrhage within the first two years of life. Acta Neurochir (Wien) *143*, 997-1004.
Sung, H., Kanchi, K., Wang, X., Hill, K., Messina, J., Lee, J., Sung, H., Kanchi, K., Wang, X., Hill, K.*, et al.* (2016). Inactivation of RASA1 promotes melanoma tumorigenesis via R-Ras activation. Oncotarget *7*, 23885-23896.
Swanstrom, S., Flodmark, O., and Lasjaunias, P. (1994). Conditions for treatment of cerebral arteriovenous malformation associated with ectasia of the vein of Galen in the newborn. Acta paediatrica (Oslo, Norway : 1992) *83*, 255-257.
Szklarczyk, D., Franceschini, A., Wyder, S., Forslund, K., Heller, D., Huerta-Cepas, J., Simonovic, M., Roth, A., Santos, A., Tsafou, K.P.*, et al.* (2015). STRING v10: protein-protein interaction networks, integrated over the tree of life. Nucleic Acids Res *43*, D447-452.
Tanaka, M., Kamata, R., and Sakai, R. (2005a). EphA2 phosphorylates the cytoplasmic tail of Claudin-4 and mediates paracellular permeability. J Biol Chem *280*, 42375-42382.
Tanaka, M., Kamata, R., and Sakai, R. (2005b). Phosphorylation of ephrin-B1 via the interaction with claudin following cell-cell contact formation. The EMBO journal *24*, 3700-3711.
Tham, E., Lindstrand, A., Santani, A., Malmgren, H., Nesbitt, A., Dubbs, H.A., Zackai, E.H., Parker, M.J., Millan, F., Rosenbaum, K.*, et al.* (2015). Dominant mutations in KAT6A cause intellectual disability with recognizable syndromic features. American journal of human genetics *96*, 507-513.

Tiedeken, J.J., 3rd, and Rovainen, C.M. (1991). Fluorescent imaging in vivo of developing blood vessels on the optic tectum of Xenopus laevis. Microvascular research *41*, 376-389.
Timberlake, A.T., Choi, J., Zaidi, S., Lu, Q., Nelson-Williams, C., Brooks, E.D., Bilguvar, K., Tikhonova, I., Mane, S., Yang, J.F.*, et al.* (2016). Two locus inheritance of non-syndromic midline craniosynostosis via rare SMAD6 and common BMP2 alleles. Elife *5*.
Timberlake, A.T., Furey, C.G., Choi, J., Nelson-Williams, C., Yale Center for Genome, A., Loring, E., Galm, A., Kahle, K.T., Steinbacher, D.M., Larysz, D.*, et al.* (2017). De novo mutations in inhibitors of Wnt, BMP, and Ras/ERK signaling pathways in non-syndromic midline craniosynostosis. Proceedings of the National Academy of Sciences of the United States of America *114*, E7341-E7347.
Tinsley, R.C., and Kobel, H.R. (1996). The biology of Xenopus (Oxford New York: Published for the Zoological Society of London by Clarendon Press ; Oxford University Press).
Trahey, M., Wong, G., Halenbeck, R., Rubinfeld, B., Martin, G., Ladner, M., Trahey, M., Wong, G., Halenbeck, R., Rubinfeld, B.*, et al.* (1988). Molecular cloning of two types of GAP complementary DNA from human placenta. Science *242*, 1697-1700.
Tsai, Y.S., Chen, Y.R., and Chen, L.W. (2015). Mystery Case: Intracranial hemorrhage in adult vein of Galen malformation. Neurology *85*, e94-95.
Tsutsumi, Y., Kosaki, R., Itoh, Y., Tsukamoto, K., Matsuoka, R., Shintani, M., Nosaka, S., Masaki, H., and Iizuka, Y. (2011). Vein of Galen aneurysmal malformation associated with an endoglin gene mutation. Pediatrics *128*, e1307-1310.
Tsygankova, O., Kupperman, E., Wen, W., Meinkoth, J., Tsygankova, O., Kupperman, E., Wen, W., and Meinkoth, J. (2000). Cyclic AMP activates Ras. Oncogene *19*, 3609-3615.
Ureta-Vidal, A., Ettwiller, L., and Birney, E. (2003). Comparative genomics: genome-wide analysis in metazoan eukaryotes. Nature reviews Genetics *4*, 251-262.
Van der Auwera, G.A., Carneiro, M.O., Hartl, C., Poplin, R., del Angel, G., Levy-Moonshine, A., Jordan, T., Shakir, K., Roazen, D., Thibault, J.*, et al.* (2013). From FastQ Data to High-Confidence Variant Calls: The Genome Analysis Toolkit Best Practices Pipeline. Current Protocols in Bioinformatics *43*, 11.10.11-11.10.33.
Van Itallie, C.M., and Anderson, J.M. (2013). Claudin interactions in and out of the tight junction. Tissue Barriers *1*, e25247.
Van Laarhoven, P.M., Neitzel, L.R., Quintana, A.M., Geiger, E.A., Zackai, E.H., Clouthier, D.E., Artinger, K.B., Ming, J.E., and Shaikh, T.H. (2015). Kabuki syndrome genes KMT2D and KDM6A: functional analyses demonstrate critical roles in craniofacial, heart and brain development. Human Molecular Genetics *24*, 4443-4453.
Venugopal, A. (2014). Disseminated intravascular coagulation. Indian J Anaesth *58*, 603-608.
Vigil, D., Cherfils, J., Rossman, K., Der, C., Vigil, D., Cherfils, J., Rossman, K., and Der, C. (2010). Ras superfamily GEFs and GAPs: validated and tractable targets for cancer therapy? Nat Rev Cancer *10*, 842-857.
Vissers, L.E., de Ligt, J., Gilissen, C., Janssen, I., Steehouwer, M., de Vries, P., van Lier, B., Arts, P., Wieskamp, N., del Rosario, M.*, et al.* (2010). A de novo paradigm for mental retardation. Nature genetics *42*, 1109-1112.

Vivanti, A., Ozanne, A., Grondin, C., Saliou, G., Quevarec, L., Maurey, H., Aubourg, P., Benachi, A., Gut, M., Gut, I.*, et al.* (2018). Loss of function mutations in EPHB4 are responsible for vein of Galen aneurysmal malformation. Brain : a journal of neurology *141*, 979-988.
Wagner, M.W., Vaught, A.J., Poretti, A., Blakemore, K.J., and Huisman, T.A. (2015). Vein of galen aneurysmal malformation: prognostic markers depicted on fetal MRI. The neuroradiology journal *28*, 72-75.
Walker, E.J., Su, H., Shen, F., Choi, E.J., Oh, S.P., Chen, G., Lawton, M.T., Kim, H., Chen, Y., Chen, W.*, et al.* (2011). Arteriovenous malformation in the adult mouse brain resembling the human disease. Annals of neurology *69*, 954-962.
Wang, H.U., Chen, Z.F., and Anderson, D.J. (1998). Molecular distinction and angiogenic interaction between embryonic arteries and veins revealed by ephrin-B2 and its receptor Eph-B4. Cell *93*, 741-753.
Wang, K., Li, M., and Hakonarson, H. (2010a). ANNOVAR: functional annotation of genetic variants from high-throughput sequencing data. Nucleic Acids Res *38*, e164.
Wang, Y., Nakayama, M., Pitulescu, M.E., Schmidt, T.S., Bochenek, M.L., Sakakibara, A., Adams, S., Davy, A., Deutsch, U., Luthi, U.*, et al.* (2010b). Ephrin-B2 controls VEGF-induced angiogenesis and lymphangiogenesis. Nature *465*, 483-486.
Wang, Z., Miura, N., Bonelli, A., Mole, P., Carlesso, N., Olson, D.P., and Scadden, D.T. (2002). Receptor tyrosine kinase, EphB4 (HTK), accelerates differentiation of select human hematopoietic cells. Blood *99*, 2740-2747.
Ware, J.S., Samocha, K.E., Homsy, J., and Daly, M.J. (2015). Interpreting de novo Variation in Human Disease Using denovolyzeR. Curr Protoc Hum Genet *87*, 7 25 21-15.
Wattenhofer, M., Reymond, A., Falciola, V., Charollais, A., Caille, D., Borel, C., Lyle, R., Estivill, X., Petersen, M.B., Meda, P.*, et al.* (2005). Different mechanisms preclude mutant CLDN14 proteins from forming tight junctions in vitro. Hum Mutat *25*, 543-549.
Wei, Q., Zhan, X., Zhong, X., Liu, Y., Han, Y., Chen, W., and Li, B. (2015). A Bayesian framework for de novo mutation calling in parents-offspring trios. Bioinformatics *31*, 1375-1381.
Wiederstein, M., and Sippl, M.J. (2007). ProSA-web: interactive web service for the recognition of errors in three-dimensional structures of proteins. Nucleic Acids Res *35*, W407-410.
Willsey, A.J., Fernandez, T.V., Yu, D., King, R.A., Dietrich, A., Xing, J., Sanders, S.J., Mandell, J.D., Huang, A.Y., Richer, P.*, et al.* (2017). De Novo Coding Variants Are Strongly Associated with Tourette Disorder. Neuron *94*, 486-499 e489.
Wolfe, J.M., and Myers, L. (2010). Fur in the midst of the waters: visual search for material type is inefficient. J Vis *10*, 8.
Xiao, Z., Carrasco, R., Kinneer, K., Sabol, D., Jallal, B., Coats, S., and Tice, D.A. (2012). EphB4 promotes or suppresses Ras/MEK/ERK pathway in a context-dependent manner: Implications for EphB4 as a cancer target. Cancer Biol Ther *13*, 630-637.
Xu, D.S., Usman, A.A., Hurley, M.C., Eddleman, C.S., and Bendok, B.R. (2010). Adult presentation of a familial-associated vein of galen aneurysmal malformation: case report. Neurosurgery *67*, E1845-1851; discussion 1851.
Yang, X., Boehm, J.S., Yang, X., Salehi-Ashtiani, K., Hao, T., Shen, Y., Lubonja, R., Thomas, S.R., Alkan, O., Bhimdi, T.*, et al.* (2011). A public genome-scale lentiviral expression library of human ORFs. Nature methods *8*, 659-661.

Yuval, Y., Lerner, A., Lipitz, S., Rotstein, Z., Hegesh, J., and Achiron, R. (1997). Prenatal diagnosis of vein of Galen aneurysmal malformation: report of two cases with proposal for prognostic indices. Prenatal diagnosis *17*, 972-977.
Zaidi, S., Choi, M., Wakimoto, H., Ma, L., Jiang, J., Overton, J.D., Romano-Adesman, A., Bjornson, R.D., Breitbart, R.E., Brown, K.K.*, et al.* (2013). De novo mutations in histone-modifying genes in congenital heart disease. Nature *498*, 220-223.
Zerah, M., Garcia-Monaco, R., Rodesch, G., Terbrugge, K., Tardieu, M., de Victor, D., and Lasjaunias, P. (1992). Hydrodynamics in vein of Galen malformations. Childs Nerv Syst *8*, 111-117; discussion 117.
Zhang, J., and Hughes, S. (2006). Role of the ephrin and Eph receptor tyrosine kinase families in angiogenesis and development of the cardiovascular system. The Journal of pathology *208*, 453-461.
Zhang, J., Schwartz, M.P., Hou, Z., Bai, Y., Ardalani, H., Swanson, S., Steill, J., Ruotti, V., Elwell, A., Nguyen, B.K.*, et al.* (2017). A Genome-wide Analysis of Human Pluripotent Stem Cell-Derived Endothelial Cells in 2D or 3D Culture. Stem Cell Reports *8*, 907-918.
Zhang, Y.E. (2009). Non-Smad pathways in TGF-beta signaling. Cell Res *19*, 128-139.